Water Temperature as a Tracer in Karst Aquifers

A DISSERTATION
SUBMITTED TO THE FACULTY OF THE GRADUATE SCHOOL
OF THE UNIVERSITY OF MINNESOTA
BY

Andrew James Luhmann

IN PARTIAL FULFILLMENT OF THE REQUIREMENTS
FOR THE DEGREE OF
DOCTOR OF PHILOSOPHY

E. Calvin Alexander, Jr., Advisor

July 2011

Acknowledgements

I have received help and support from many people while working on my thesis. First, I would like to thank my advisor, Dr. E. Calvin Alexander, Jr. Coming into graduate school, I had a general interest in hydrogeology. Calvin certainly led me into the field of karst hydrogeology. He initially showed me numerous springs, sinkholes, and caves, and introduced me to many leaders in the field at scientific meetings. He has been readily accessible and always supportive of my ideas, which has involved a significant amount of his time and energy in the field. Furthermore, his useful critiques have consistently led us to further scientific understanding. Calvin has been a great advisor.

I also want to thank members of my PhD committee: Dr. Martin O. Saar (chair), Dr. William (Bill) E. Seyfried, Jr., and Dr. Anthony (Tony) Runkel. Each of these individuals has provided invaluable help in my scientific development through coursework and research. Thank you for your time and input into my studies. Thank you also to the rest of the faculty in the Department of Geology and Geophysics for promoting a superb educational environment.

Thank you to Dr. Matthew D. Covington. Matt has been a godsend, and his one and a half years as a postdoctoral researcher at Minnesota's Department of Geology and Geophysics enabled the foundation to be set for significant collaboration. Even since he has moved on to another postdoctoral position in Slovenia, we have continued to collaborate via several hundred emails and many Skype calls. Matt's influence has affected all aspects of this thesis, and his input has made my thesis much more scientifically sound.

Thank you Scott Alexander for all of your help and input along the way, especially with field logistics. Su Yi Chai, thank you for your help with data collection and analysis for the Freiheit Spring trace, among other things. Jeff Green, thank you for taking me on my first dye trace. Thanks to Cale Anger, Andrew Peters, Joel Groten, Joe Myre, Jimmy Randolph, Maria Davis, Ravi Appana, Robert (Bob) Tipping, Greg Brick, Chad Geppert, Mina Rahimi, Dr. Po-Hao Kao, Dr. Xiangzhao Kong, Ben Tutolo, Dr. Stuart Walsh, Judy Andrews, Rick Knurr, Dr. Yongli Gao, and Dr. Benjamin Schwartz for your help over the years. I am also grateful to National Science Foundation (NSF) Research Experiences for Undergraduates (REU) summer interns Erik Larson, Julie Greene, and Masaru Nobu for help in the field and lab. Thank you to all the staff for all you do every day to take care of the daily practicalities for me and the entire department.

The ongoing permission of Susan, Aaron, and Matt Kolling to access their property at Freiheit Spring and numerous other local property owners is gratefully acknowledged. Ongoing access to caves in southeastern Minnesota by John Ackerman and his Minnesota Cave Preserve is much appreciated.

I am grateful to Dr. Grant Ferguson and Dr. Abe Springer for providing formal reviews and Dr. Carol Wicks and Dr. Daniel Doctor for offering helpful reviews of an earlier version of Chapter 2. Constructive comments from all of these individuals have improved this chapter.

I have received support as a research assistant with funding provided by the Minnesota Environment and Natural Resources Trust Fund as recommended by the Legislative-Citizen Commission on Minnesota Resources (LCCMR). I have also been a

grateful beneficiary of the Richard C. Dennis and Francis A. Gibson Graduate Fellowships from the University of Minnesota's Department of Geology and Geophysics, and the Doctoral Dissertation Fellowship from the University of Minnesota Graduate School.

Finally, thank you to my parents, family, and friends for all of your love, encouragement, and support throughout the years. Thank you especially to my chief editor and lovely wife Audrey. I would not have finished my thesis without your continual encouragement. Thank you for discussing karst hydrogeology way more than you ever wanted to. Thank you also to my sons, Benjamin and Samuel. Your lives are a continual reminder to make time to stop and enjoy the simple, but incredibly important, things of life. Benjamin, drafts of this thesis will forever be preserved on the backs of your precious drawings. Samuel, the rocks we find in your pockets make Daddy proud.

Table of Contents

List of Tables

List of Figures

List of Notations

A	cross-sectional area of flow path
a	Gaussian peak height
α_r	thermal diffusivity of rock
b	Gaussian peak center
C	concentration
C_e	electrical conductivity
$C_{e,1}$	electrical conductivity of pool for Aug. 30, 2010 trace
$C_{e,2}$	electrical conductivity of pool for Sept. 2, 2010 trace
C_B	background spring chloride concentration
C_S	spring chloride concentration
c	controls Gaussian peak width
$c_{p,r}$	specific heat capacity of rock
$c_{p,w}$	specific heat capacity of water
D_H	conduit hydraulic diameter
D_L	longitudinal dispersivity
E_j	Nash-Sutcliffe efficiency
ε	conduit wall roughness height
F	combined function related to thermal peak lag
f	Darcy-Weisbach friction factor
g	gravitational acceleration
H	height of water above v-notch bottom
h	height of flow path
h_c	heat transfer coefficient
Δh	hydraulic head difference
K	constant characterizing the temperature dependence of electrical conductivity
k_r	thermal conductivity of rock
k_w	thermal conductivity or water
L	conduit length
λ	skin depth

M	salt mass
M_1	salt mass used in Aug. 30, 2010 trace
M_2	salt mass used in Sept. 2, 2010 trace
μ_w	dynamic viscosity of water
Nu	Nusselt Number
P	period of thermal oscillations
Pe	longitudinal dispersion Peclet Number
Pr	Prandtl Number
Ψ	$\rho_w c_{p,w} (\rho_r c_{p,r})^{-1}$
Q	discharge
Q_{ref}	reference discharge
R	conduit radius
R_A	recharge amplitude (i.e., Gaussian peak height or a)
R_D	recharge duration (i.e., Gaussian FWHM or $2c\sqrt{2\ln 2}$)
R_S	total salt recovery
Re	Reynolds Number
r^*	dimensionless radial distance
ρ_r	density of rock
ρ_w	density of water
St	Stanton Number
T	temperature
T_B	background spring temperature
T_C	conservative spring temperature
T_P	pool water temperature
T_r	rock temperature
$T_{r,0}$	initial rock temperature
T_r^*	dimensionless rock temperature
T_s	conduit rock surface temperature
T_s^*	dimensionless conduit wall temperature
T_w	water temperature

T_w^*	dimensionless water temperature
t	time
t^*	dimensionless time
t_{CP}	conservative tracer peak time at outlet
t_{TP}	thermal peak time at outlet
Θ	advection and conduction time ratio
τ	thermal peak lag
τ_{ft}	flow-through time
V_P	volume of pool water at spring per time step
V_T	total pool volume
V_1	pool volume for Aug. 30, 2010 trace
V_2	pool volume for Sept. 2, 2010 trace
v	flow velocity in conduit
v_{ref}	average or reference flow velocity
x^*	dimensionless longitudinal distance along flow path
y^*	dimensionless distance from conduit

Chapter 1

Introduction

Scattered widely over the Earth is a rather peculiar landscape known as "karst."
–Dr. William B. White (1989)

1.1. Karst

The word "karst" describes terrain with a "distinctive hydrology and landforms that arise from a combination of high rock solubility and well developed secondary (fracture) porosity" (Ford and Williams 2007). Klimchouk and Ford (2000) define a karst system as "an integrated mass-transfer system in soluble rocks with a permeability structure dominated by conduits dissolved from the rock and organized to facilitate the circulation of fluid." Soluble karst rocks include limestone, dolostone, gypsum, and salt, and ~20% of the Earth's dry and ice-free land consists of these rocks at or near the surface (Ford and Williams 2007). Most dissolution occurs in preexisting openings that consist of either bedding planes or structures. In an analysis of ~500 caves, Palmer (1991) found that 57% of the total length of cave passages formed due to dissolution along favorable beds or bedding-plane partings. In addition, 42% of the total length of cave passages formed due to dissolution along prominent fractures, and only 1% of the total length of cave passages formed due to dissolution of intergranular pores. Characteristic surface karst features include sinkholes, sinking streams, and springs.

Below the surface, fractures and bedding planes dissolve to form conduits or caves (Figure 1.1).

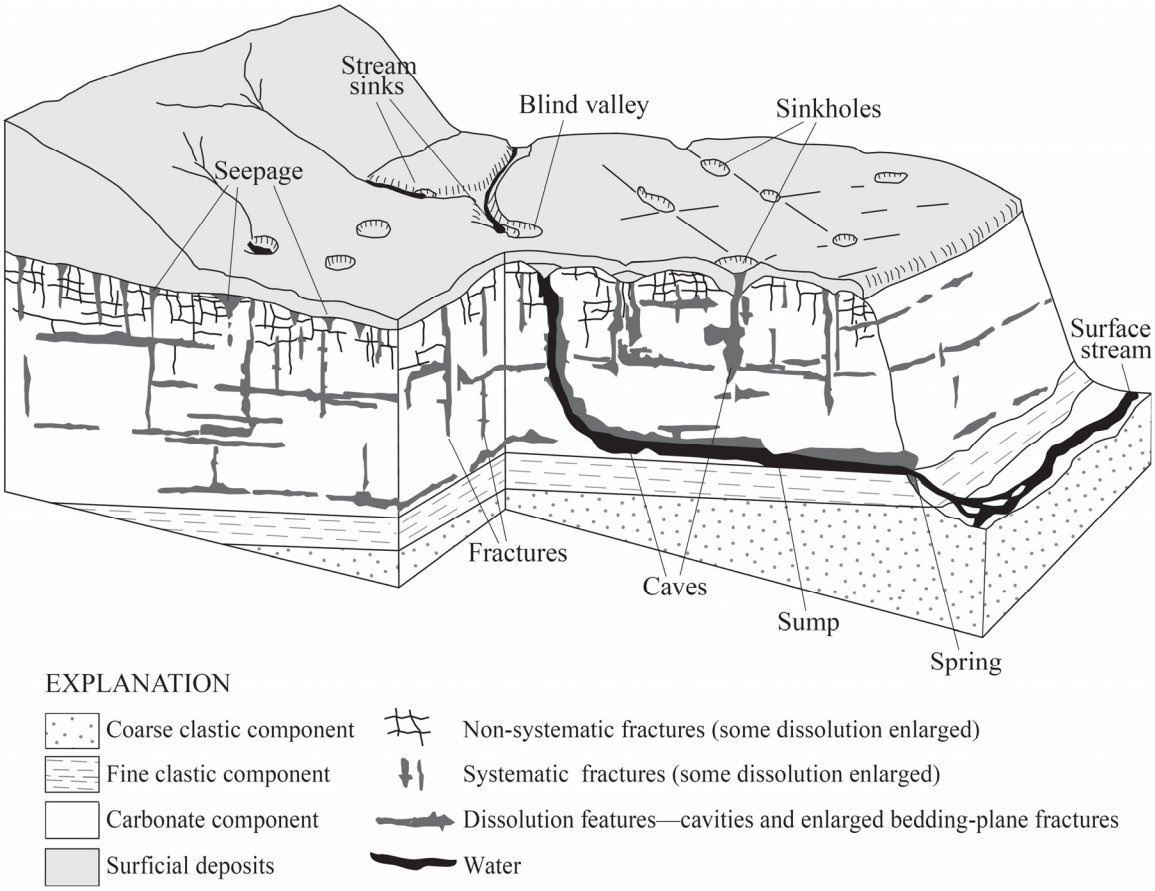

Figure 1.1. Common karst features. From Runkel et al. (2003).

The world distribution of carbonate rocks is shown in Figure 1.2 (Williams and Fong 2010). Carbonate karst aquifers are important water resources, as 20-25% of the world's population is largely or entirely dependent on groundwater from these reservoirs (Ford and Williams 2007). While some believe this estimate is too high, they still affirm the importance of karst groundwater for humanity (Goldscheider et al. 2007).

Some of the most important aquifers in Minnesota are the Paleozoic aquifers in the southeastern part of the state, from which most public wells and more than 50% of private wells in this area draw their water (Runkel et al. 2003). A significant portion of this stratigraphy includes limestone and dolostone, which has undergone karst development. Figure 1.3 shows the karst lands of southeastern Minnesota, indicating the amount of surficial cover between the carbonate bedrock and the surface. Dissolution of these carbonates involves a sequence of reactions which may be summarized with the

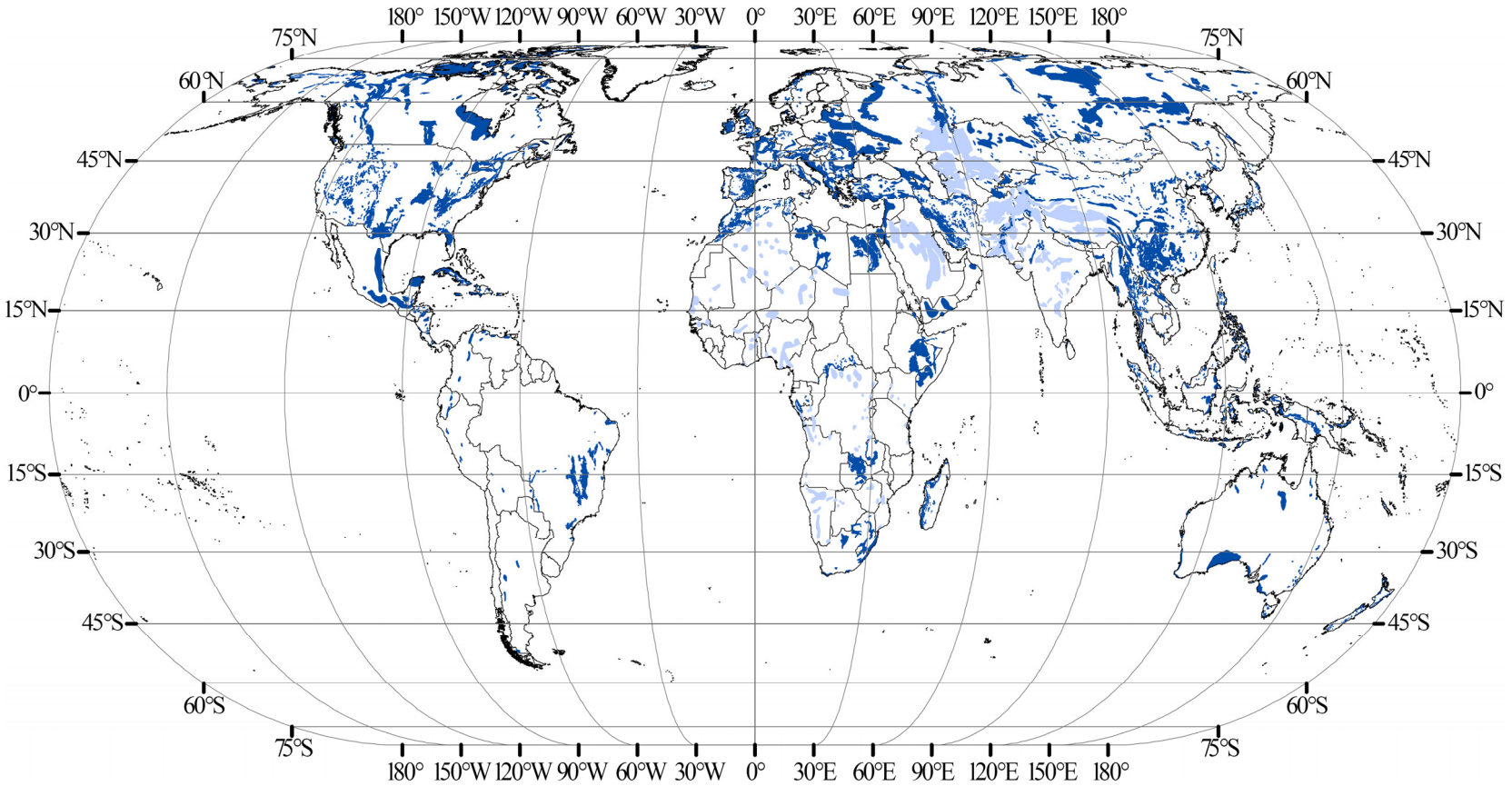

Figure 1.2. The world distribution of carbonate rock outcrops. The dark blue areas indicate regions of relatively pure and continuous carbonate rock, and the lighter blue areas indicate significant, but impure or discontinuous, carbonate strata. From Williams and Fong (2010).

following two reactions for calcite and dolomite, respectively:

$$CaCO_3 + CO_2 + H_2O \leftrightarrow Ca^{2+} + 2HCO_3^-, \quad (1.1)$$

and

$$CaMg(CO_3)_2 + 2CO_2 + 2H_2O \rightarrow Ca^{2+} + Mg^{2+} + 4HCO_3^-. \quad (1.2)$$

One estimate of rock dissolution in Minnesota karst is approximately 1 mm per thousand years (Alexander and Lively 1995). The largest caves in Minnesota occur in the Upper Ordovician Galena Group. Joint-controlled maze caves commonly occur at the Stewartville-Dubuque contact, and dendritic stream caves are found in the lower Cummingsville Formation (Alexander et al. 2009). Mystery Cave at the Stewartville-Dubuque contact is the only Minnesota cave with more than 10 km of mapped passages, but nine others caves in the Galena or Prairie du Chien Groups include more than 1 km of cave passage. See Alexander et al. (2009) for more detail about caves in Minnesota.

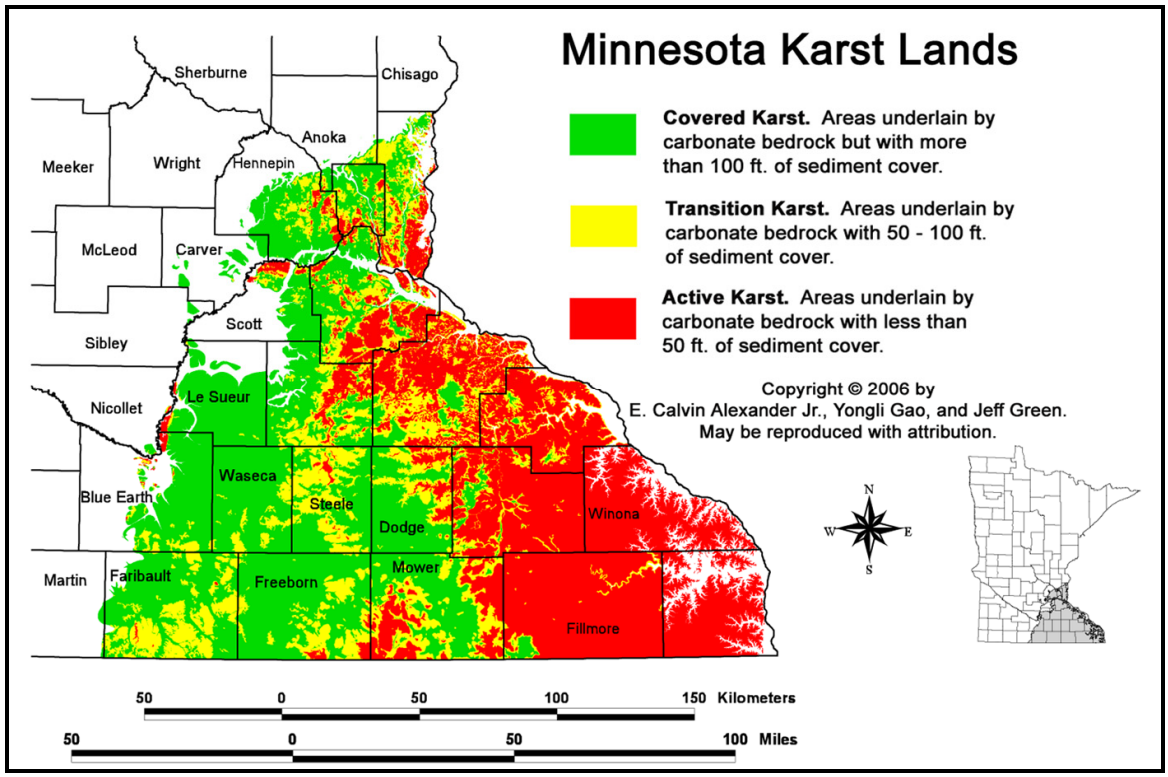

Figure 1.3. Karst lands of southeastern Minnesota. From Gao and Alexander (2008).

Figure 1.4 illustrates how water may flow through a karst aquifer. Karst aquifers are complex, heterogeneous systems (e.g., Tipping et al. 2006) where hydraulic conductivity depends on a study's scale (Kiraly 1975; Quinlan et al. 1992). A karst

aquifer conceptual model incorporates the triple permeability nature of these systems, including matrix permeability, fracture permeability, and conduit permeability (White 1999). While the rock matrix provides most of the storage in karst aquifers, most water flows through channels or conduits because of the greater permeability (Atkinson 1977b; Worthington 1999; Worthington et al. 2000). Primary porosity and permeability in young limestone rocks may be relatively high (e.g., Budd and Vacher 2004), potentially causing groundwater flow through interstitial spaces to be significant (e.g., Martin and Dean, 2001; Screaton et al., 2004; Ritorto et al. 2009; Moore et al. 2009). Vacher and Mylroie (2002) identify this as eogenetic karst, which is common in young carbonates that have undergone only meteoric diagenesis at the site of deposition. In contrast, telogenetic karst (Vacher and Mylroie 2002) is common in Paleozoic carbonates. With a history of burial and uplift, the matrix porosity of telogenetic karst is greatly reduced from the amount present when the sediments were deposited. This causes most of the groundwater to flow through fractures and conduits (e.g., White and White 1989), potentially producing flashy responses (e.g., Florea and Vacher 2006). The karst of Minnesota is this latter type.

Karst aquifers are particularly vulnerable to contamination from land surface activities since contaminants may be rapidly transported into a karst aquifer via conduits or other preferential pathways (e.g., Borchardt et al. 2011). Identifying these preferential pathways and their characteristics thus provides critical information for water resource management.

For a more thorough discussion of karst or karst aquifers, see excellent texts by White (1988), Ford and Williams (2007), and Palmer (2007).

1.2. Geology of southeastern Minnesota

Basement rocks of southeastern Minnesota include sedimentary rocks that are approximately 1000-1200 Ma (Keweenawan), deposited when volcanic activity associated with the Midcontinent rift system waned (Mossler 2002). After volcanism widened the rift, sedimentary material accumulated in basins that arose due to subsidence associated with significant fracturing and faulting in the Belle Plaine structural zone

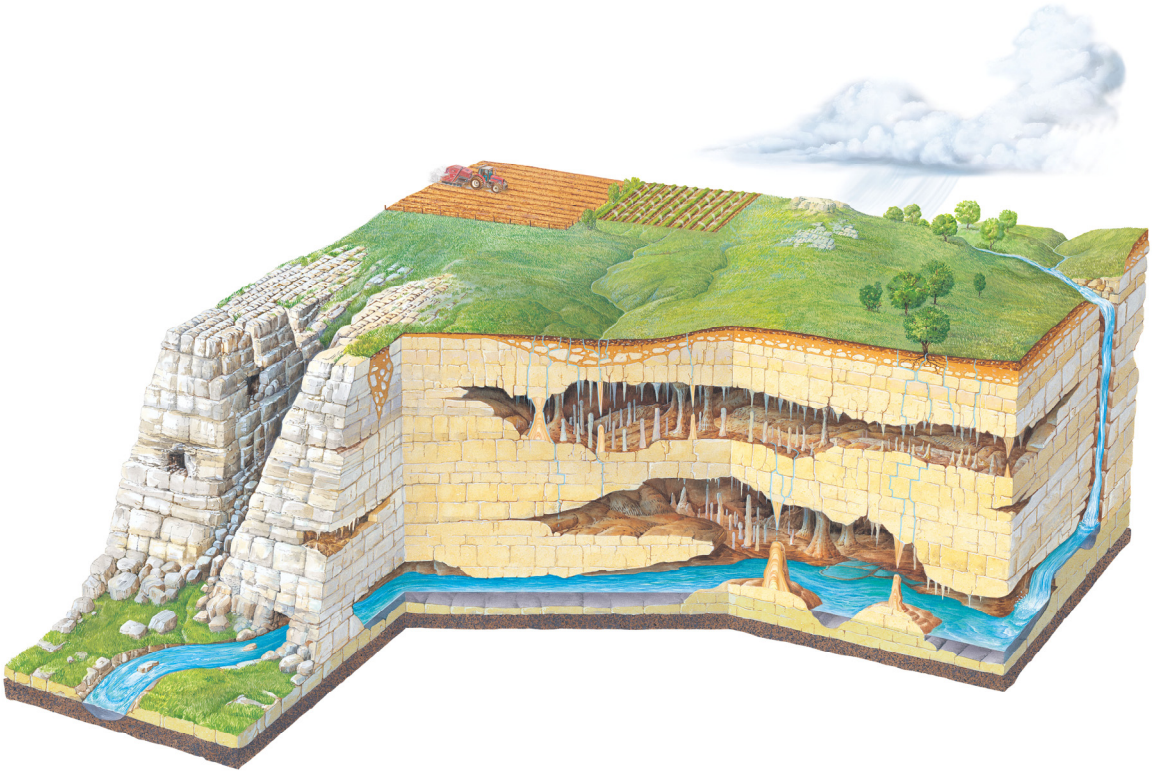

Figure 1.4. Karst aquifer. From Lascu and Feinberg (2011).

(Mossler 2002). While no Keweenawan rocks resulting from this rift system outcrop in any part of southeastern Minnesota, the Fond du Lac Formation and the overlying Hinckley Sandstone have been mapped by gravity, magnetic, and seismic surveys (Craddock 1972). Furthermore, sedimentary rocks distinct from the Fond du Lac and the Hinckley have been attributed to the Solor Church Formation (Morey 1972). There are also some older Middle Proterozoic volcanic and mafic intrusive rocks related to the Midcontinent rift system and Archean and Early Proterozoic metamorphic and igneous rocks below the Keweenawan sedimentary strata (Mossler 2008).

More sedimentary rocks accumulated on top of these rocks during the Early to Middle Paleozoic Era (Cambrian to Devonian), deposited in a low-lying depositional basin that Austin (1969) named the Hollandale embayment (Figure 1.5), which was associated with the erosion of Proterozoic sedimentary rocks (Mossler 2002). These Paleozoic sedimentary rocks were deposited in shallow epicontinental seas (Morey 1982), and they form the bulk of the cover rocks present throughout southeastern Minnesota. Late Cambrian to Early Ordovician rocks were deposited during the Sauk sequence, Middle and Late Ordovician rocks were deposited during the Tippecanoe

sequence, and Middle Devonian rocks were deposited during the Kaskaskia sequence (Mossler 2008). While lower Paleozoic rocks are predominantly sandstones, upper Paleozoic rocks are predominantly carbonates. See Figures 1.6 and 1.7 for a generalized bedrock geologic map and the Paleozoic stratigraphic column of southeastern Minnesota, respectively.

Nonmarine sedimentary rocks occur in isolated areas in southeastern Minnesota and are Late Cretaceous in age (Austin 1972), and Quaternary deposits of till and other glacial material, alluvium, colluvium, and loess are present at the surface (e.g., Hobbs and Goebel 1982). Activity associated with Wisconsinan glaciers left thick glacial deposits throughout much of Minnesota. However, the Wisconsinan glacial lobes did not reach Minnesota's southeastern corner (Hobbs 1995; Hobbs 2002). Therefore, glacial till in this region consists of older deposits resulting from earlier glacial periods. These deposits are thin and isolated because of erosion. Thus, the region is part of the pseudo-driftless area (Hobbs 2002).

Runkel et al. (2003) have shown that, based upon the measured permeabilities and porosities of plug samples, all of southeastern Minnesota Paleozoic sedimentary rocks fall into three hydrostratigraphic components: coarse clastic rocks, fine clastic rocks, and carbonate rocks. The behavior of each of these three components is largely dependent on their depth beneath overlying bedrock. Shallow bedrock is characterized by the presence of secondary pores, including systematic fractures, nonsystematic fractures, and dissolution features (see Figure 1.1). In contrast, secondary pore features in deep bedrock are less prevalent, making these units less productive as groundwater resources. While a lithostratigraphic unit may be characterized by high permeability near the bedrock surface due to the presence of secondary pores, the same unit may be characterized by much lower permeability at greater depths. Runkel et al. (2003) generalized this transition from shallow to deep bedrock to occur at 200 feet below the bedrock surface or 200 horizontal feet from a valley wall throughout southeastern Minnesota, although subsequent publications (e.g., Runkel et al. 2006) indicated that 50 feet might be more appropriate for some types of bedrock.

In deep bedrock settings, flow is minimal through fine clastic and carbonate rocks with little secondary porosity, and these units generally occur as layers of confinement.

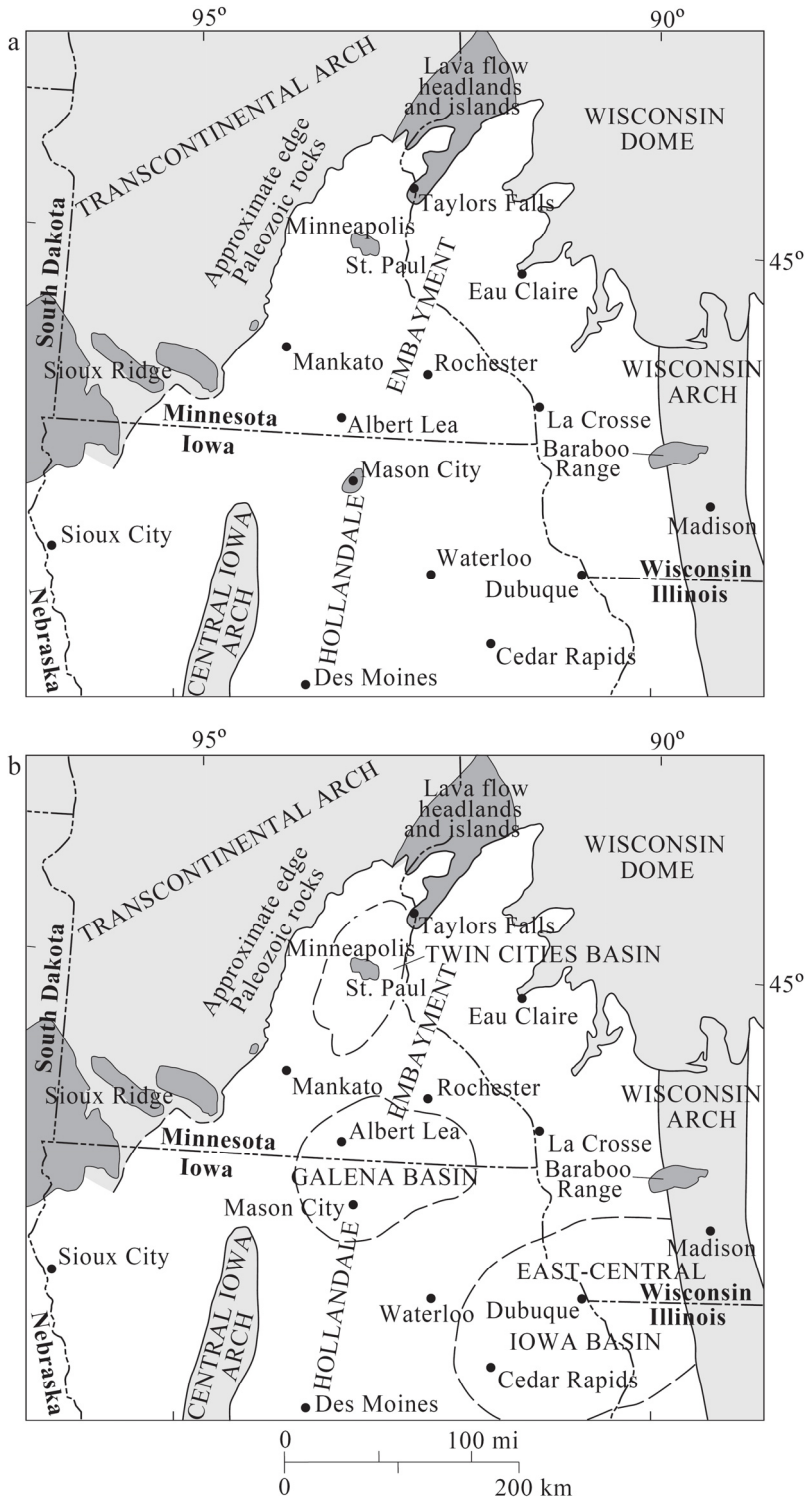

Figure 1.5. The Hollandale Embayment during (a) the Sauk sequence (upper Cambrian to lower Ordovician) and (b) the Tippecanoe sequence (Upper Ordovician). From Mossler (2008).

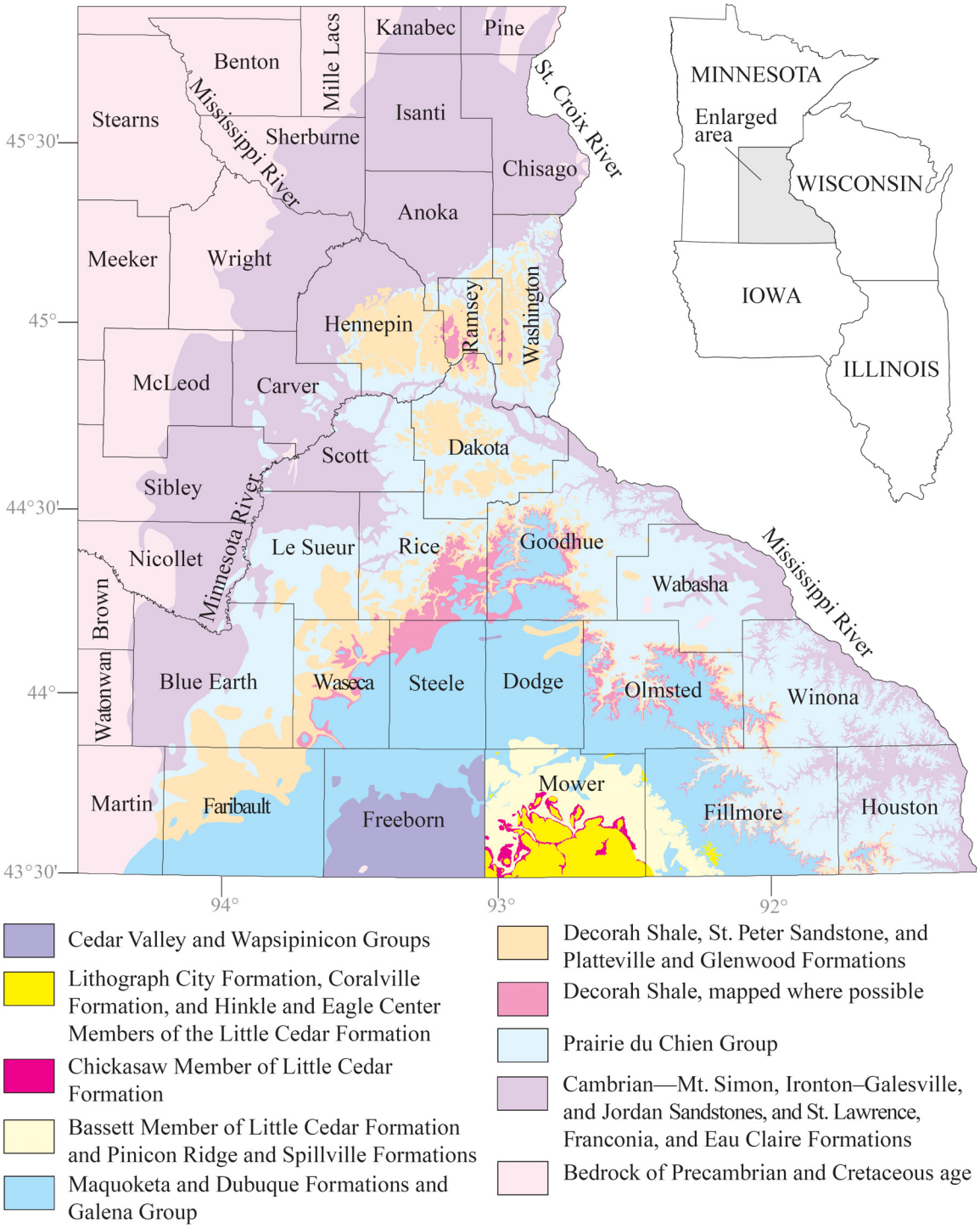

Figure 1.6. Bedrock geology of southeastern Minnesota. Modified from Runkel et al. (2003).

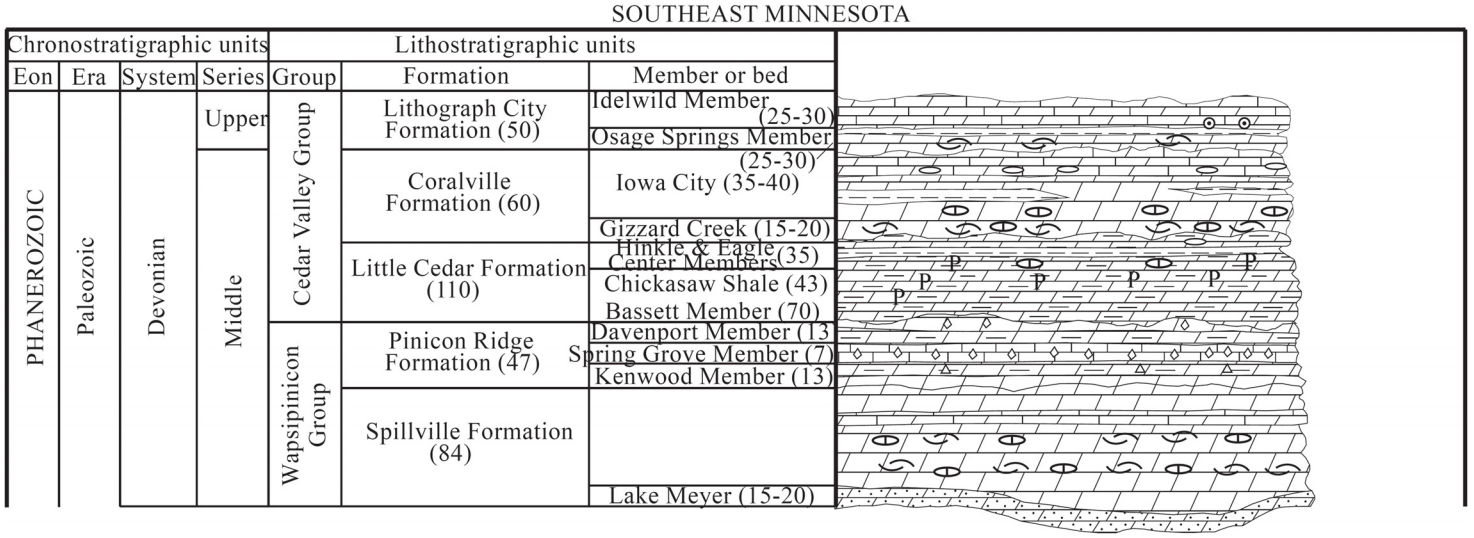

(continued on following page)

Figure 1.7. Stratigraphic column of southeastern Minnesota (on this and following pages). From Mossler (2008).

(continued from previous page)

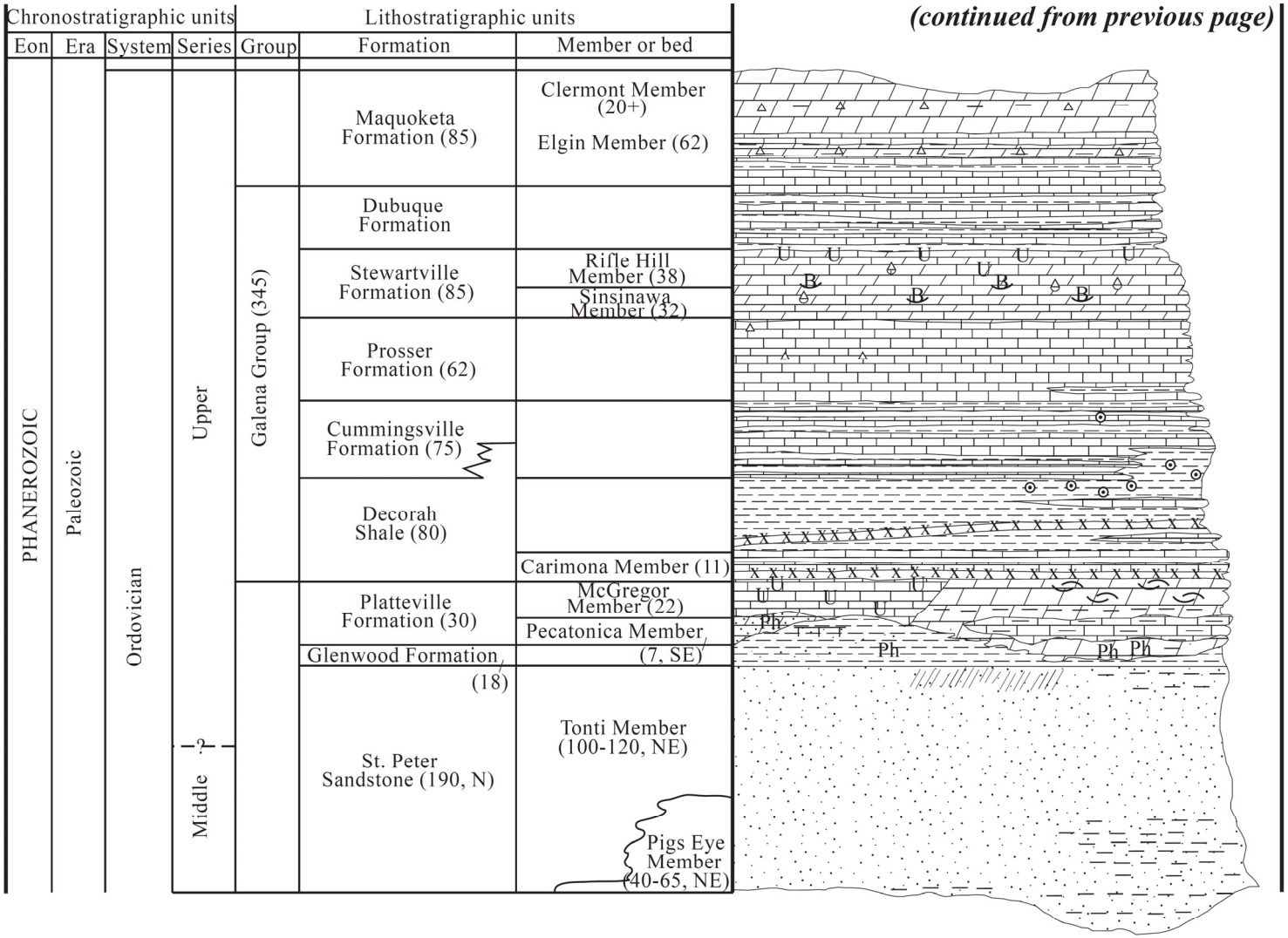

(continued on following page)

(continued from previous page)

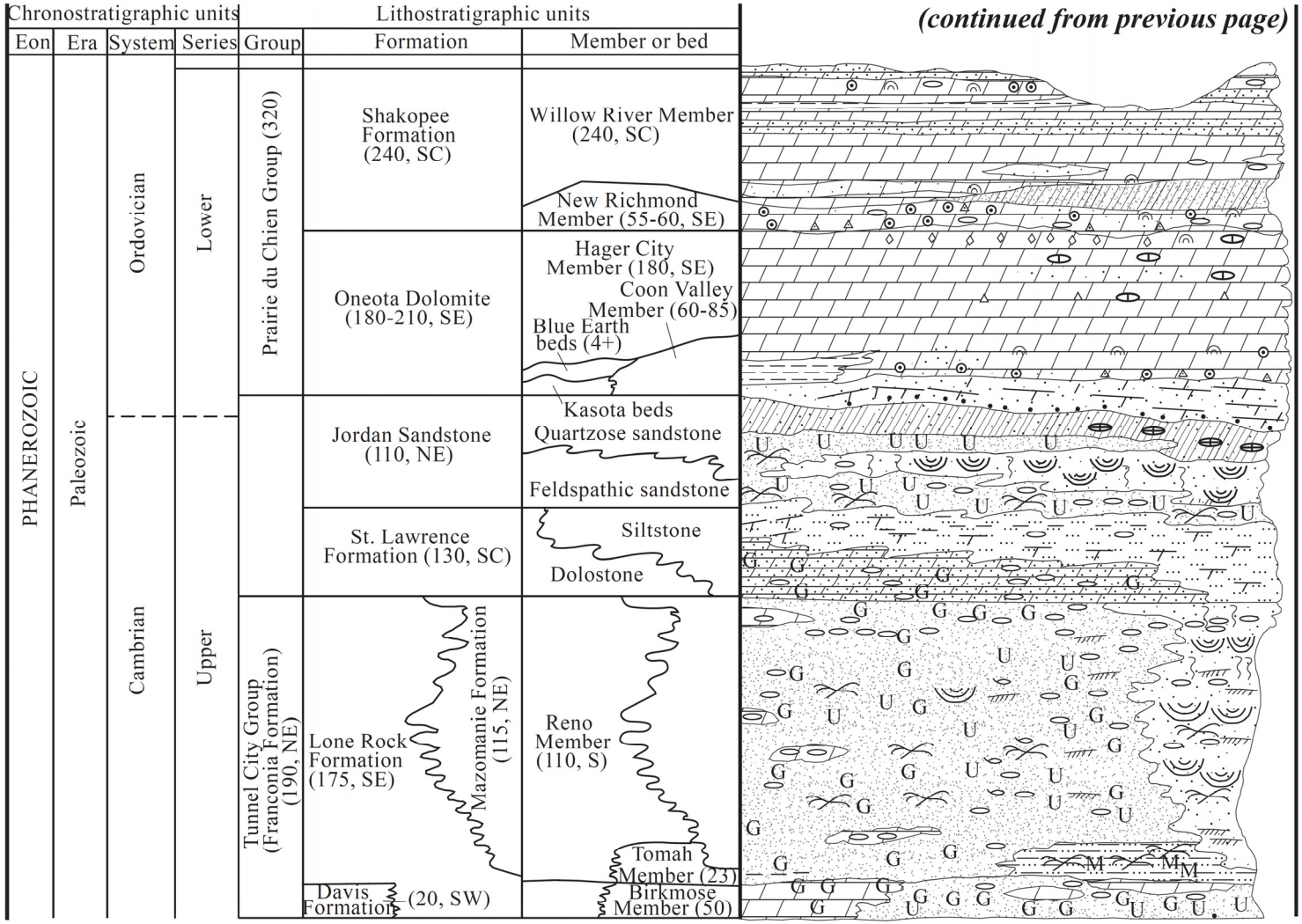

(continued on following page)

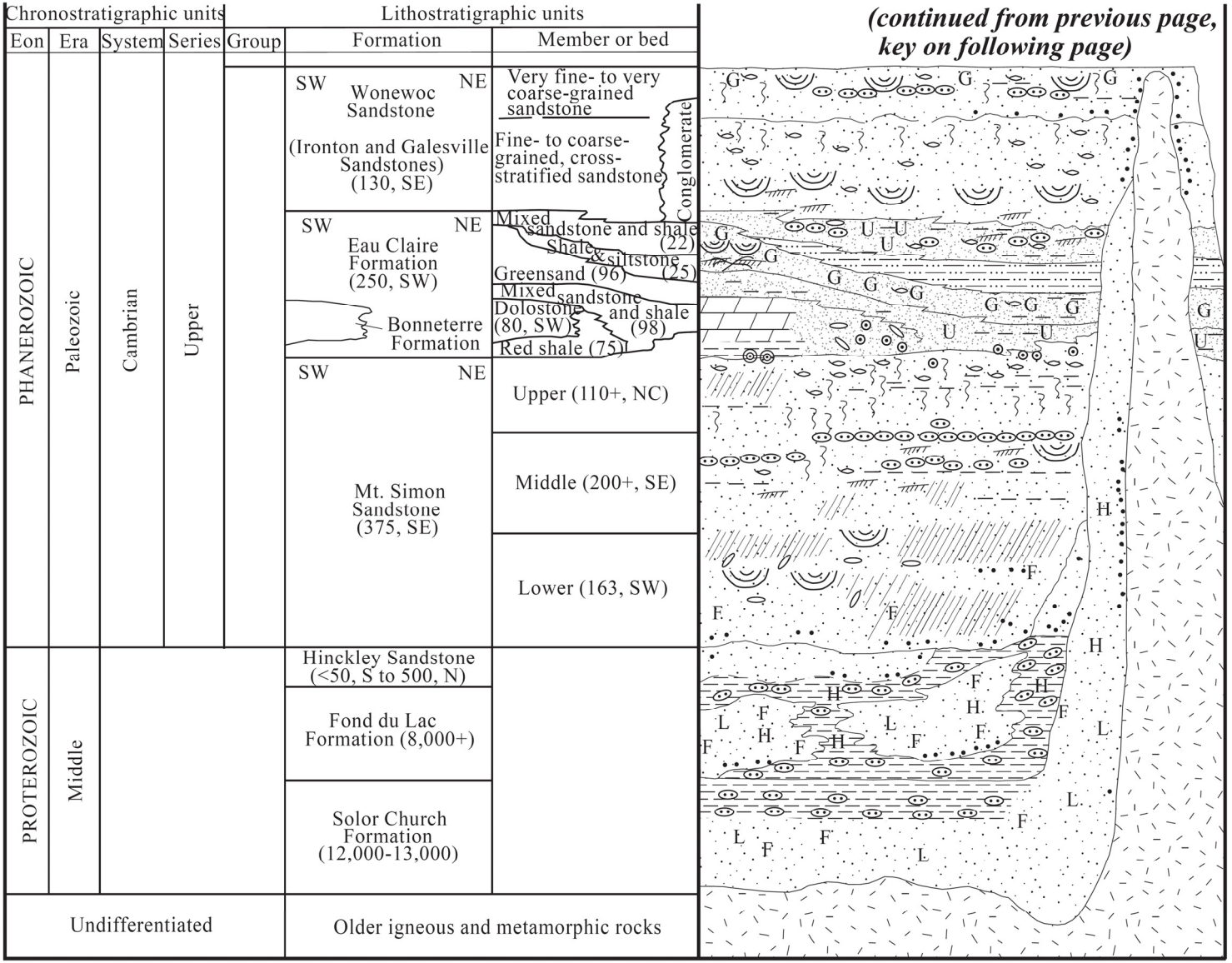

(continued from previous page, key on following page)

EXPLANATION

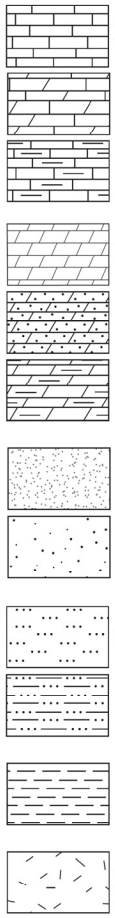

LIMESTONE
Dolomitic
Shaly
DOLOSTONE
Sandy
Shaly
SANDSTONE
Very fine- to fine-grained
Principally medium- to coarse-grained
SILTSTONE
Shaly
SHALE
OLDER IGNEOUS AND METAMORPHIC ROCKS

Chert
Oolitic chert
Oolites
Vugs filled with calcite
Calcareous concretions
Intraclasts
Breccia
Dolomitic
Calcareous
Silty
x x x x Bentonite
G Glauconite
P Pyrite
L Lithic (sand grains)
M Mica
F Feldspathic
H Hematitic
Ph Phosphatic
Fossils, primarily inarticulate brachiopods
Fossils, primarily as molds and/or finely comminuted
Receptaculites
Gastropods
Stromatolites

Oncolites
U Worm bored (general)
Skolithos borings
Conglomeratic
Ripple cross-stratification
Large-scale cross-stratification to tangential cross-stratification
Trough cross-stratification
Swaly and hummocky cross stratification

(60, SW) Numbers in parentheses in formation and member columns refer to maximum thickness of unit (in feet). Letters in parentheses by number refer to part of southeast Minnesota (SW = southwest part, NC = north-central part, etc.) where unit is thickest.

SW-NE Letters in formation column not in parentheses denote direction of facies changes shown on columnar section.

For example, horizontal hydraulic conductivities for mostly unfractured shale, interbedded shale and very fine-grained sandstone, and unfractured carbonates are 10^{-7} ft/day, 10^{-2} to 10^{-1} ft/day, and $\leq 10^{-4}$ ft/day, respectively. In contrast, flow is much higher in coarse clastic rocks and along stratigraphically discrete intervals of carbonate and fine clastic rocks with significant secondary porosity features in deep bedrock settings. For example, horizontal hydraulic conductivities for coarse clastic rocks and carbonate rocks with significant dissolution features are a few ft/day to 60 ft/day and hundreds of ft/day to miles/day, respectively. In shallow bedrock conditions, all three components have higher and greater ranges of hydraulic conductivities, primarily due to the increase in secondary pores, and the integrity of the aquitards in a vertical direction may be compromised. For a more thorough discussion of hydrogeology in southeastern Minnesota, see Runkel et al. (2003).

1.3. Structure and stress of southeastern Minnesota

The sedimentary rocks of southeastern Minnesota have undergone little deformation. However, the rocks of the Hollandale embayment were compressed to form the southward-plunging (Morey 1982), southern Minnesota syncline and smaller basins and synclines during the Paleozoic Era, with the deformation possibly caused by mountain building in the eastern United States (Mossler 2002). This synclinal folding causes the rocks of Minnesota's southeastern corner to have a small regional dip to the southwest (Mossler 1995; Mossler 2002). However, the local dip in any area may have been influenced by the reactivation of Proterozoic or older faults during the Phanerozoic Eon (Mossler 2002). Butler et al. (1997) provide a brief synopsis of work conducted concerning basement reactivation, in which pre-existing heterogeneities in the form of faults and shear zones may influence later continental deformation. Despite extensive work, Butler et al. (1997) concluded that the role of basement reactivation remains a problem. Yet, faults in Minnesota are almost certainly caused by basement reactivation (Hudleston 2007b). Furthermore, Paleozoic structures may be best explained by reactivation of Precambrian faults (Craddock et al. 1963; Morey 1972; Mossler 2008).

Mechanical twins in carbonates indicate that the bedding-parallel, subhorizontal shortening fabric present throughout the eastern North American craton is due to late Paleozoic stresses associated with the Appalachian-Ouachita orogeny, as compressional stresses perpendicular to the orogenic front were transmitted more than 1200 km (Craddock and van der Pluijm 1989) and likely up to ~2100 km from the plate margin (Craddock et al. 1993). This fabric, preserved in Paleozoic limestones of southeastern Minnesota, is perpendicular to the E-W layer-parallel shortening fabric associated with the Sevier Orogeny recorded by Cretaceous limestones in western Minnesota (Craddock and van der Pluijm 1999). The current overall orientation of the maximum horizontal stress field of the midplate central and eastern United States "plate-tectonic" province averages ENE (Zoback and Zoback 1989).

Systematic fractures or joints are prevalent throughout southeastern Minnesota, and these extensional fractures (Hudleston 2007a) are perpendicular to bedding planes at relatively constant intervals with consistent strike orientations (Runkel et al. 2003). According to Mossler (1995), some of the fractures most likely formed from compression due to regional stresses, which eventually opened after these stresses waned. Nonsystematic fractures are also prevalent, although their distribution and shapes are more variable. Because regional stresses most likely cause systematic fractures, systematic fractures seen at the surface are also present in deep bedrock settings, although less developed (Runkel et al. 2003). Regardless, the fractures in shallow bedrock settings throughout southeastern Minnesota are better developed because of uplift, unloading, and weathering, as the rocks were relieved of stress due to the removal of overlying material (Runkel et al. 2003).

1.4. Research goals

I began my graduate school days working on dye tracing projects and setting up a spring monitoring network to collect water level, discharge, temperature, electrical conductivity, and precipitation data to learn about complex karst flow paths. Upon analysis of my data and a review of pertinent karst hydrogeology literature, it became apparent that there were questions to address regarding water temperature as a tracer.

Most fundamental, what information does water temperature communicate about an aquifer? To begin to address this question, my first research goal was to develop a framework for understanding the different types of thermal patterns and to determine the information content they carry about flow through an aquifer.

During the summer of 2009, we conducted an artificial recharge tracer test, with the goal of estimating geometrical properties of the flow path. We added tracers to a pool full of water, and then dumped the water into a sinkhole and monitored the responses at a spring approximately 95 horizontal meters away. Water temperature interacted with the soil and bedrock along this short flow path, producing a lagged, damped thermal signal at the spring. Responses at the spring were small, so we repeated the trace with a larger slug of water and more tracers to illustrate the interactive nature of temperature and to demonstrate how the lagged, damped thermal signal may be used to estimate a conduit's hydraulic diameter.

The tracer test results led to the development of a new goal: to determine which variables affect the thermal lag. Furthermore, I sought to address the relative importance of all dependent variables. Then, given high resolution data during recharge event thermal perturbations at a spring, one might potentially estimate values for unknown variables such as conduit diameter or length with approximations for the other dependent variables.

1.5. Thesis organization

This thesis consists of five chapters. The first chapter includes the introduction that you are currently reading, and the fifth chapter concludes this thesis and proposes questions for future work.

Chapter 2 summarizes spring and cave stream thermal data collected at several sites throughout southeastern Minnesota. Collaborators and I developed a thermal pattern classification scheme that correlates distinct thermal patterns with aquifer system geometry and recharge. This chapter concludes that thermal patterns are a function of conduit geometry, recharge mode and duration, and aquifer depth, and it has been published in *Ground Water* (Luhmann et al. 2011).

Chapter 3 documents a controlled recharge event using multiple natural and artificial tracers to Freiheit Spring in western Fillmore County, MN. A plastic pool was set up next to a sinkhole and was filled with approximately 13,000 liters of water. The water was heated, and salt, deuterium oxide, and uranine were added. After the tracers were well mixed, the pool was emptied into the sinkhole. Data were collected to illustrate breakthrough curves at the spring. This chapter demonstrates that multiple tracers may provide a better estimate of tracer recovery and compares the breakthrough curves for each of the tracers. The breakthrough curves are then used to estimate flow path geometry using two different methods. The first estimates conduit volume using a well known method in the karst hydrologic community. The second is a new method which independently estimates a conduit's hydraulic diameter using known inputs, the thermal breakthrough curve at the spring, and a heat transport simulation. This chapter incorporates two papers: one that was presented at a conference (Luhmann et al. in press, 2011) and another that was submitted to the *Journal of Hydrology* (Luhmann et al. in review, 2011)

Chapter 4 illustrates thermal retardation in karst conduits using heat transport simulations. A series of simulations were run to determine which variables affect the lag of a thermal peak at a spring. Controlling variables were then combined to produce an equation relating controlling variables to thermal peak lag. This relationship may ultimately be used to estimate some of the controlling variables given high resolution data of a conservative tracer (e.g., conductivity) and temperature at a spring when thermal perturbations occur.

Finally, this thesis includes six Appendices. Appendix A includes manual measurements and field notes from monitoring sites in southeastern Minnesota. It also lists the names of text files for the data that were recorded by data loggers. Data text files are included online as supplementary files with this thesis. The water temperature data are summarized in Chapter 2. Appendix B includes the data that were collected for the trace on Aug. 30, 2010 that is discussed in Chapter 3. Appendix C lists details about simulations from Chapter 4. This includes the thermal peak lag, the output peak temperature, and the variables different from those given in Table 4.1 for each

simulation. Appendices D, E, and F include discharge measurements from several sites, recharge event water chemistry and suspended sediment from Freiheit Spring, and snow chemistry above Tyson Spring Cave and near Freiheit Spring, respectively. Much of the data in Appendices D, E, and F were not specifically used in this thesis. However, it is included with the rest of the Appendices to be of use for those working with southeastern Minnesota hydrology in particular and with karst hydrology in general.

Chapter 2

Classification of thermal patterns at karst springs and cave streams

Summary

Thermal patterns of karst springs and cave streams provide potentially useful information concerning aquifer geometry and recharge. Temperature monitoring at 25 springs and cave streams in southeastern Minnesota has shown four distinct thermal patterns. These patterns can be divided into two types: those produced by flow paths with ineffective heat exchange, such as conduits, and those produced by flow paths with effective heat exchange, such as small fractures and pore space. Thermally ineffective patterns result when water flows through the aquifer before it can equilibrate to the rock temperature. Thermally ineffective patterns can be either event-scale, as produced by rainfall or snowmelt events, or seasonal scale, as produced by input from a perennial surface stream. Thermally effective patterns result when water equilibrates to rock temperature, and the patterns displayed depend on whether the aquifer temperature is changing over time. Shallow aquifers with seasonally varying temperatures display a phase-shifted seasonal signal, whereas deeper aquifers with constant temperatures display a stable temperature pattern. An individual aquifer may display more than one of these

patterns. Since karst aquifers typically contain both thermally effective and ineffective routes, we argue that the thermal response is strongly influenced by recharge mode.

2.1. Introduction

Karst aquifers are heterogeneous and anisotropic systems, where characteristic parameters such as hydraulic conductivity are dependent on the scale of interest (Quinlan et al. 1992). The network of conduits largely determines the flow and transport through the system (Atkinson 1977b; Worthington et al. 2000), but the geometry and location of these preferential flow paths is typically poorly constrained. Some of the greatest challenges of karst hydrology revolve around the unknown location and characteristics of conduits.

One approach frequently applied to these challenges is to observe the behavior of springs within a karst aquifer, since a spring provides a characteristic signal that is integrated over an entire basin. Much of the analysis of springs has focused on the characterization of hydrographs, particularly during storm event recessions. However, work by Covington et al. (2009) showed that analysis of hydrographs alone may only provide information about the recharge into the conduit system rather than the geometry. On the contrary, combinations of hydraulic and chemical or thermal responses can provide useful geometrical information. Specifically, lags between the hydraulic and chemical or thermal responses have been used to estimate conduit volumes (Ashton 1966; Atkinson 1977b; Sauter 1992; Ryan and Meiman 1996). Birk et al. (2004) demonstrated that this procedure produced a reasonable first-order estimate of conduit volume for a simulated conduit system with a known geometry.

Additionally, many previous workers have used chemical or isotopic monitoring of springs to separate different water sources or to provide information about the flow system (Hess and White 1988; Dreiss 1989; Lakey and Krothe 1996; Lee and Krothe 2001; Desmarais and Rojstaczer 2002; Grasso and Jeannin 2002; Grasso et al. 2003; Liu et al. 2004; Perrin et al. 2007). Shuster and White (1971) classified karst spring chemical responses into two types: those that displayed a large variation in hardness, which they called conduit systems, and those that displayed little variation in hardness, which they

called diffuse. However, many authors have argued that variability in chemical parameters is largely dependent on the proportion and variability of allogenic recharge, rather than flow conditions within an aquifer (Jakucs 1959; Newson 1971; Ternan 1972; Atkinson 1977a, 1977b; Worthington et al. 1992; White 2002). Regardless, chemical and isotopic studies are labor intensive and expensive.

Reactive solute transport and heat transport are mathematically analogous processes (e.g., Incropera et al. 2007, chap. 8). Thus, we might expect to be able to derive similar information concerning geometry and recharge by observing thermal responses of springs. Importantly, temperature is a more reactive tracer than dissolved calcite (Birk et al. 2006), and therefore it should probe different scales within the aquifer, providing some unique information. Additionally, in comparison to chemical loggers, temperature data loggers are robust and economical, making it more practical to deploy them simultaneously in many springs for time-scales of years.

In general, heat has proven to be a useful tracer in groundwater systems (Anderson 2005), providing potentially powerful constraints on groundwater velocity (Suzuki 1960; Stallman 1965; Bredehoeft and Papadopulos 1965). Specifically, a combination of temperatures and heads can be used jointly in the inverse modeling of groundwater velocities and hydraulic conductivities (Stallman 1963; Woodbury and Smith 1988; Wang et al. 1989; Bravo et al. 2002; Jiang and Woodbury 2006). Temperature measurements are often conducted in boreholes. However, when springs exist, they provide key locations for obtaining signals integrated over an entire basin (Manga 2001). Manga (2001) notes that temperature data are only useful as convective heat transport becomes important.

In karst aquifers, springs are ubiquitous. Furthermore, heat transport in a karst aquifer is dramatically disturbed by convection, and thus represents an extreme case in the continuum of conduction- to convection-dominated systems. (Note the word ‘convection’ refers to ‘forced convection’ throughout this chapter.) Therefore, it seems likely that karst spring temperatures are a crucial source of information for constraining aquifer characteristics. However, few studies have examined thermal responses of karst springs. Benderitter et al. (1993) studied temperature variations in a shallow carbonate

aquifer, observing both seasonal and short-term fluctuations. They interpreted the rapid variations as resulting from water transmitted quickly through fractures and conduits, and the seasonal variations as resulting from a changing aquifer temperature, ultimately using this information to calculate the depth of the aquifer. Bundschuh (1993, 1997) also studied temperature variations of shallow aquifers, but the influence of quick flow paths such as conduits and fractures on these temperature variations remains poorly understood. Using numerical heat transport models, numerous studies have demonstrated that temperature variations and breakthrough curves at springs are quite sensitive to conduit geometry (Hückinghaus et al. 1997; Liedl et al. 1998; Liedl and Sauter 1998). Martin and Dean (1999) and Screaton et al. (2004) used temperature to determine residence time and gain insight about interaction between the conduit system and porous matrix.

Despite the growing body of work on thermal responses, little has been done to develop a general framework for characterizing thermal responses and understanding how they correlate with system geometry and recharge. While others have developed classification systems for springs (e.g., Springer and Stevens 2009) or in particular for karst springs (Smart and Worthington 2004) or carbonate aquifers (Smart and Hobbs 1986), we take a more process-based approach and attempt to classify the spectrum of possible thermal responses, connecting observed thermal patterns and the geometries and recharge modes that produce them. Ultimately, this scheme could be incorporated into a more generalized classification of springs, but we do not attempt that here.

Southeastern Minnesota provides an ideal setting for studying the variety of thermal patterns displayed at karst springs. Karst aquifers dominate the local and regional hydrogeology in southeastern Minnesota, where a thick sequence of Paleozoic carbonate and siliciclastic rocks are found. Because of differences in lithology and hydrological settings, individual aquifers have variable karst development. There are both well-developed and poorly-developed karst basins. Furthermore, the large range of surface temperatures in Minnesota (average seasonal surface temperatures fluctuate approximately 30°C with approximately 70°C variation between extremes) accentuates thermal behaviors. While no local study can hope to capture all possible types of thermal responses, the karst aquifers of southeastern Minnesota provide a useful starting point for

understanding the variety of possible patterns. Here, we classify the thermal patterns observed at 25 different springs and cave streams in southeastern Minnesota. Heat transport theory elucidates connections between the observed patterns and the respective system geometries and recharge modes, and thus motivates our particular classification scheme.

2.2. Study area

The bedrock geology of southeastern Minnesota consists of Cambrian and Ordovician carbonate and siliciclastic rocks (Mossler 2008), shown by the stratigraphic column in Figure 2.1. The rocks were deposited in the Hollandale Embayment and have gentle dips towards the center of the basin to the southwest of the study area (Mossler 2002). Locally, dips may have been influenced by the reactivation of Proterozoic or older faults during the Phanerozoic (Mossler 2002). Systematic extensional fractures or joints are prevalent throughout southeastern Minnesota (Hudleston 2007a) and are perpendicular to bedding planes at relatively constant intervals with consistent strike orientations (Runkel et al. 2003). Systematic fractures seen at the surface may extend to deep bedrock settings, but are less developed (Runkel et al. 2003). Nonsystematic fractures can be locally prevalent. Fractures in shallow bedrock settings throughout southeastern Minnesota are more developed because of unloading by removal of overlying or adjacent material in addition to weathering (Runkel et al. 2003).

Dissolution along these systematic fractures or joints and bedding planes has led to extensive karst development including numerous sinkholes, sinking streams, caves, springs, and other karst features (Alexander et al. 2009). Known caves include branchwork, network, and anastomotic patterns in Palmer's (2007) classification scheme. Individual karst groundwater basins are drained by one or more springs, providing accessible monitoring locations for recording aquifer response.

With the large number of monitoring sites in this study, we present data from selected sites in Minnesota that illustrate the range of observed behaviors. Goliath's Cave (MN23:C0085) is located in southwestern Fillmore County in the Dubuque and Stewartville Formations. The temperature/conductivity probe and the pressure transducer

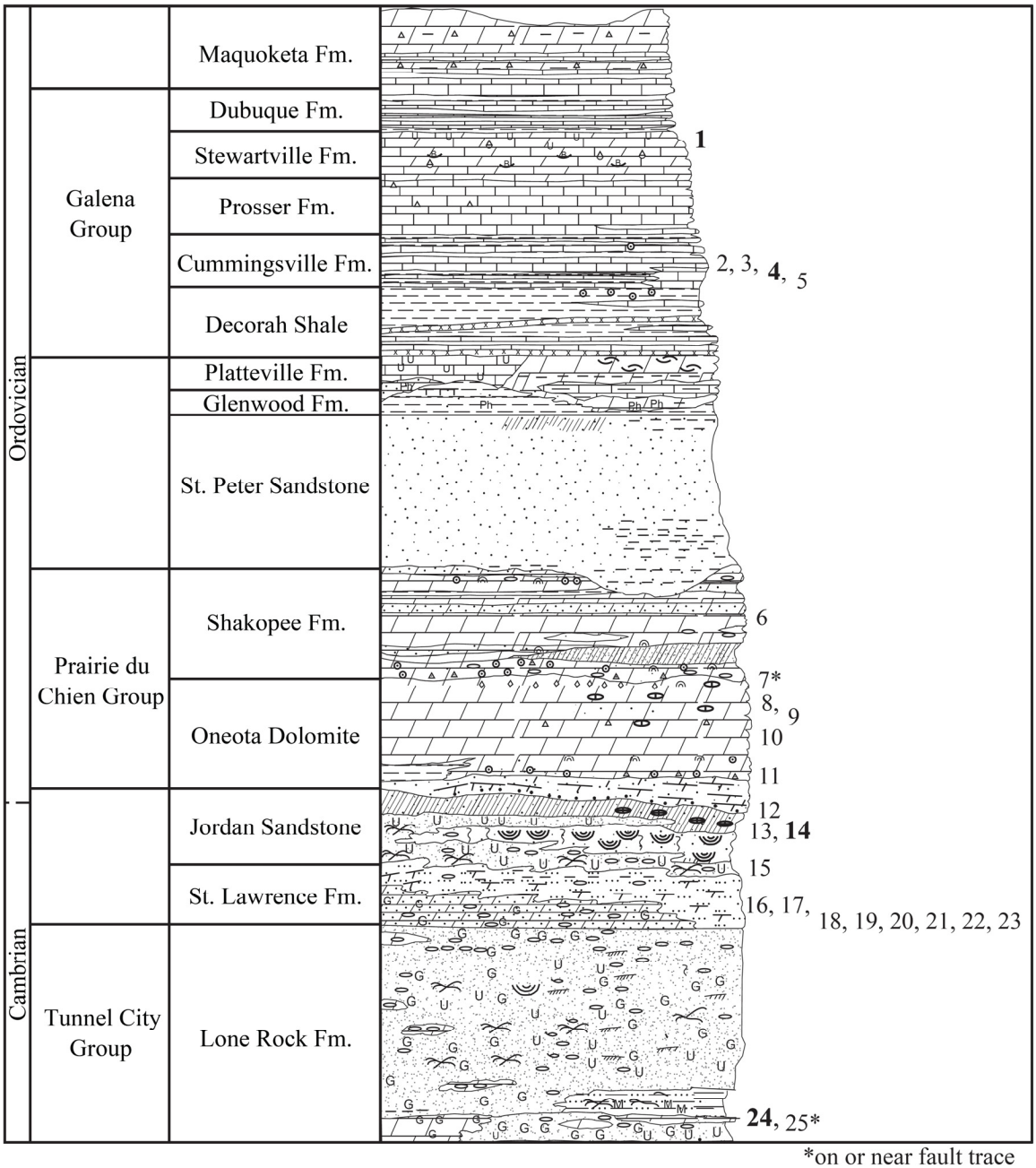

Figure 2.1. Stratigraphic column of southeastern Minnesota. Numbers on right correspond to monitoring locations in Figure 2.2 and Table 2.1 and indicate the stratigraphic location of each site. Bold numbers indicate monitoring locations that are shown and discussed in the text. Modified from Mossler (2008).

at David's Entrance to Goliath's Cave are approximately 26 m below the surface in a stream that runs through the cave. Vreeman Spring (MN23:A0875) is located in southwestern Fillmore County. This spring is in the Cummingsville Formation, and it flows into the South Branch of the Root River (SBRR). Krage Spring (MN85:A0266) is

located in southern Winona County. This spring is in the Lone Rock Formation, and it flows into Corey Creek. Highway 76 MNDNR Spring (MN28:A0076) is located in central Houston County. This spring is in the Jordan Sandstone, and it flows into Badger Creek.

2.3. Methods

Campbell Scientific CR10 Data Loggers were installed at four springs and two cave streams, five Schlumberger CTD Divers were installed along one flow system, and HOBO Pendant Temperature Data Loggers were installed at 21 springs to monitor basic physical and chemical parameters (Figure 2.2). Three sites contained both Campbell and HOBO loggers. Campbell loggers were connected to either a Campbell Scientific 247 Conductivity/Temperature Probe or a Campbell Scientific CS547A Conductivity and Temperature Probe and A547 Interface. Druck PDCR 830 or 1230 pressure transducers were also connected to the Campbell loggers to measure water level. Schlumberger loggers measured temperature, conductivity, and pressure. (For the purpose of this paper, conductivity data are not shown.) HOBO loggers measured temperature alone. Measurements were made every second and 30 min averages were recorded on the Campbell loggers. Measurements were made and recorded every 5 or 10 min on the Schlumberger loggers. HOBO loggers measured and recorded temperature every 30 min. The Campbell loggers recorded temperature with a resolution of 0.01°C and an accuracy of ±0.4°C over the range of -24°C to 48°C. Temperature resolution for Schlumberger loggers was 0.01°C, with an accuracy of ±0.1°C from -20°C to 80°C. Temperature resolution with HOBO loggers was 0.1°C at 25°C, with an accuracy of ±0.5°C at 25°C.

To calibrate and correct sensor drift over time, hand measurements were taken each time the monitoring locations were visited. Temperature measurements were taken with an ASTM 63C traceable glass thermometer near the probe. The glass thermometer had 0.1°C tick marks and was factory calibrated at 0, 10, 20, and 30°C.

Hourly surface temperature and precipitation data were obtained for Rochester, MN (Midwestern Regional Climate Center 2010) and are presented (Figure 2.3a) to

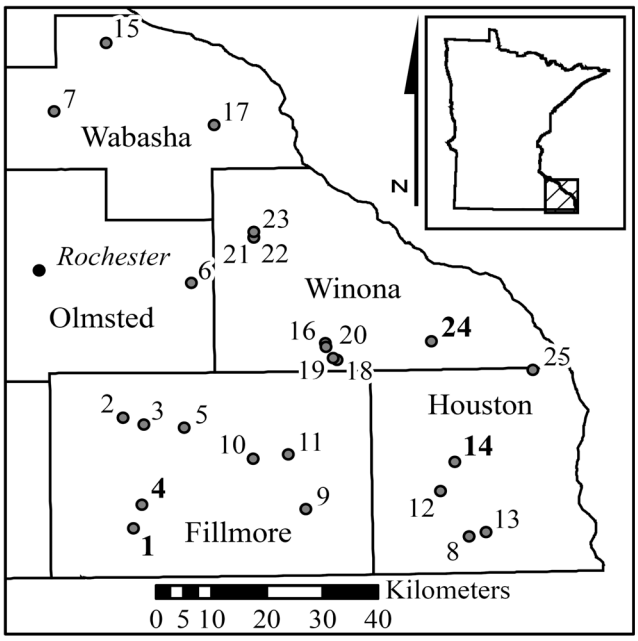

Figure 2.2. Spring and cave stream monitoring locations in southeastern Minnesota. Thermographs from the monitoring locations in bold are shown and discussed in the text. Numbers correspond to numbers in Figure 2.1 and Table 2.1. The hatched area on the inset map shows the study area with respect to Minnesota. Note: Sites 21 and 22 appear as the same location at this scale.

facilitate comparison of spring responses to surface events. Snowmelt occurred when temperatures exceeded 0°C when snow was present.

2.4. Results

The thermographs recorded in this study contain four distinct patterns, and all of our sites portray one or more of these temperature patterns (Table 2.1). However, we acknowledge there may be other patterns, particularly in other climates. Pattern 1 is an event-scale temperature fluctuation that occurs over hours or days. Pattern 2 is a seasonal fluctuation in temperature that is in phase with surface temperatures. Pattern 3 is a seasonal fluctuation in temperature that is out of phase with surface temperatures. Pattern 4 is long-term temperature stability, over time-scales of weeks to years.

Figure 2.3 shows surface temperature and precipitation at Rochester, MN and the thermographs and hydrographs (where applicable) from one cave stream and three springs. Patterns 1 and 4 are illustrated by the thermograph from the stream running through Goliath's Cave (Figure 2.3b). The data during March 2008 portrayed daily

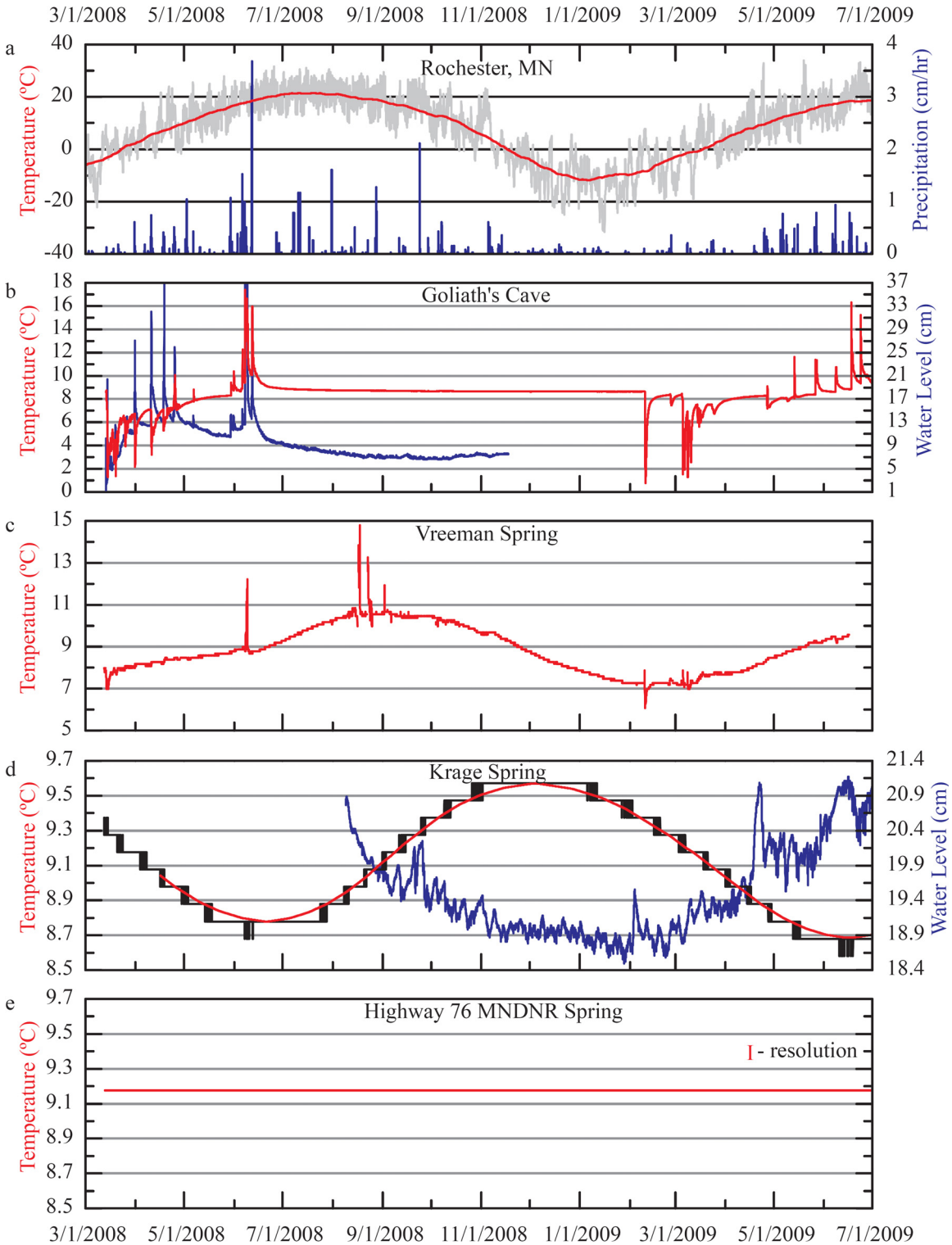

Figure 2.3. (a) Surface temperature and precipitation at Rochester, Minnesota, (b) temperature and water level of a stream running through Goliath's Cave at David's Entrance, (c) temperature of Vreeman Spring, (d) temperature and water level of Krage Spring, and (e) temperature of Highway 76 MNDNR Spring. Hourly surface

temperature data in gray in (a) were smoothed with a two-month running average shown in red. Temperature data in black in (d) were smoothed with a ten-week running average shown in red. Note the changes in temperature scales: 0°C to 18°C in (b), 5°C to 15°C in (c), and 8.5°C to 9.7°C in (d) and (e). Temperature resolution is 0.01°C in (b) and 0.1°C in (c), (d), and (e).

Table 2.1. Monitoring locations & associated thermal patterns.

Site	Name	Thermal Pattern
1	**Goliath's Cave**	**1 and 4**
2	Bat River Cave	1 and 4
3	Tyson Spring	1 and 4
4	**Vreeman Spring**	**1 and 2 or 3**
5	Big Spring at Fountain	1 and 3
6	Crow Spring	4
7	Cold Spring at Zumbro Falls	3
8	Schuldt Spring	3
9	Hvoslef WMA[a] Spring	1 and 4
10	Lanesboro SFH[b] Spring	4
11	Gribben Mill Spring	1 and 4
12	Big Spring at BCVSP[c]	3
13	Camp Winnebago Spring	1 and 4
14	**Highway 76 MNDNR[d] Spring**	**4**
15	Miller Creek Spring	3
16	Wunderlich Spring	3
17	Canfield Spring	1 and 4
18	Borson Spring	3
19	Wolfram Spring	3
20	Ehlenfeldt Spring	3
21	Crystal Springs Hatchery #1	3
22	Crystal Springs Hatchery #2	3
23	Little Green Spring East	1 and 3
24	**Krage Spring**	**3**
25	Kathan's Spring	1 and 3

Note: Bold rows indicate monitoring locations that are shown and discussed in the text.
[a]Wildlife Management Area.
[b]State Fish Hatchery.
[c]Beaver Creek Valley State Park.
[d]Minnesota Department of Natural Resources.

variability due to snowmelt (Pattern 1). During this interval, higher surface temperatures during the day caused the snow to melt. The resulting approximately 0°C runoff water produced the drops in temperature of the water flowing through Goliath's Cave. (When surface runoff is present, it drains into a sinkhole approximately 350 m northwest of the monitoring location, contributing to the flow running through Goliath's Cave.) Minimums in temperature also corresponded to maximums in water level. As the snowmelt moved quickly through the system via conduits and interacted little with the

surrounding rocks, it caused a significant decrease in temperature and a significant increase in water level. As the surface temperature dropped below freezing at night, the snow stopped melting. The supply of cold runoff water decreased and the temperature of the cave stream rose because of the greater relative contribution of the warmer stored water to the stream.

The data from Goliath's Cave following the 2008 snowmelt season also portrayed event-scale variations caused by rainfall events that produced either minimums or maximums in temperature and maximums in water level (Pattern 1). In late May, a warm, rainy period began that culminated in a 35 cm rainfall event that fell in 24 h from June 7 to 8, 2008. The pressure transducer over-ranged, and when the site was visited two days later a clear debris ring was visible in the entrance shaft 11.5 m above the bottom. The cave passage at the bottom of David's Entrance is approximately 2 m high. This system portrayed significant event-scale variability during the snowmelt and spring rain seasons. However, temperature and water level showed little to no variability after large precipitation events in the summer of 2008 (Pattern 4). (A small, gradual decrease in temperature may have been caused by thermal recovery following the large, warm rains in early June 2008.) Evapotranspiration from warm summer days and maturing nearby crops was able to remove a significant amount of water from this system. Temperature was essentially stable for more than half of the year before additional event-scale variations were observed in the 2009 snowmelt season.

The thermograph from Vreeman Spring is shown in Figure 2.3c. This spring, like Goliath's Cave, displayed a few event-scale variations (Pattern 1). Some or all of these events may have been caused by backflooding of the SBRR. There was also an annual sinusoidal temperature cycle at this spring of approximately 3.5°C (Pattern 2). Outside of event-scale variations, maximum and minimum temperatures were roughly in phase with surface temperatures and occur around early September and late February, respectively.

The thermograph at Krage Spring portrayed an annual sinusoidal temperature cycle of approximately 1°C (Figure 2.3d). However, temperatures at Krage Spring were approximately five months out of phase with surface temperatures (Pattern 3).

Furthermore, the thermograph displayed no event-scale variations. Due to the resolution of the logger at Krage Spring, the data were smoothed with a ten-week running average.

The thermograph of Highway 76 MNDNR Spring is shown in Figure 2.3e. This spring portrayed stable water temperature for more than a year of data (Pattern 4). Interaction with the soil and bedrock either warmed or cooled recharge water to a constant 9.2°C ±0.1°C by the time it reached the spring. (Nine short events were removed where ephemeral surface flow apparently affected logger temperature.)

2.5. Discussion

Pattern 1 occurs during transient recharge events when water traverses the aquifer before reaching thermal equilibrium. The water enters at a different temperature than the aquifer and quickly moves through the system, retaining some degree of the input temperature signal. This pattern results from focused run-in during snowmelt or rainfall events and is seen in the thermographs from Goliath's Cave and Vreeman Spring.

Seasonal variations can occur when recharge water retains the annual temperature signal as it flows through the aquifer. A relatively continuous supply of recharge that flows quickly through the system produces Pattern 2. This pattern typically arises in aquifers that receive a significant contribution of water from perennial sinking streams. Surface streams are directly affected by surface temperatures. If a stream sinks underground, moves through the aquifer within days, and composes a significant proportion of the water moving through the aquifer, then water temperature at the monitoring location will likely portray seasonal fluctuations that are in phase with surface temperatures. Our only possible example of this pattern to date is shown in the Vreeman Spring thermograph. After we saw this pattern at this site, we hypothesized that it was fed by a sinking stream. A dye trace was then conducted from the SBRR to Vreeman Spring. A previously unknown sinking reach of the SBRR was found.

However, water temperature at Vreeman Spring is approximately 40 days out of phase with surface temperature. Because of this phase difference, it is possible that the seasonal variation in temperature at Vreeman Spring is actually Pattern 3 (described in the following paragraphs) instead of Pattern 2. The Vreeman Spring basin is downstream

of a complex flow system with several sinks and rises. Surface water sinking into this system has a significant groundwater component. Therefore, water temperature of the sinking reach of the SBRR may also be slightly out of phase with surface temperature. Further temperature data from the sinking reach of the SBRR would be required to determine whether Vreeman Spring is displaying Pattern 2 or 3. Regardless of whether Vreeman Spring is demonstrating Pattern 2 responses, such responses are expected to be found in systems dominated by input from perennial streams.

Patterns 3 and 4 occur when recharge water moves relatively slowly through the aquifer and has time to equilibrate to the aquifer temperature. For systems displaying these patterns, the average residence time of the water is likely larger than the residence time of flow producing Patterns 1 and 2. If the rock temperature in the aquifer changes seasonally, this may produce Pattern 3, as seen at Krage Spring. Alternatively, a constant rock temperature in the aquifer produces Pattern 4. This stable pattern occurs both in systems during quiescent periods between Pattern 1 events and in systems that show no event-scale response. Specifically, the entire thermograph from Highway 76 MNDNR Spring is stable, while a portion of the thermograph from Goliath's Cave is also stable.

The thermal behavior of a karst spring is largely determined by the effectiveness of heat exchange along the flow paths in the aquifer. The effectiveness of heat exchange in a given flow path can be quantified using a Stanton number (St), analogous to the Peclet number used to quantify heat transport in porous media (Domenico and Palciauskas 1973; van der Kamp and Bachu 1989; Mongelli and Pagliarulo 1997). Peclet numbers are calculated using a characteristic velocity, characteristic length, and thermal diffusivity (as well as other potential geometrical factors, see van der Kamp and Bachu 1989), and are derived through the non-dimensionalizing of the equation for heat transport. The St for a conduit can be similarly derived by considering conservation of energy during flux of water through a differential section of pipe, giving:

$$\frac{dT_w}{dx} = \frac{4h_c}{\rho_w c_{p,w} v D_H}(T_r - T_w), \tag{2.1}$$

where T_w is the water temperature, T_r the rock temperature at the conduit wall, x the position along the length of the conduit, h_c the convective heat transfer coefficient, ρ_w the

density of water, $c_{p,w}$ the specific heat of water, v the average cross-sectional velocity of water through the conduit, and D_H the conduit hydraulic diameter (Incropera et al. 2007, Section 8.3). Non-dimensionalizing this equation using a reference temperature, T_0, and the conduit length, L, and substituting in the relation $h_c = k_w \mathrm{Nu}/D_H$, where k_w is the thermal conductivity of water, and Nu is the Nusselt number, results in a modified St:

$$\mathrm{St} = \frac{4k_w \mathrm{Nu} L}{\rho_w c_{p,w} v D_H^2}, \tag{2.2}$$

which represents the ratio of heat flux into the wall and the heat flux along the conduit. Nu is generally a function of the Reynolds and Prandtl numbers.

Two limiting cases emerge. When the St is large (St>>1), heat exchange is effective, and inflowing water will equilibrate with the rock temperature. Water flowing through such a path would be unlikely to display any event-scale pattern. Large St can be produced by small conduits, long flow paths, or slow velocities. When the St is small (St<<1), heat exchange is ineffective, and thermal signals will move through the conduit to the spring. Small St are produced by large diameter conduits or short flow paths, combined with fast flow-through times. Therefore, Patterns 1 and 2 are expected for systems where a significant portion of the flow occurs in conduits with small St, though they will only be present during conditions where recharge temperatures differ significantly from the rock temperature. Similarly, Patterns 3 and 4 indicate domination by flow paths with large St, where any fluctuations of recharge temperature are completely damped.

It is useful to place each component of the triple-permeability karst aquifer model in its relative position on the scale of St. Specifically, the largest St is found in the porous matrix component where heat transport is better expressed using a Peclet number. Fractures have an intermediate value of St, while conduits have the smallest St. Therefore, in moving from flow paths dominated by porous media toward flow paths dominated by conduits there is a shift toward smaller St and the rapid thermal responses found in Patterns 1 and 2. Observations of Patterns 1 and 2 in nature illustrate the fact that karst conduits are frequently ineffective in exchanging heat.

For cases where the heat transport between water and rock is very effective, the water exiting at a spring will be in equilibrium with the rock temperature. This can lead to the stable signal of Pattern 4. However, if the rock temperature of the aquifer is changing over a seasonal scale, then it can also lead to the out of phase seasonal signal of Pattern 3. Two primary mechanisms influence the seasonal temperature fluctuation of an aquifer: heat flux from the changing seasonal surface temperatures, and heat flux via water moving through the aquifer. In the first mechanism, a seasonal heat pulse is conducted from the surface through the rock. This pulse both decays with depth and shifts in phase (Roy and Benderitter 1986). Therefore, a seasonal sinusoidal temperature dependence at the surface would be manifested as a damped, out of phase sinusoidal signal at depth. This is precisely what is observed in Pattern 3. However, this signal decays rapidly with depth, with a skin depth, λ, given as:

$$\lambda = \sqrt{\frac{\alpha_r P}{\pi}}, \tag{2.3}$$

where α_r is the thermal diffusivity of the rock and P is the period of thermal oscillations (Carslaw and Jaeger 1959, Section 2.6, Equation 10). Adopting a thermal diffusivity for rock of roughly 1 mm^2/s and a period of 365 days results in a thermal skin depth of approximately 3 m. Thermal fluctuations at depth as the result of conduction from surface temperature fluctuations would only be expected to penetrate to a few times this skin depth, and thus could only be observed in relatively shallow aquifers.

As aforementioned, water moving through the aquifer can also have a thermal influence on the aquifer rock because of convection. Therefore, convection may increase the skin depth beyond what is possible with conduction alone. Others have developed solutions for heat transport in porous media (Suzuki 1960; Stallman 1965; Bredehoeft and Papadopulos 1965), which demonstrate the potential influence of flow on perturbing subsurface temperatures. However, in karst flow occurs rapidly and heterogeneously through fractures and conduits, allowing water out of thermal equilibrium with the rock to penetrate deep into the aquifer. This may further enhance the depth of influence of recharged surface water, but heat transport in such systems is poorly understood. Qualitatively, there is a trade-off between penetration depth and thermal exchange

between the rock and water. Flow routes that are less effective in exchanging heat will allow for deeper penetration of nonequilibrium water. However, decreasing effectiveness in heat exchange ultimately results in escape of water from the aquifer that has not transferred all of its available energy (as in Patterns 1 and 2). If the heat exchange is too ineffective, there will not be significant heating or cooling of the rock. It is likely that an intermediate area of the parameter space exists, where convective thermal exchange enhances the depth to which the aquifer can be heated and cooled with the season. Such convective heating and cooling would also result in an out of phase sinusoidal signal in the rock temperature, where the phase and damping of the signal are primarily a function of the mass of rock being heated and cooled. However, further work is needed to understand this process in detail.

An individual karst aquifer often contains both thermally effective and ineffective flow paths. The pattern observed at the spring is an integration of the response of all of the flow paths in the system weighted by the amount of flow through each path. The aforementioned discussion and observations suggest that heat exchange from mature karst conduits is often ineffective enough to allow transport of nonequilibrium water deep into or all of the way through the system. Therefore, whether one sees Patterns 1 and 2 responses or Patterns 3 and 4 responses is likely a function of the flow path between the surface and the mature conduit system. If water enters the aquifer directly into the conduit network via a localized input, then Patterns 1 and 2 behaviors are possible. Alternatively, if water is infiltrating into the conduit system via relatively distributed flow paths with large St, such as narrow aperture fractures and intergranular pores, then Patterns 3 and 4 would be expected. Our distinction between localized and distributed recharge is similar to that made by Worthington et al. (1992), which suggested that the coefficient of variation of hardness at a karst spring is an indicator of the fraction of allogenic and autogenic recharge. We prefer the terms localized and distributed, since point sources of recharge need not necessarily be allogenic, and distributed inputs need not necessarily be autogenic.

A given karst aquifer will have different distributions of recharge at different times. For example, large storms may produce significant runoff that can subsequently

enter the aquifer via localized recharge points, whereas during low flow many systems will be dominated by distributed sources of recharge. Indeed, this alternation between behaviors is seen at Goliath's Cave. A given flow path may also respond differently under different flow conditions. Increasing the flow velocity in a particular path will reduce the residence time in that path, and may allow the flow path to cross over from the thermally effective regime into the thermally ineffective regime, producing short-term temperature fluctuations at the output. The extent to which this switching effect occurs in nature is unknown.

In general, the thermal response of a karst spring is determined by the effectiveness with which the aquifer exchanges heat along its flow paths. Since karst aquifers typically contain both thermally effective and ineffective flow paths, the pattern at the spring is primarily a function of what fraction of the flow has occurred through thermally ineffective routes. Localized recharge typically drains directly into the conduit network, which is relatively thermally ineffective, whereas distributed recharge filters through more thermally effective components of the aquifer such as soil, rock matrix, and narrow aperture fractures before entering the conduit network. Thus the relative percentage of localized and distributed recharge has a strong influence on the type of thermal response.

Patterns 1 and 2 are end members on a continuum of signals produced by thermally ineffective flow paths, where the location on this continuum is controlled by recharge duration. Pattern 1 approaches Pattern 2 as a thermally ineffective flow path receives recharge for longer and longer durations. Similarly, Patterns 3 and 4 are end members on a continuum of signals produced by thermally effective flow paths. Where on this continuum a system lies is a function of the aquifer depth versus the penetration depth of seasonal surface temperature signals into the rock. As aquifer depth extends beyond the range of seasonal temperature variations, Pattern 3 signals will approach the stable signature of Pattern 4. Equipment resolution ultimately limits the degree to which you can see this transition. While Patterns 2 and 3 seem quite similar, and can be difficult to distinguish in the field, as evidenced by Vreeman Spring, they are produced by quite different mechanisms and cannot be smoothly graded into one another by

adjusting a single physical parameter. Any lag between recharge temperature and spring temperature for a system displaying Pattern 2 is directly correlated with the flow-through time of the system. On the contrary, lags seen in Pattern 3 are decoupled from flow-through times and instead are a function of the time required for surface temperature fluctuations to propagate to the aquifer depth. Recharge water may contain a significant lag if it has recently exited an upgradient aquifer that displays Pattern 3. In this case, distinguishing Patterns 2 and 3 will require time series data of recharge temperature. The flow chart portrayed in Figure 2.4 illustrates the factors responsible for producing each pattern.

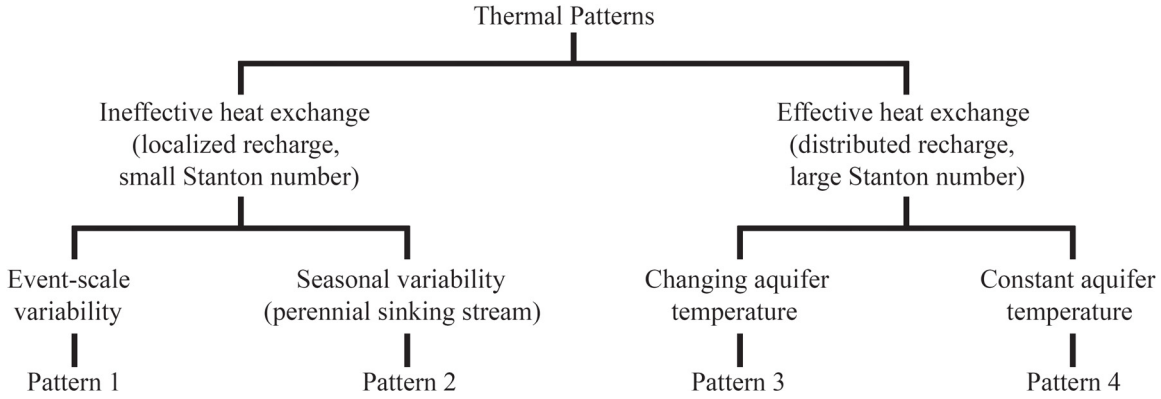

Figure 2.4. Flow chart summary of heat transport discussion.

Most of our examples of Pattern 1 and our only potential example of Pattern 2 are seen at sites in Fillmore County. There are more mapped karst features in Fillmore County than the rest of Minnesota combined (Gao et al. 2005). While mapped karst features represent only a small portion of the karst features actually present, it is probably safe to assume that there are more surface karst features in this county than any of the surrounding counties. Fillmore County contains more carbonate strata as uppermost bedrock with a relatively thin cover of unconsolidated sediment when compared to the rest of our study area in southeastern Minnesota. Numerous point inputs facilitate localized recharge and flow along thermally ineffective paths. In surrounding counties with fewer karst features recharge is more distributed. Most of our sites that portray only Pattern 3 or 4 occur in these counties. Therefore, for our example cases, the intensity of surface karstification is correlated with the type of thermal pattern seen within an aquifer.

Most of our examples of Pattern 1 and our only potential example of Pattern 2 are also seen at sites where the springs emanate from Ordovician carbonate bedrock.

Conversely, most of our sites that portray only Pattern 3 or 4 emanate from Cambrian siliciclastic bedrock. Siliciclastic matrix hydraulic conductivity may be several orders of magnitude higher than the carbonate bedrock matrix (Runkel et al. 2003). However, transport in the carbonate bedrock is dominated by conduits. Still, preferential flow paths that facilitate high groundwater flow velocities exist in all of our systems, including the sandstone aquifers (Runkel et al. 2006; Swanson et al. 2006), regardless of the type of thermal pattern seen at the spring. For example, a qualitative dye trace (Green et al. 2008) that was later repeated quantitatively (unpublished data) has shown that maximum flow velocity is on the order of hundreds of m/d in the flow systems that discharge at Borson, Ehlenfeldt, and Wolfram Springs, each of which portray thermal Pattern 3. This evidence motivates a cautionary note, that the existence of a thermally effective pattern at a spring does not imply that preferential flow paths are absent.

A given monitoring location may show multiple patterns. Flow paths may respond in different ways at different times due to the complex nature of flow systems. These different responses may produce a different thermal pattern. When the thermal pattern at a monitoring location changes, it may be impossible to identify a distinct point in time when the transition occurred. Patterns may be superimposed on each other during these times, as different flow paths become relatively active or inactive. Therefore, transitions may take place over a larger period, ultimately controlled by relative changes in different flow path contributions to the entire flow system through time.

2.6. Conclusion

Thermographs are an underutilized means for characterizing karst aquifers. Temperature probes are stable, sturdy, and economical, allowing the deployment of probes at numerous sites for a fairly low cost. We observe the following four general patterns: event-scale temperature variations (Pattern 1), seasonal variations in temperature in phase with surface temperatures (Pattern 2), seasonal variations in temperature out of phase with surface temperatures (Pattern 3), and long-term temperature stability (Pattern 4). Whether a system displays thermally ineffective patterns (1 and 2) or thermally effective patterns (3 and 4) is a function of the relative

proportions of flow occurring through thermally ineffective and effective routes, where this effectiveness can be quantified using a St. Location on the continuum of thermally ineffective patterns is controlled by recharge duration, whereas location on the continuum of thermally effective patterns is primarily controlled by aquifer depth. Therefore, thermal patterns observed at a spring carry information about the nature of heat transport through the aquifer, which depends critically on the geometries of the flow paths in the system. While more work is needed, we suggest that the types of thermal patterns observed during a given period are typically indicative of recharge mode.

Addendum: Pattern 2

After this chapter was published (Luhmann et al. 2011), additional data collection provided a great example of Pattern 2. Figure 2.5 shows nearly a year of temperature data collected at the South Branch of the Root River (SBRR) at Mystery Cave (MN23:X0143/MN23:X0144) and at Seven Springs (MN23:A0001), both in Fillmore County, MN. To further illustrate daily variability, Figure 2.6 includes the first month and a half of this record. The SBRR at Mystery Cave is a surface stream, and thus closely follows surface temperatures when groundwater inputs are minimal. Therefore, water temperature at the SBRR at Mystery Cave portrays seasonal changes in temperature that are in phase with surface temperatures, along with daily temperature fluctuations that follow the relatively warmer and cooler periods of a day. Just downstream of the monitoring location at the SBRR at Mystery Cave, the stream sinks, flows underground, and reappears at Seven Springs, with approximately 2.4 km of straight-line distance between the sinking stream and spring. Water temperature at Seven Springs is similar to water temperature at the SBRR at Mystery Cave, with some modification due to interaction with the flow path as the water moves through the aquifer and due to mixing with other water. The SBRR at Mystery Cave provides a continuous, localized recharge source that is only partially damped as it moves through the aquifer, and thus provides an excellent example of Pattern 2 at Seven Springs.

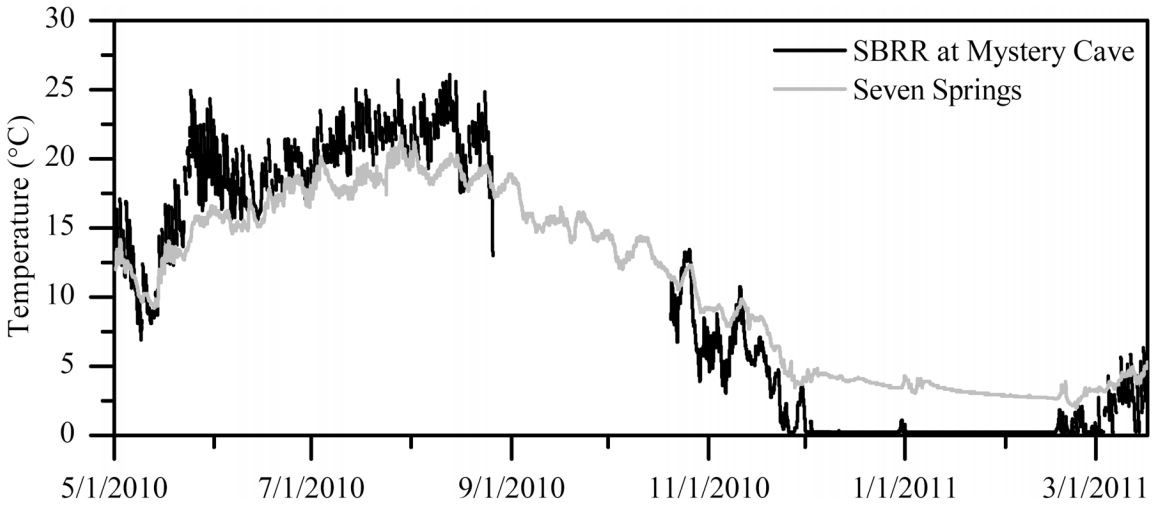

Figure 2.5. Seasonal variability in water temperature at the South Branch of the Root River (SBRR) at Mystery Cave and at Seven Springs. Note the data logger at the SBRR at Mystery Cave was not recovered on Oct. 20, 2010, leaving a nearly two-month gap in the record.

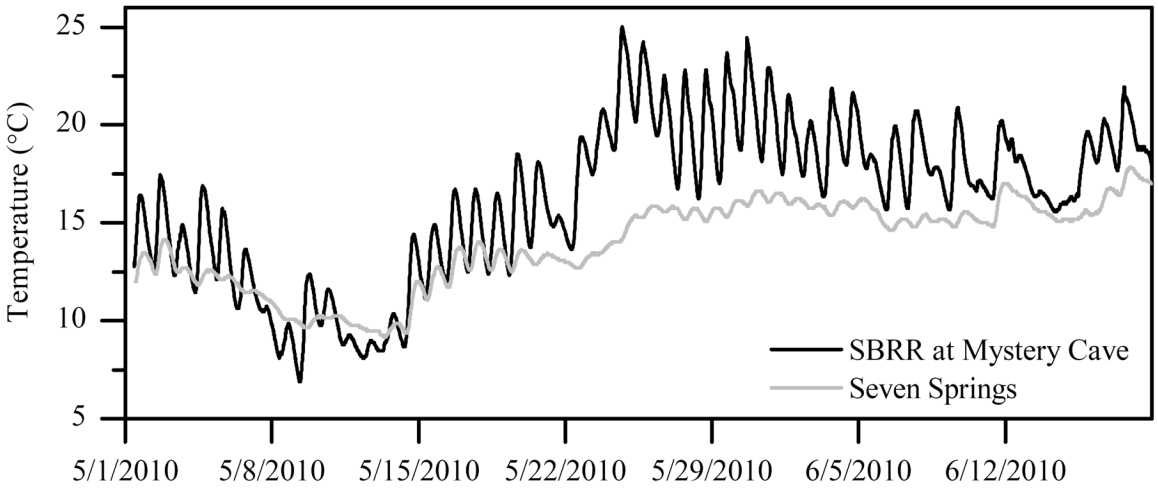

Figure 2.6. Daily variability in water temperature at the South Branch of the Root River (SBRR) at Mystery Cave and at Seven Springs.

Chapter 3

Comparing natural and artificial tracers in karst and using them to estimate flow path geometry

Summary

A controlled recharge event was conducted with multiple tracers. A pool adjacent to a sinkhole was filled with approximately 13,000 L of water. After tracers were added and thoroughly mixed, the pool was emptied into the sinkhole. Data were collected at Freiheit Spring approximately 95 m north of the sinkhole to monitor spring responses.

Flow peaked first at the spring and was followed by a suspended sediment peak; then essentially identical uranine, chloride, and δD peaks; and finally a temperature peak. The initial increase in flow at the spring recorded the time at which the water reached a submerged conduit, sending a pressure pulse to the spring at the speed of sound. The initial increase in uranine, chloride, and δD at the spring recorded the arrival of the recharge water. The initial change in temperature and its peak occurred later than the same features in the uranine, chloride, and δD breakthrough curves. As water flowed along this flow path, water temperature interacted with the aquifer, producing a lagged, damped thermal peak at the spring. The combination of hydraulic response and conservative and non-conservative tracers illustrates unique pressure, advective, and interactive processes.

Geometrical properties of the flow system may be estimated using these tracers. By summing discharge between the time of the initial increase in stage produced by a pressure pulse and the time of the chloride peak, the conduit volume is estimated as 51 m^3. Using a heat transport simulation to reproduce the modified thermal signal requires a planar flow path with a hydraulic diameter of 7 cm. These two estimates together suggest a bedding plane flow path that is 3.5 cm high by 10 m wide. The different tracers provide complementary information, and the combination of parameters provides useful constraints on flow path geometry.

3.1. Introduction

Natural and artificial tracers are often used in aquifer studies to provide basic information about a flow system. However, little has been done in terms of controlled field-scale tracer experiments to identify similarities or differences in tracer responses at a spring or to exploit complementary information that each tracer provides. Atkinson et al. (1973) conducted a multiple tracer test using malachite green dyed *Lycopodium clavatum* spores, blue polyethylene dust, lithium acetate, and pyranine. All tracers except pyranine were injected at a stream sink; the pyranine was injected more than 150 m upstream. They did not recover either the polyethylene dust or the lithium acetate. The concentration curves of the Lycopodium spores and the pyranine dye were similar, with the initial arrival of the spores occurring just before the dye. Goldscheider et al. (2003) injected sodium-napthionate and clubmoss spores of *Lycopodium clavatum* into one well and eosin and fluorescent microspheres into another well to compare soluble and particle tracers. However, they only recovered 0.81% of the sodium-napthionate and negligible amounts of the other tracers. Geyer et al. (2007) injected uranine, sulforhodamine G, and tinopal CBS-X simultaneously into a sinkhole. Uranine peaked first at the spring and was followed by sulforhodamine G and tinopal CBS-X peaks 25 and 45 min later, respectively. Geyer et al. (2007) used the different breakthrough curves of the conservative and reactive tracers to estimate reactive transport and conduit parameters. After diluting uranine and mud in 40 L of water, Goldscheider et al. (2008) sprayed the mixture on an irrigated land surface and monitored the responses in a cave 32 m below

the surface. Uranine and turbidity started to increase simultaneously approximately one h after injection, but the turbidity reached its peak and returned to background faster than uranine under nearly constant discharge. Goldscheider et al. (2008) concluded that this is potentially due to preferential transport of particles in the middle of the largest pore spaces with higher mean velocities or due to a time-dependent loss function. Smart and Hodge (1980) and Birk et al. (2004) combined tracer studies with artificial recharge. Smart and Hodge (1980) injected a Rhodamine WT solution 15 min after an artificial flood pulse was initiated to determine the vadose portion of a cave passage and to calculate conduit volume. Birk et al. (2004) used a combined tracer and recharge test to estimate conduit volume. After injecting sodium fluorescein dissolved in 100 L of demineralized water into a sinkhole, they poured two slugs of water (6.9 and 7.0 m^3) that were at a lower electrical conductivity and higher temperature than spring water at five to ten and 50-55 min later. Water level at the spring began to increase shortly after injection, indicating a phreatic conduit. A few hours later, dye began to appear at the spring 59 min before conductivity began to change. The dye peak occurred 35 min before the conductivity peak. The relatively warm water used for the trace actually produced a small decrease in temperature at the spring.

This study documents a controlled field-scale recharge experiment using multiple natural and artificial tracers that are commonly used in aquifer studies. Tracers employed with our recharge pulse include conductivity/chloride, temperature, uranine, δD, and suspended sediment. One objective of this study was to inject the tracers simultaneously into a sinkhole to facilitate comparison of spring breakthrough curves, providing further understanding for general hydrologic monitoring of these parameters. Another objective of this study was to estimate geometrical properties of conduits using two methods that make use of the different tracers. Using natural recharge events or tracer tests, several studies have estimated conduit volume by summing discharge until the arrival of event water or a tracer (e.g., Atkinson et al. 1973; Atkinson 1977b; Smart and Hodge 1980; Smart 1988; Sauter 1992; Ryan and Meiman 1996; Birk et al. 2004; Vojtechovska et al. 2010). We use this method and then present a new method that estimates the hydraulic

diameter of a flow path using a modified temperature signal caused by interaction with an aquifer. In this study, the two methods provide complementary information.

3.2. Study area

Freiheit Spring (MN23:A0041) is located in western Fillmore County in southeastern Minnesota (4,839,431 N, 554,981 E, (UTM, zone 15), shown on the Wykoff Quadrangle 7.5 min topographic map) and is shown in Figure 3.1. The spring emanates from the Ordovician Stewartville Formation of the Galena Group. The Stewartville Formation consists of limestone and dolostone (see Mossler (2008) for more detail). The Galena Group has very low to low matrix porosity and permeability, but caves and other dissolution features in the Stewartville Formation produce high bulk permeabilities (Runkel et al. 2003).

Freiheit Spring typically emanates from three distinct discharge locations at the base of a north-facing hillslope. The flow at the farthest upstream emanation point is relatively minor. A majority of the flow discharges at two downstream emanation points 1.5 m apart along a low rock face. The furthest downstream emanation is 9 m from the furthest upstream emanation. During high flow, the three emanation points are less distinct and become a relatively continuous discharge feature. The spring run flows approximately 85 m into Spring Valley Creek.

The Freiheit Spring springshed, or karst groundwater basin, is currently being delineated. To date, three dye traces have reached the spring from injection locations to the southwest (Figure 3.1a-b). Using the base-flow discharge method proposed by Quinlan and Ray (1995), springshed size is approximately 7 km^2. However, additional dye traces are necessary to further delineate the basin and refine this estimate.

3.3. Methods

A plastic swimming pool was set up next to sinkhole MN23:D2631 and filled with groundwater from a nearby well for use as a recharge source to trace the flow path from the sinkhole to Freiheit Spring. The pool was filled with approximately 13,000 L of water on 25-26 Aug. 2010 to allow the water to heat up above groundwater temperature,

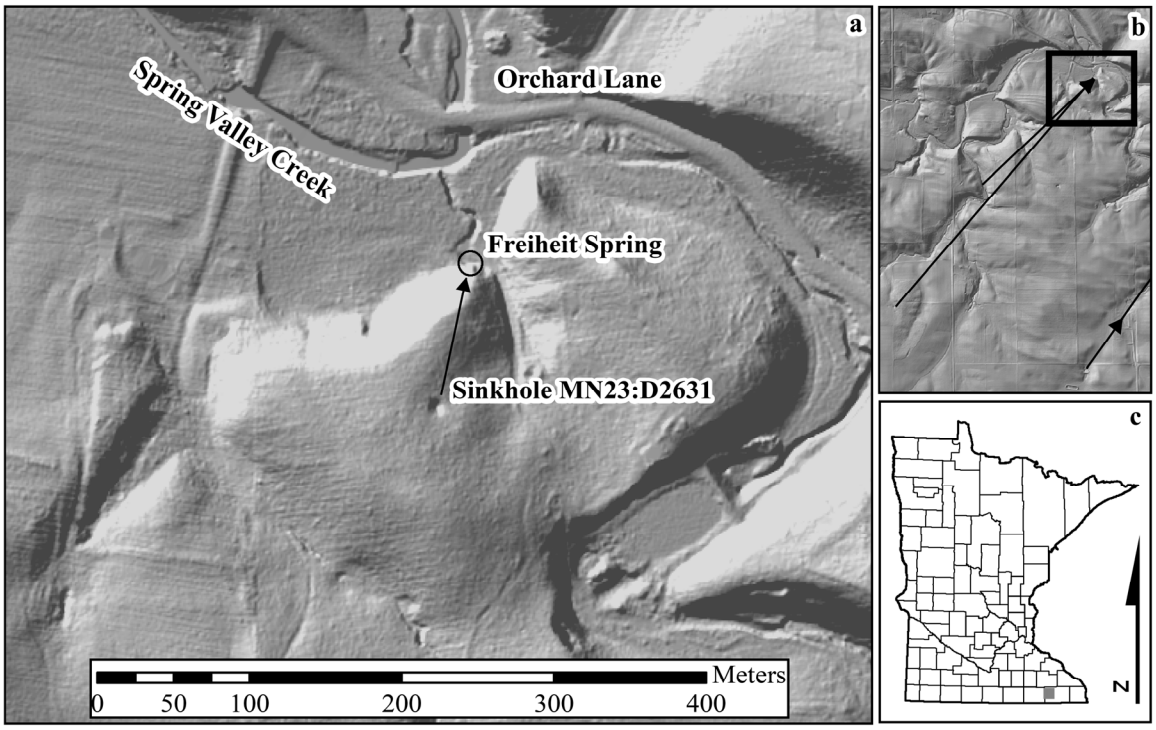

Figure 3.1. (a) Hillshade showing the study area surrounding Freiheit Spring. Water and tracers were poured into Sinkhole MN23:D2631, and data were collected at Freiheit Spring. (b) Hillshade showing a greater extent of the Freiheit Spring basin. Lines with arrows show two additional dye traces to Freiheit Spring and the beginning of another dye trace to Mahood Spring northeast of Freiheit. The black square outline shows the location of (a). (c) The location of (a) within Minnesota is found within the gray square. Hillshades in (a) and (b) were created using LiDAR data with an azimuth of 315° (i.e., light source from the northwest) and an altitude of 45°.

which averages approximately 9°C. On 30 Aug. 2010, the water was further heated using two propane burners, each with a 55 L washtub. After water in each tub was heated, it was exchanged with cooler water from the pool. This process was repeated for 5 h. At the same time, 32.91 kg of salt were added to the water to increase conductivity/chloride concentration in the pool. 200.82 g of deuterium oxide and 14.660 g of a 35 wt % uranine solution were later added to the pool. Samples were collected in 1 L HDPE Nalgene bottles both before and after tracers were added to the pool. The pool was released into the sinkhole in three min and thirty-four s, beginning at 16:01 on 30 Aug. 2010. Water initially ponded in the sinkhole, but completely drained as the last of the pool was emptied.

Two Campbell Scientific CR10 data loggers monitored and recorded spring response for this trace. A Campbell Scientific conductivity/temperature probe (247 or CS547A with A547 Interface) and a Druck PDCR 1230 pressure transducer were connected to each logger to continuously monitor electrical conductivity, temperature, and water level. Conductivity resolution is 0.001 mS cm^{-1}, and conductivity accuracy is ±5% between 0.44 and 7.0 mS cm^{-1}. Temperature resolution is 0.01°C, and temperature accuracy is ±0.4°C over the range of -24°C to 48°C. The first logger monitored temperature and conductivity at the farthest downstream emanation point and has been in place for the past two years. The pressure transducer is approximately 10 m downstream of the furthest downstream emanation point. A 120° v-notch weir is approximately 20 m downstream of the furthest downstream emanation point and enables the conversion from stage to total discharge for all three emanation points. Salt dilution stream flow measurements were also performed on the day of and the days surrounding the pool trace to calibrate and confirm weir measurements. Both the pressure transducer and the temperature/conductivity probe from the second logger were placed in the intermediate emanation point. For the first approximately 100 min, data were recorded every s. At the end of the breakthrough curve tails, data were recorded with one and then ten min output intervals.

Direct water samples were collected in 30 ml clear borosilicate glass vials from the intermediate emanation point every 30 s until 16:38. Water samples were then collected every min until 17:02, every two min until 18:00, and every ten min until 19:00. Two automated ISCO samplers continued to collect samples from this emanation every 20 min until 11:00 on 31 Aug. 2010 and then every 90 min until 15:30 on 2 Sept. 2010.

Direct water samples were analyzed on a Shimadzu RF5000U scanning spectrofluorophotometer. All samples were scanned synchronously at 5nm bandwidths and 15 nm $\Delta\lambda$. Spectral components were then fitted using PeakFit™ (Version 4.04) nonlinear curve-fitting software to provide uranine peak characteristics for each sample. Standards were prepared to determine uranine concentration. Sediment was filtered from the water samples onto a 1 μm glass fiber filter and dried overnight in an oven at 104°C as per Standard Method 2540D from the American Public Health Association, American

Water Works Association, Water Environment Federation. The mass of sediment and water was used to calculate suspended sediment concentration. Selected samples were analyzed for anions using anion chromatography following EPA method 300.1. These samples were also analyzed for stable isotopes of hydrogen and oxygen using a Model 908-0008, Los Gatos Research, Liquid Water Stable Isotope Analyzer that uses Off-Axis Integrated Cavity Output Spectroscopy (OA-ICOS) laser technology at the Schwartz Isotope Lab in the Department of Biology at Texas State University in San Marcos. All δD values are relative to VSMOW standard, and all reported errors are 1 σ.

3.4. Results

Figure 3.2 portrays the tracer breakthrough curves at the spring, and Table 3.1 summarizes the initial change and peak times as well as background and peak values for each of the tracers. Table 3.1 also includes volume and tracer concentrations of the pool water. A chloride-conductivity relationship (R^2 = 0.99993) was determined using samples from the trace analyzed for anions, and this relationship was used to determine chloride concentration through time (Figure 3.2d).

Dye recovery was determined by integrating the product of the uranine breakthrough curve and discharge through time and then dividing by the amount of uranine used in the trace. Approximately 9.7 grams of the 35 wt % uranine solution were recovered by 18:00 on the day of the trace, giving a dye recovery of 66% at this time (Figure 3.2c). Chloride recovery was determined by subtracting the background chloride concentration from the entire chloride time series and then integrating the product of this resultant chloride time series and discharge through time. Because samples were not analyzed for cations, sodium recovery was attained by multiplying the chloride recovery by the atomic mass ratio of sodium to chloride. Finally, salt recovery was determined by summing sodium and chloride recovery and then dividing by the amount of salt used in the trace. We recovered approximately 25.7 kg of salt by 18:00, giving 78% recovery (Figure 3.2d). Subtracting the background temperature from the entire temperature time series gives the thermal signal from this trace. Heat recovery was determined by integrating the product of this resultant temperature time series, discharge through time,

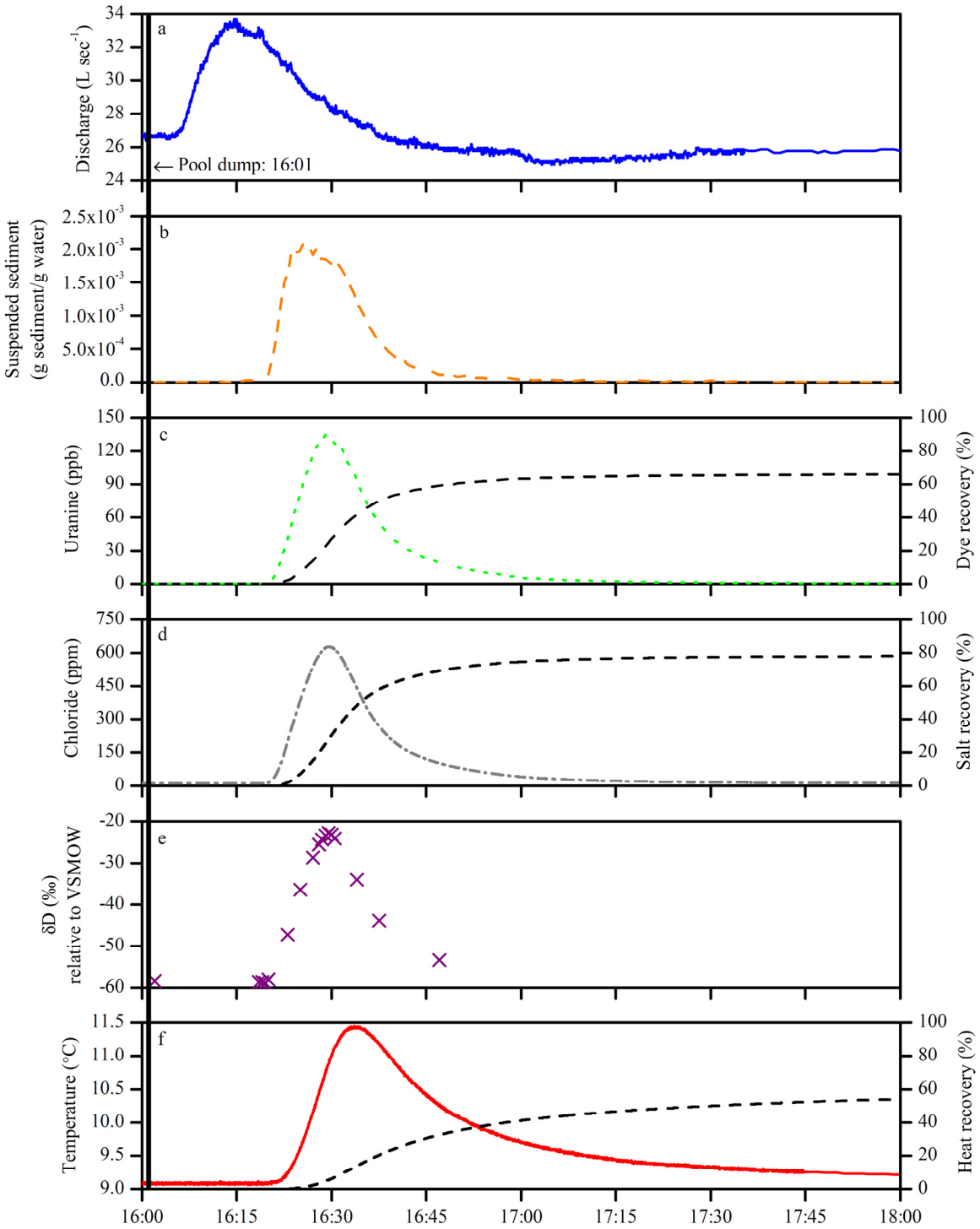

Figure 3.2. (a) Discharge, (b) suspended sediment, (c) uranine, (d) chloride, (e) δD, and (f) temperature breakthrough curves at Freiheit Spring on 30 Aug. 2010. (c) Dye, (d) salt, and (f) heat recovery curves are shown with black dashed lines.

and water's heat capacity, and then dividing by the thermal energy of the pool water. The thermal energy of the pool water is the product of the temperature difference between the

Table 3.1. Trace summary.

Tracer	Initial change	Peak time	Peak	Background
Shown in Figure 3.2				
Discharge[a]	16:05:22	16:14:40	33.7 L s^{-1}	26.7 L s^{-1}
Suspended sediment[b]	16:14:30	16:25:30	2.09 x 10^{-3} g sed./g water	0 g sed./g water
Uranine[b]	16:19:00	16:29:00	135.2 ppb	0 ppb
Chloride[b]	16:19:02	16:29:27	628.6 ppm	11.8 ppm
δD[b]	16:20:00	16:29:30	-22.8 ± 0.3 ‰	-58.6 ± 0.3 ‰
Temperature[b]	16:20:05	16:33:35	11.45°C	9.08°C
Not shown in Figure 3.2				
Stage[b]	16:04:15	16:09:58	17.1 cm	16.1 cm
Conductivity[c]	16:19:51	16:30:46	2.416 mS cm^{-1}	0.704 mS cm^{-1}
Temperature[c]	16:20:43	16:34:11	11.33°C	9.08°C

Pool: 13,065 ± 2% L of water, uranine = 369 ppb, chloride = 1529 ppm, temp = 24.1°C, and δD = +29.8 ± 0.3 ‰

Pool dump: 16:01

[a]Data from downstream of emanation points.

[b]Data from intermediate emanation.

[c]Data from downstream emanation.

pool water and background spring water, the water volume in the pool, and water's heat capacity. The pool's water volume was determined using salt (which is described in Section 3.5). 54% of the pool's thermal energy was recovered by 18:00 (Figure 3.3f).

3.5. Discussion

As mentioned earlier, 78% of the salt was recovered at the spring during the first two hours, 12% higher than uranine recovery. Calculating the pool's water volume using these tracers provides insight into this discrepancy. Pool volume may be calculated by dividing tracer mass by tracer concentration in the pool due to our tracer addition to the water. Salt concentration was attained by the summation of the chloride concentration less background and sodium concentration (i.e., the product of chloride concentration less background and the atomic mass ratio of sodium to chloride). The pool water volume calculated using the salt concentration is 13,065 ± 2% liters. A similar calculation with uranine concentration gives 13,892 ± 2% liters. Uranine is known to degrade in light (e.g., Käss 1998). The uranine was added approximately 30-60 minutes before the pool was emptied to facilitate complete mixing. After mixing, two pool water samples were

collected 16 minutes before the pool was emptied. The samples were put in a cooler and kept in the dark until they were analyzed 10 days later. If some of the uranine was degraded, then the calculated pool water volume would be overestimated. Consequently, salt concentration provides a better estimate of pool water volume.

Dividing uranine mass by the water volume estimate using salt concentration gives the uranine concentration that would have been expected if there were no degradation. Comparing this to actual concentration shows that the uranine degraded by 6% by the time the samples were analyzed. With this loss accounted for, the 66% (of 94%) uranine recovery at 18:00 becomes 70% uranine recovery. The remaining difference between the salt and uranine recoveries is not caused by preferential storage within the aquifer because uranine is conservative in karst aquifers (Käss 1998; Benischke et al. 2007). Perhaps the remaining discrepancy is due to the additional degradation from light that occurred after the samples were collected at the spring but before they were put in the dark a couple hours later. Other possible explanations for this discrepancy include either non-light degradation that may have occurred during the ten days before the samples were analyzed or light exposure during sample preparation and analysis. If any of these are true, then only 85% (i.e., 66% uranine recovery / 78% salt recovery) of the 14.660 g of the 35 wt % uranine solution poured into the pool was available for this trace by the time the samples were analyzed, or approximately 12 grams. We did not anticipate this degradation of uranine. The pool was surrounded by trees and mostly shaded, and spring samples were never exposed to direct sunlight. However, it seems likely that 78% of the non-degraded uranine had also been recovered by 18:00.

A negligible amount of salt (0.1%) was recovered from 18:00 to 18:37 (when conductivity returned to its background level). After 18:00, an additional 3% of uranine was recovered over the following three days, although this is a minimum due to uranine degradation before samples were analyzed. However, it is easier to determine uranine recovery at this point of the breakthrough curve because other factors may influence conductivity measurements and because uranine was absent from the flow path before the trace began. Furthermore, uranine's detection limit is much lower than the resolution on

the conductivity probe. Still, it is likely that a proportional amount of salt was also recovered over the following three days, giving a minimum total of 81% recovery for both tracers.

There are several potential explanations for why this trace did not produce 100% recovery. The first is the uranine degradation that has already been discussed. Furthermore, uranine was still reaching the spring when the sampling was terminated, although in very low concentrations that would have produced minimal additional recovery. Another explanation is the error associated with all of the measurements and lab analysis, including approximately ±10% error in discharge measurements. Additionally, some of the tracers may have been temporarily stored within the soil at the sinkhole or along the flow path. Finally, some of the tracers may have traveled along a different route to an undetected spring or seep into Spring Valley Creek. Our large slug of water likely activated one or more previously inactive flow paths. Still, this trace confirms that a majority of recharge sinking into this sinkhole will reach Freiheit Spring.

Whereas dye and salt recoveries were leveling off by 18:00, the thermal recovery continued to climb until temperature returned to background at 10:30 the following morning, yielding 69% recovery.

Normalization of the data permits a comparison of breakthrough curves for each of the different tracers. We use two different normalization techniques. The first involves dividing the difference between each data point and background value by the difference between peak and background values (Figure 3.3a). This technique illustrates the shape and timing of the different breakthrough curves. The second normalization method involves dividing each data point of a given time series less background by the total area of the breakthrough curve less background (Figure 3.3b). While this method also portrays the shape and timing of the different breakthrough curves, it also provides additional mathematical insight. The area under each area-normalized breakthrough curve is equal (i.e., 1), and therefore this method allows a quantitative comparison of the different breakthrough curves, where the values of all the area-normalized curves represent the fraction of total tracer emerging as a function of time.

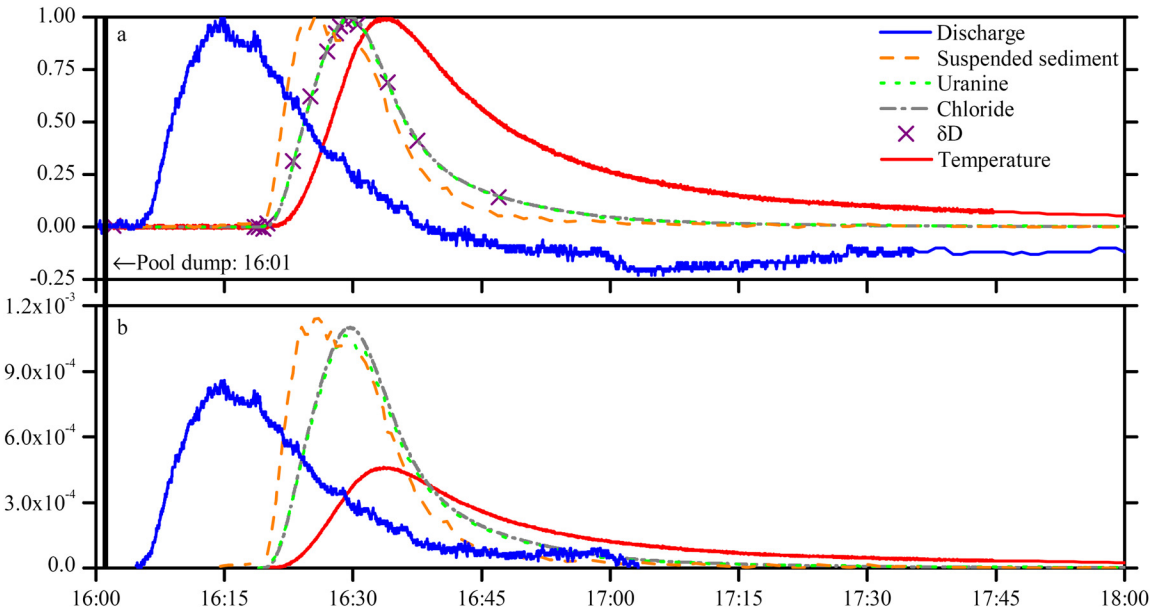

Figure 3.3. Normalized breakthrough curves setting either the (a) peaks or (b) areas of the breakthrough curves equal to one.

Either normalization technique clearly illustrates that discharge began to increase and even reached its peak before significant changes in the other parameters at the spring (Figure 3.3). While it takes a finite time for flood or event water to physically move through an aquifer, an increase in discharge at a spring may occur almost instantaneously. In a fully submerged conduit, a pressure pulse propagates at a velocity on the order of the speed of sound in open water (approximately 1500 m s^{-1}), and momentum effects have been shown to produce negligible delays (Covington et al. 2009). We started emptying the pool at 16:01, and the level at the intermediate emanation began to increase at 16:04:15. This time difference likely records the time required for the water to move down from the sinkhole to a fully submerged conduit, sending a pressure pulse on its arrival. A portion of this interval may include the time that the water flowed in an open channel, where flood waves propagate at roughly 1.5 times the water velocity (Chanson 2004, Equation 17.28). Given the time difference between the initial increase in discharge and the other parameters at the spring, however, it seems likely that the flow path is mostly submerged. At the later stages of the hydrograph recession, discharge dropped below the background value (Figure 3.3a). We do not fully understand this process, but the same general feature was reproduced during a similar trace three days later. It may be the result of momentum or siphoning effects or hysteresis associated with

the transition of some portion of the conduit from full pipe flow to open channel flow (Raeisi et al. 2007).

Peak normalization illustrates that transport mechanisms for uranine, chloride, and δD are similar, as the three breakthrough curves are essentially identical (Figure 3.3a). These breakthrough curves are largely dependent on advection along the flow path, producing conservative tracer responses. The curves indicate event water and record contributions from the pool. In the area-normalized plot (Figure 3.3b), the uranine curve around the peak is a little lower than the chloride curve because the uranine curve has a longer tail due to uranine's low detection limit. δD was not included in the area-normalized plot (Figure 3.3b) because the breakthrough curve is defined by only 19 data points.

Suspended sediment began to appear after changes in discharge, but before changes in uranine, chloride, and δD (Figure 3.3). We did not anticipate including suspended sediment in the study. All samples were analyzed for suspended sediment after they were analyzed for uranine. Suspended sediment analyses were also conducted after select samples were analyzed for anions and δD. Furthermore, samples were split into three discontinuous groups due to additional ongoing analyses and run on different days. This ad hoc analysis introduces additional uncertainty. Still, minor amounts of sediment were picked up and transported from within the flow path before the event water arrived. The arrival of sediment before event water has been documented by Hallberg et al. (1984); they concluded that large discharges were able to remove stored sediment from within conduits. However, the bulk of sediment that reached Freiheit Spring was likely from the sinkhole, washed down into the flow path when the pool was emptied, since significant increases in sediment did not occur until the arrival of event water. The rising limb of the suspended sediment breakthrough curve is likely steeper than the rising limb of the uranine, chloride, and δD breakthrough curves because of the discharge variation. If the flow path's cross-sectional area (A) remained relatively constant during the trace, then the decrease in discharge (Q) during most of the suspended sediment breakthrough curve was produced by a decreasing flow velocity (v) since $Q = v\,A$. A lower flow velocity moves less sediment, so the steep rising limb and

early peak of the suspended sediment breakthrough curve is likely an artifact of increasing deposition within the flow path through time. Alternatively, this may be due to the aforementioned preferential transport of sediment along flow lines with higher mean velocities (Goldscheider et al. 2008).

Finally, the initial change and peak in temperature occurred later than the initial changes and peaks for all other parameters (Figure 3.3). Other researchers have observed temperature peaks later than conductivity peaks in gypsum karst (Bundschuh 1997; Birk 2002). Bundschuh's (1997) explanation is that dilute recharge water approaches saturation quickly because of the rate at which gypsum is dissolved. However, conductivity/chloride in the present study is essentially conservative. In contrast, temperature interacted significantly with the aquifer. As the pool water moved along the flow path, some of the heat was lost into the surrounding rock (Molson et al. 2007). This produces an apparent velocity from the thermal pulse that is less than the actual groundwater velocity because of a thermal retardation factor (Palmer et al. 1992). Due to the interactive nature of temperature, the area-normalized temperature peak is much lower than the peaks of the conservative tracers (Figure 3.3b). However, the heated rock surrounding the conduit was able to heat subsequent water moving along the flow path, thus shifting much of the breakthrough curve into an elongated tail that extended beyond the tails of the conservative tracers. Temperature remained higher than its pre-dump value long after chloride reached its pre-dump level, indicating the end of the pool water.

Not only did the temperature peak lag behind the chloride peak, but it was also damped. To illustrate, we determine the volume of pool water (V_P) that discharged at the spring for each time step:

$$V_P = \frac{(C_S - C_B)}{\int (C_S - C_B)dt} V_T R_S \,, \tag{3.1}$$

where C_S is spring chloride concentration, C_B is background spring chloride concentration, V_T is total pool volume, and R_S is total salt recovery expressed as a decimal. We use chloride in this calculation because of its conservative behavior in this trace and because we have one s resolution data from the conductivity-chloride calibration.

Conservative spring temperature (T_C) for each time step is then given by a simple mixing relationship:

$$T_C = \frac{V_P}{Q} T_P + \frac{(Q - V_P)}{Q} T_B, \tag{3.2}$$

where T_P is pool water temperature, Q is spring discharge, and T_B is background spring temperature. If temperature had behaved conservatively, then the peak temperature would have been 15.06°C. Actual peak temperature at the spring was 11.45°C, only 40% of the change from background (9.08°C) to the conservative value, T_C. Therefore, water temperature interacted with the soil and rock along the flow path, producing a lagged, damped signal.

3.6. Estimating Flow Path Geometry

3.6.1. Method 1: Summing discharge

Conduit volume for fully submerged conduits may be estimated using the lag between hydraulic and chemical or thermal responses. This method was first suggested by Ashton (1966) and has been used by other researchers (Atkinson 1977b; Sauter 1992; Ryan and Meiman 1996; Birk et al. 2004). The technique generally uses flood pulses from recharge events as tracers. As mentioned in Section 3.5, spring discharge may increase almost instantaneously because of a pressure pulse in a fully submerged conduit. In this situation, conduit volume may be estimated by totaling the spring's discharge between the initial increase in flow and the initial increase in other physical or chemical parameters. The latter indicates the arrival of the actual flood water.

Conduit volume may also be estimated by summing discharge through time between injection and detection of a tracer. Detection time has been defined as initial arrival time, peak time (Atkinson et al. 1973), or mean tracer time (Smart 1988; Field and Nash 1997; Goldscheider et al. 2008). Birk et al. (2004) calculated conduit volume using all three time definitions. Vojtechovska et al. (2010) compared conduit volumes calculated using various detection time definitions and found that volumes calculated using mean transit time provided the most accurate results. Our tracer injection was not instantaneous; it took three min and thirty-four s. Furthermore, the tracers were injected

into a dry sinkhole where they flowed down a dry infeeder before reaching water in the main conduit. This further spread out our injection. Therefore, our breakthrough curve is skewed towards the tail, which would likely cause conduit volume determined by mean transit time to be overestimated. Therefore, we use peak time. Furthermore, we use the chloride peak because of its conservative behavior in this trace.

51 m^3 of water were discharged from Freiheit Spring between the initial increase in stage and the peak in chloride. Dividing by the 95 m distance from the sinkhole to the spring gives a conduit cross-sectional area of 0.54 m^2. This corresponds to a diameter of 0.83 m in a circular conduit. Flow path distance is often about 1.5 times longer than straight-line distance (Field and Nash 1997). Accounting for this sinuosity correction, the conduit cross-sectional area and diameter are 0.36 m^2 and 0.68 m, respectively. If there is a significant infeeder between the spring and the point where the injection intersected the main conduit, then this cross-sectional area would be an overestimate. Therefore, these estimates are an upper bound of the actual conduit volume, cross-sectional area, and diameter.

3.6.2. Method 2: Modeling thermal pulse

Conduit diameter may also be estimated using the thermal pulse that was modified by the flow path. Heat transport along a 1D flow path is given by the heat advection-dispersion equation:

$$\frac{\partial T_w}{\partial t} = D_L \frac{\partial^2 T_w}{\partial x^2} - v\frac{\partial T_w}{\partial x} + \frac{4h_c}{\rho_w c_{p,w} D_H}(T_s - T_w), \tag{3.3}$$

where T_w is the water temperature, D_L the longitudinal dispersivity, x the flow path position, v the water velocity, h_c the heat transfer coefficient, ρ_w the density of water, $c_{p,w}$ the specific heat of water, D_H the hydraulic diameter of the flow path, and T_s the conduit wall surface temperature. The terms on the right side of Equation (3.3) track heat dispersion, heat advection, and heat exchange with the surrounding rock. The heat transfer coefficient is given by

$$h_c = \frac{k_w \mathrm{Nu}}{D_H}, \tag{3.4}$$

where k_w is the thermal conductivity of water and Nu the Nusselt number, which is the ratio of convection to pure conduction heat transfer through the convective boundary layer in the water. The Nu for turbulent flow is given by the empirically-derived Gnielinski correlation (Incropera et al. 2007, Equation 8.62),

$$\mathrm{Nu} = \frac{(f/8)(\mathrm{Re}-1000)\,\mathrm{Pr}}{1+12.7\sqrt{f/8}\,(\mathrm{Pr}^{2/3}-1)}, \tag{3.5}$$

where f is the Darcy-Weisbach friction factor, $\mathrm{Re} = \rho_w\, v\, D_H\, \mu_w^{-1}$ the Reynolds number, and $\mathrm{Pr} = c_{p,w}\mu_w\, k_w^{-1}$ the Prandtl number of water. μ_w is the dynamic viscosity of water.

Heat exchange in karst conduits is strongly controlled by conduction through the rock surrounding the conduit (Covington et al. in review, 2011). 2D heat conduction in cylindrical coordinates with no energy generation is given by

$$\rho_r c_{p,r} \frac{\partial T_r}{\partial t} = \frac{1}{r}\frac{\partial}{\partial r}\left(k_r r \frac{\partial T_r}{\partial r}\right) + \frac{\partial}{\partial x}\left(k_r \frac{\partial T_r}{\partial x}\right), \tag{3.6}$$

where ρ_r is the density of rock, $c_{p,r}$ the specific heat of rock, T_r the rock temperature, and k_r the thermal conductivity of rock. The corresponding equation in planar coordinates is given by

$$\rho_r c_{p,r} \frac{\partial T_r}{\partial t} = \frac{\partial}{\partial y}\left(k_r \frac{\partial T_r}{\partial y}\right) + \frac{\partial}{\partial x}\left(k_r \frac{\partial T_r}{\partial x}\right). \tag{3.7}$$

Boundary conditions include:

$$\frac{\partial T_r}{\partial r} \to 0 \text{ as } r \to \infty, \tag{3.8}$$

and

$$k_r \frac{\partial T_r}{\partial r}\left(\text{at conduit wall}\right) = h_c\left(T_s - T_w\right). \tag{3.9}$$

In planar coordinates, r is replaced by y in these boundary conditions.

Conservative solute transport along a 1D flow path is given with a similar advection-dispersion equation:

$$\frac{\partial C}{\partial t} = D_L \frac{\partial^2 C}{\partial x^2} - v\frac{\partial C}{\partial x}, \tag{3.10}$$

where C is chloride concentration.

The advection-dispersion and conduction equations were solved numerically using the finite element package COMSOL Multiphysics® (Version 3.5). For each simulation, one of the heat conduction equations was solved using the Conduction Heat Transfer application mode, and the advection-dispersion equations were solved using the Coefficient Form PDE mode. The values used for the parameters in the simulations are given in Table 3.2. Values for rock variables are for the Salem Limestone (Incropera et al. 2007).

Table 3.2. Values used for variables in simulations.

Parameter	Value	Units
ρ_w	1000	kg m^{-3}
$c_{p,w}$	4200	J kg^{-1} K^{-1}
k_w	0.58	W m^{-1} K^{-1}
μ_w	1.3×10^{-3}	kg s^{-1} m^{-1}
ρ_r	2320	kg m^{-3}
$c_{p,r}$	810	J kg^{-1} K^{-1}
k_r	2.15	W m^{-1} K^{-1}
D_L	0.01	m^2 s^{-1}
f	0.05	-
Pr	9.5	-

One complication in this particular study is that the water flowed through a dry infeeder before reaching the main submerged flow path. Consequently, upon reaching the main flow path, the water had already lost some of its thermal signal. To account for this heat loss, our model consists of two flow paths: the infeeder and the submerged flow path (see Figure 3.4). Equations (3.3) and (3.10) were solved along two 1D lines in COMSOL to represent the infeeder and main passage. Equation (3.6) or (3.7) was solved throughout two 2D rectangles in COMSOL to simulate conduction into the rock surrounding the infeeder and main passage. Conduction was modeled in cylindrical or planar coordinates to represent a circular conduit or a bedding plane parting, respectively. For each flow path, the 1D line and one edge of the 2D rectangle were coupled using the Extrusion Coupling Variables feature in COMSOL. To again account for sinuosity (Field and Nash 1997), the entire lengths of the infeeder and the main flow path were set to 1.5 times the vertical and horizontal distances, respectively, between the sinkhole and the spring, which represent rough approximations of the expected geometry.

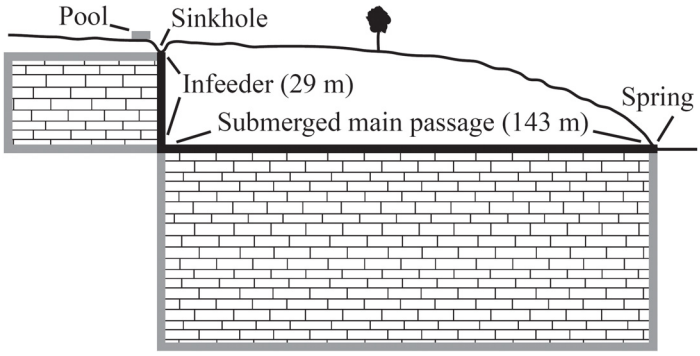

Figure 3.4. Cross-sectional schematic of field site. The thick black "infeeder" line and the adjacent limestone rectangle represent the infeeder portion of the simulation. The thick black "submerged main passage" line and the adjacent limestone rectangle represent the main passage portion of the simulation. Gray limestone boundaries perpendicular to the infeeder and main passage are insulated rock boundaries. Gray limestone boundaries parallel to the infeeder and main passage are sufficiently far from flow path lines to satisfy Equation (3.8) and were set to background temperature.

In COMSOL, the 1D conduit or bedding plane line and the rock at the conduit or bedding plane wall were discretized into 1000 finite elements along both the infeeder and the main flow path for all simulations. Mesh resolution gradually coarsens in each 2D rectangle rock away from the flow path wall, but each 2D rectangle was generally discretized into 20,000 elements. COMSOL uses an implicit method when solving and user-defined relative and absolute tolerances that are compared to the estimated error to modify timesteps (COMSOL 2008). Relative and absolute tolerances for the infeeder portion of the simulations were set to 10^{-5} and 10^{-6}, respectively. Relative and absolute tolerances for the main flow path portion of the simulations were set to 10^{-4} and 10^{-5}, respectively.

To determine instantaneous velocity, $v(t)$, we use the equation

$$v = \frac{Q v_{ref}}{Q_{ref}}, \tag{3.11}$$

where v_{ref} is a reference velocity and Q_{ref} a reference discharge. This equation is valid so long as cross-sectional area of the flow path is constant through time. Because of the pipe flow conditions required to transmit the pressure pulse, the flow path's cross-sectional area was likely constant over much of its length. The infeeder's v_{ref} is defined as 1.5 times the vertical distance between the sinkhole and the spring, divided by the time

difference from the beginning of the pool dump to the initial increase in stage at the spring. The main passage's v_{ref} is defined as 1.5 times the horizontal distance from the sinkhole to the spring, divided by the time difference from the initial increase in stage to the initial increase in chloride at the spring. The main passage's Q_{ref} is defined as spring discharge at the initial increase in stage at the spring. The exact second of the beginning of the pool dump is unknown, although it began sometime between 16:01:00 and 16:01:59. With this uncertainty, the main passage's v_{ref} falls within the range of potential v_{ref}s for the infeeder. Because of this overlap, the $v(t)$ time series determined by Equation (3.11) for the main passage was also used for the infeeder, until discharge reached a minimum, likely indicating when all of the pool water had passed through the infeeder. Infeeder velocity was set to 0 m s^{-1} after the discharge minimum. However, this indirect $v(t)$ time series for the infeeder was moved back in time to account for the time difference between the start of the pool dump and the initial increase in spring stage.

Pool temperature and pool chloride concentration were used as input into the dry infeeder (Table 3.1). The infeeder output was then mixed with non-pool groundwater (i.e., background spring water) at the intersection of the infeeder and main conduit. To determine the fraction of pool water as a function of time at the junction, we first calculated the pool water fraction at the spring using chloride concentration, and then shifted the fraction back in time by the flow-through time $\tau_{ft}(t)$ of the main conduit. Since velocity varied over time during the trace, the $\tau_{ft}(t)$ also varied over time, with

$$L = \int_{t-\tau_{ft}(t)}^{t} v(t')dt' . \tag{3.12}$$

Since this equation cannot be explicitly solved for $\tau_{ft}(t)$, in practice $\tau_{ft}(t)$ was determined by summing $v(t)dt$ backwards over time until reaching the conduit length L (again, 1.5 times the horizontal distance from the sinkhole to the spring for the sinuosity correction) at a time that corresponds to $\tau_{ft}(t)$. Non-pool groundwater attributes were defined as background spring temperature and background spring chloride concentration (Table 3.1).

The Nash-Sutcliffe efficiency, E_j, may be used to quantify simulation results and is given by

$$E_j = 1 - \frac{\sum_{i=1}^{N} \left| O_i - P_i \right|^j}{\sum_{i=1}^{N} \left| O_i - \bar{O} \right|^j}, \tag{3.13}$$

where O_i, P_i, and $\bar{O}$ are observed, predicted, and average observed values, respectively, and j is a positive integer. E_j ranges from 1.0 (perfect fit) to -∞. A positive E_j indicates that model predictions are better than the mean value of the observed time series, and a negative E_j indicates that the mean value of the observed time series is better than model predictions. Nash and Sutcliffe (1970) initially defined E_j with $j = 2$. However, Legates and McCabe (1999) and Krause et al. (2005) have noted that E_j is too dependent on extreme values when differences are squared (i.e., $j = 2$). Therefore, we use E_1.

Simulation results are shown in Figure 3.5. If the infeeder and main passage are modeled with the same D_H, the best cylindrical solution occurs with a D_H of 8 cm (Figure 3.5a). However, the infeeder is likely smaller than the main conduit. If the infeeder's D_H is set to one half of the previous solution (i.e., 4 cm), then the best cylindrical solution occurs with a D_H of 9 cm for the main passage (Figure 3.5b). Both of these values for the main passage are significantly less than the value derived from Method 1 if a conduit with a circular cross-section is assumed. However, the water at the spring discharges from a bedding plane parting, suggesting that a wide rectangular cross section may be a more appropriate assumption than circular. If the infeeder and main passage are modeled with the same D_H, the best planar solution occurs with a D_H of 6 cm (Figure 3.5c). For wide conduits, $D_H = 2h$, where h is the height of the conduit. This would suggest a conduit height of 3 cm, and, if combined with the cross-sectional area estimate using Method 1, a conduit width of 12 m. If the infeeder's D_H is set to one half of the initial planar solution (i.e., 3 cm), then the best planar solution occurs with a D_H of 7 cm for the main passage (Figure 3.5d). This corresponds to a flow path that is 3.5 cm high by 10 m wide. This estimate seems reasonable since the spring water emerges along a bedding plane from three locations that span 9 m.

While cylindrical simulations approximately reproduced the damping of the thermal signal (Figure 3.5a-b), they were not as successful in reproducing the lag. The simulated temperature peak occurred earlier than the actual temperature peak. A smaller

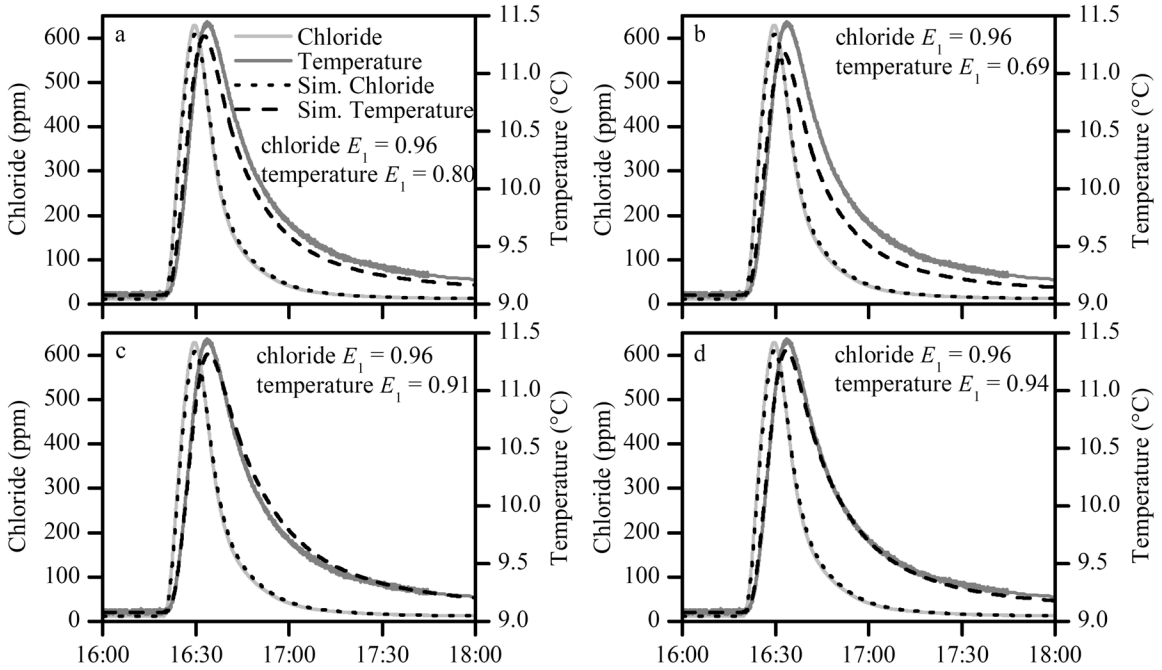

Figure 3.5. (a-b) Cylindrical and (c-d) planar simulations. The D_H of the main passage was set to (a) 8 cm, (b) 9 cm, (c) 6 cm, and (d) 7 cm. The infeeder's D_H was the same as the main passage's D_H in (a) and (c). The infeeder's D_H in (b) was 4 cm (half of best-fit solution in (a)), and the infeeder's D_H in (d) was 3 cm (half of best-fit solution in (c)). See text for details.

D_H would be necessary to reproduce the lag. However, this would reduce the magnitude of the thermal signal. In contrast, planar simulations were able to reproduce both the damping and the lag and produced higher values of E_1 for the temperature curve (Figure 3.5c-d). The ability of the planar simulations to match not only the damping, but also the lag of the thermal signal, also suggests that a bedding plane parting geometry is more appropriate for this flow path.

Method 1 is often employed to estimate geometrical properties of unknown conduits. In this study, this method alone with a circular cross-sectional assumption estimates a small, but traversable passage for humans. However, Method 2 suggests that a much smaller cylindrical passage would be necessary to match the thermal response. The two methods provide the most information when used in combination. In the planar case, this allows estimates of both conduit height and width.

3.7. Conclusions

A controlled recharge event with multiple tracers was conducted to manually perturb a karst system. Given the time difference between the initial increase in discharge and the initial increase in the other parameters at the spring, it seems likely that the conduit from below the injected sinkhole to the spring is mostly submerged. If the water flowed along an open channel, we would expect there to be a smaller time difference between the initial changes. Normalization of the data shows that the breakthrough curves of uranine, chloride, and δD from this trace are essentially identical, dominantly controlled by advection. This trace also illustrates the interactive nature of temperature, where interaction with the soil and rock produced a lagged, damped thermal signal at the spring.

Comparison of salt and uranine recovery curves and calculation of pool water volumes from salt and uranine concentrations shows that uranine degradation may occur within an hour, even in a mostly shaded setting. If this study would have simply been a dye trace, then the actual percent dye recovery would have been underestimated. Therefore, salt was useful to determine tracer recovery early in the trace. However, uranine proves valuable in determining tracer recovery on the tail portion of the breakthrough curve primarily because of its low detection limit.

Due to the correlation between conduit geometry and the rate of heat exchange between water and rock, water temperature signals provide potential constraints on flow path characteristics. This study demonstrates how a partially modified temperature signal may be used to estimate a flow path's D_H (Method 2). Previously, researchers have summed discharge until the arrival of event water or a tracer to estimate conduit volume (Method 1). When both methods are used together, however, they provide more information than either method can alone. In this study, this permits an estimate of a water-filled bedding plane parting 3.5 cm high and 10 m wide, in agreement with the observed spring geometry.

The model used to make this estimation relies on approximate values of a number of unknowns, such as the conduit length. The largest uncertainties arise from the unknown differences between the infeeder and main conduit diameters. Two simulations

with different ratios between these diameters both produce good fits to the observed curve. The exact uncertainty in the diameters is not known, but we are currently developing a faster simulation code that can be used to more fully characterize the parameter space. Additional tracer experiments might also provide more powerful constraints on geometry. In particular, since temperature signals are dependent upon the time scale of the recharge event (Covington et al in review, 2011), multiple tests at the same site with different durations may prove useful.

Researchers often use responses to natural recharge events to characterize karst aquifers. This study demonstrates that manual perturbations to a karst system, particularly if they exploit the differences between a variety of conservative and interactive tracers, may provide insight into flow path geometry. This type of field experiment would be met with some limitations when dealing with larger, more complex systems, but is likely to be useful in many conduit-dominated systems where total system discharge is small enough to be significantly perturbed. Furthermore, flow path geometry may be estimated using responses to natural recharge events, given sufficient input and output data. Combinations of physical, chemical, and isotopic tracers with conservative or interactive characteristics permit a flow path to be probed in many ways, and each tracer potentially provides unique information.

Chapter 4

Thermal retardation during full pipe flow in karst conduits

Summary

Numerical simulations were run to determine variables controlling thermal retardation in karst conduits. The lag of a thermal peak in the water is proportional to a conduit's length; is proportional to the square root of recharge duration, rock thermal conductivity, rock specific heat, and rock density; and is inversely proportional to a conduit's hydraulic diameter, velocity, water specific heat, and water density. These individual relationships were then combined to form one collective function, which, when plotted against thermal peak lag produced a line in log-log space. The relationship between the thermal peak lag and the combined function potentially enables estimates of conduit geometry using thermal peak lag data.

4.1. Introduction

As water flows through an aquifer, numerous processes occur between the water and the aquifer material. One of these processes is thermal exchange, causing the water to approach thermal equilibrium with the aquifer materials through time (e.g., Anderson 2005; Saar 2011). However, preferential flow paths facilitate fast flow-through times and may enable nonequilibrium thermal perturbations to reach a spring (Benderitter et al.

1993; Bundschuh 1997; Martin and Dean 1999; Screaton et al. 2004; Luhmann et al. 2011, Chapter 2 in this thesis). The interaction modifies a water thermal signal, producing a thermal signal that lags behind actual groundwater velocity, i.e., thermal retardation (Luhmann et al. in review, 2011, Chapter 3 in this thesis).

Retardation is well known in porous media and fractures, generally presented in the context of adsorption during solute transport (e.g., Freeze and Cherry 1979; Domenico and Schwartz 1998; Fetter 2001; Singhal and Gupta 2010). Studies have demonstrated thermal retardation in porous media (e.g., Molson et al. 1992; Palmer et al. 1992; Markle and Schincariol 2007) and fractures (e.g., Molson et al. 2007). However, little is known about thermal retardation in karst conduits, let alone the variables that are responsible for producing thermal lags in these preferential flow paths. For flow paths where thermal signals are not completely damped, which are common in karst, some degree of thermal retardation will occur.

Here, we use numerical simulations to demonstrate the effect of several variables on thermal retardation in karst conduits. Variables we consider include flow velocity, conduit geometry, recharge characteristics, and rock and water physical properties. We then combine controlling variables into one function and demonstrate its relationship to thermal peak lag. Ultimately, this relationship may be used to estimate unknown conduit geometry when thermal peak lag data is attained. The importance of conduits in general to flow in karst hydrology is well known (Atkinson 1977b; Worthington 1999; Worthington et al. 2000). However, the actual geometry of a conduit is often a critical unknown.

4.2. Model Description

Heat transport along a 1D flow path is given by the heat advection-dispersion equation:

$$\frac{\partial T_w}{\partial t} = D_L \frac{\partial^2 T_w}{\partial x^2} - v\frac{\partial T_w}{\partial x} + \frac{4h_c}{\rho_w c_{p,w} D_H}(T_s - T_w), \tag{4.1}$$

where T_w is the water temperature, D_L the longitudinal dispersivity, x the flow path position, v the water velocity, h_c the heat transfer coefficient, ρ_w the density of water, $c_{p,w}$

the specific heat of water, D_H the hydraulic diameter of the flow path, and T_s the conduit wall surface temperature. The terms on the right side of Equation (4.1) describe heat dispersion (into which diffusion is lumped), heat advection, and heat exchange with the surrounding rock. The convective heat transfer coefficient is given by

$$h_c = \frac{k_w \mathrm{Nu}}{D_H}, \tag{4.2}$$

where k_w is the thermal conductivity of water and Nu the Nusselt number, which is the ratio of convection to pure conduction heat transfer through the convective boundary layer in the water. The Nu for turbulent flow is given by the empirically derived Gnielinski correlation (Incropera et al. 2007, Equation 8.62),

$$\mathrm{Nu} = \frac{(f/8)(\mathrm{Re}-1000)\,\mathrm{Pr}}{1+12.7\sqrt{f/8}\,(\mathrm{Pr}^{2/3}-1)}, \tag{4.3}$$

where f is the Darcy-Weisbach friction factor, $\mathrm{Re} = \rho_w\, v\, D_H\, \mu_w^{-1}$ the Reynolds number, and $\mathrm{Pr} = c_{p,w}\, \mu_w\, k_w^{-1}$ the Prandtl number of water. μ_w is the dynamic viscosity of water.

Conduction provides a strong control over heat exchange in karst conduits (Covington et al. in review, 2011). 3D heat conduction in cylindrical coordinates with no energy generation can be described by the 2D equation

$$\frac{1}{\alpha_r}\frac{\partial T_r}{\partial t} = \frac{1}{r}\frac{\partial}{\partial r}\left(r\frac{\partial T_r}{\partial r}\right) + \frac{\partial^2 T_r}{\partial x^2}, \tag{4.4}$$

where T_r is the rock temperature and $\alpha_r = k_r\,(\rho_r\, c_{p,r})^{-1}$ is the here-assumed isotropic and homogeneous thermal diffusivity of rock, with k_r denoting the thermal conductivity, ρ_r the density, and $c_{p,r}$ the specific heat. In 2D planar coordinates, the heat conduction equation becomes

$$\frac{1}{\alpha_r}\frac{\partial T_r}{\partial t} = \frac{\partial^2 T_r}{\partial y^2} + \frac{\partial^2 T_r}{\partial x^2}. \tag{4.5}$$

For a general analysis of thermal retardation, Equations (4.1), (4.4), and (4.5) are nondimensionalized resulting in

$$\frac{\partial T_w^*}{\partial t^*} = \frac{1}{\mathrm{Pe}}\frac{\partial^2 T_w^*}{\partial x^{*2}} - \frac{v}{v_{ref}}\frac{\partial T_w^*}{\partial x^*} + \mathrm{St}(T_s^* - T_w^*), \tag{4.6}$$

$$\Theta \frac{\partial T_r^*}{\partial t^*} = \frac{1}{r^*} \frac{\partial}{\partial r^*} \left(r^* \frac{\partial T_r^*}{\partial r^*} \right) + \frac{R^2}{L^2} \frac{\partial^2 T_r^*}{\partial x^{*2}}, \tag{4.7}$$

and

$$\Theta \frac{\partial T_r^*}{\partial t^*} = \frac{\partial^2 T_r^*}{\partial y^{*2}} + \frac{R^2}{L^2} \frac{\partial^2 T_r^*}{\partial x^{*2}}, \tag{4.8}$$

respectively. $T_w^* = T_w \, T_{r,0}^{-1}$ is the dimensionless water temperature, $T_s^* = T_s \, T_{r,0}^{-1}$ the dimensionless conduit wall temperature, $T_r^* = T_r \, T_{r,0}^{-1}$ the dimensionless rock temperature, $T_{r,0}$ the initial rock temperature (or rock temperature at infinity), v_{ref} a time-averaged or reference flow velocity, $t^* = t \, v_{ref} \, L^{-1}$ the dimensionless conduit flow-through time, L the conduit length, $x^* = x \, L^{-1}$ the dimensionless longitudinal distance along the conduit, $r^* = r \, R^{-1}$ the dimensionless radial coordinate, and R the conduit radius. The Peclet Number, Pe, is given by

$$\mathrm{Pe} = \frac{L v_{ref}}{D_L}, \tag{4.9}$$

representing the ratio of heat advection to longitudinal heat dispersion. The Stanton Number, St, is given by

$$\mathrm{St} = \frac{4 h_c L}{\rho_w c_{p,w} D_H v_{ref}}, \tag{4.10}$$

which indicates the ratio of heat flux into the conduit wall to the heat flux along the conduit. Finally,

$$\Theta = \frac{R^2 v_{ref}}{L \alpha_r} \tag{4.11}$$

is a dimensionless ratio of conduction and advection time scales as given in Covington et al. (in review, 2011).

The boundary conditions are:

$$T_w^*(x^* = 0, t) = f(t), \tag{4.12}$$

$$\left. \frac{\partial T_w^*}{\partial x^*} \right|_{x^*=1} = 0, \tag{4.13}$$

$$\frac{\partial T_r^*}{\partial r^*} \to 0 \text{ as } r^* \to \infty, \tag{4.14}$$

and

$$\left.\frac{\partial T_r^*}{\partial r^*}\right|_{r^*=1} = \frac{\Theta \Psi \mathrm{St}}{2}\left(T_s^* - T_w^*\right), \tag{4.15}$$

where $\Psi = \rho_w\, c_{p,w}\, (\rho_r\, c_{p,r})^{-1}$. Initially, rock and water temperatures are set equal to the rock temperature at infinity or $T_w^*(x^*, 0) = T_r^*(r^*, 0) = 1$.

For our recharge temperature, we use a Gaussian function of the form

$$f(t) = 1 + a \exp\left\{-\left((t-b)^2\right)/(2c^2)\right\}, \tag{4.16}$$

where a is the peak height, b the peak center, and c controls the peak width. A Gaussian function is used because it approximates spring thermal perturbations in nature. Recharge temperature may be relatively constant during recharge events. However, variations in flow during recharge events may still produce a Gaussian-like thermal perturbation. Recharge amplitude, R_A, is a in Equation (4.16). For each simulation, c is defined to attain a desired recharge duration, R_D, or full width at half maximum (FWHM) given by

$$R_D = FWHM = 2c\sqrt{2\ln 2}\,. \tag{4.17}$$

Average velocity in a closed conduit with turbulent flow is given by the Darcy-Weisbach Equation:

$$v = \sqrt{\frac{2 D_H g \Delta h}{fL}}\,, \tag{4.18}$$

where g is gravitational acceleration and Δh the hydraulic head difference between the beginning and the end of the conduit. For each simulation, we use a constant head gradient, $\Delta h\, L^{-1}$. Because all other variables are held constant for each simulation, v is also held constant, although v varies between different simulations. f may be approximated using the von Kármán Equation:

$$f = [1.74 + 2\log(R/\varepsilon)]^{-2}\,, \tag{4.19}$$

where ε is the roughness height, i.e., the average distance that irregularities on the rock wall protrude into the conduit. We define $f = 0.05$ when $R = 0.5$ m. Because R or D_H affect f, we account for variations in f while changing R. ε is held constant throughout all simulations.

The finite element package COMSOL Multiphysics® (Version 3.5) is used to numerically solve the coupled advection-dispersion and conduction equations. Using the Coefficient Form PDE mode in COMSOL, Equation (4.6) is solved along a 1D line which represents a conduit (Figure 4.1a) or fracture (Figure 4.1b). Because of axial symmetry, a simulation of conduction in the rock surrounding a circular conduit with full pipe flow may be reduced to a 2D axisymmetric problem. Thus, Equation (4.7) is solved using COMSOL's Conduction Heat Transfer application mode with a 2D axisymmetric rectangle for cylindrical simulation (Figure 4.1a). Similarly, because of reflection symmetry about the fracture plane, a simulation of conduction in the rock surrounding a water-filled fracture may be simplified to a 2D planar problem. Thus, Equation (4.8) is solved in a 2D rectangle in Cartesian coordinates for planar simulations (Figure 4.1b). The 1D line and either the 2D cylindrical or planar rectangle are coupled to each other at one of the rectangle edges using the Extrusion Coupling Variables feature in COMSOL. The 1D conduit or fracture line and the rock at the conduit or fracture wall were discretized into 1000 finite elements along the flow path length for all simulations. Mesh resolution gradually coarsens in the 2D rectangle rock away from the flow path wall, but the 2D rectangle was generally discretized into 23,000 elements. COMSOL uses an implicit method when solving and user-defined relative and absolute tolerances that are compared to the estimated error to modify timesteps (COMSOL 2008). Relative and absolute tolerances for all simulations were set to 10^{-6} and 10^{-7}, respectively.

We conduct numerous simulations to assess the dependence of a variety of parameters on thermal retardation. Parameters varied include hydraulic diameter, D_H, length, L, flow velocity, v, recharge duration, R_D, recharge amplitude, R_A, rock thermal conductivity, k_r, rock specific heat capacity, $c_{p,r}$, rock density, ρ_r, water thermal conductivity, k_w, water specific heat capacity, $c_{p,w}$, water density, ρ_w, and dynamic viscosity, μ_w. Initially, cylindrical simulations are run in groups where one variable is varied while all others are held constant. Table 4.1 lists default variables when held constant. Values for rock variables are for the Salem Limestone (Incropera et al. 2007). After the initial simulations, additional cylindrical simulations are run, where one or several variables are changed for each simulation. Some planar simulations are then run

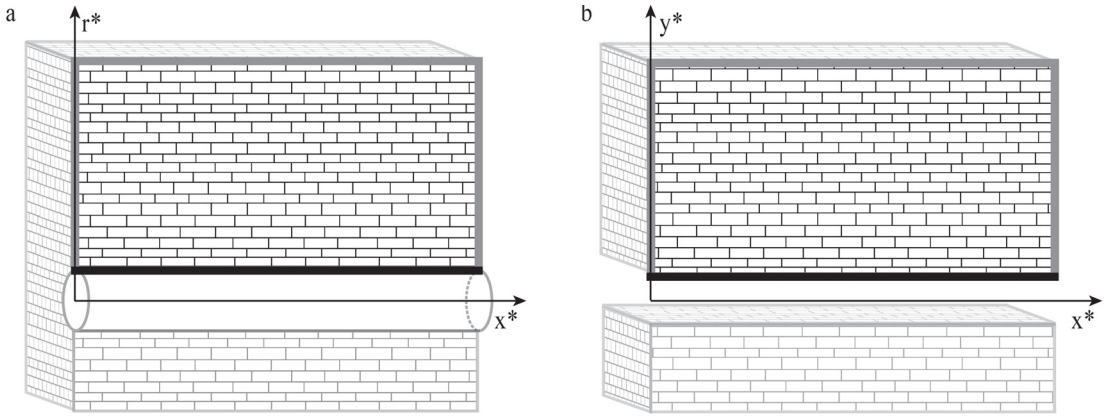

Figure 4.1. Model setup for heat transport simulations involving a (a) conduit or (b) fracture and the surrounding rock. The advection-dispersion equation is solved along the 1D (a) conduit or (b) fracture. Because of symmetry, conduction in the 3D rock surrounding the conduit or fracture may be modeled with a simple 2D rectangle (outlined in thick gray and black lines). Thus, conduction is modeled in (a) 2D cylindrical or (b) 2D planar coordinates. The two geometries are coupled to each other at each respective thick black line (i.e., the conduit/fracture wall surface). Thick gray limestone boundaries perpendicular to the conduit or fracture are insulated rock boundaries. Thick gray limestone boundaries parallel to the conduit or fracture are sufficiently far from flow path lines to satisfy Equation (4.14) and are set to background temperature.

to compare differences between cylindrical and planar geometry. The thermal peak lag, τ, for each simulation is determined by the equation

$$\tau = t_{TP} - t_{CP}, \tag{4.20}$$

where t_{TP} and t_{CP} are times of the thermal peak and a conservative tracer peak, respectively, at the outlet. t_{CP} is time of conservative tracer peak at the beginning of the conduit plus flow-through time. Simulation details are provided in Appendix C.

Table 4.1. Default variables used in simulations.

Parameter	Value	Units
D_H	1	m
L	1000	m
v	0.626	m s^{-1}
R_D	60,000	s
R_A	1	-
k_r	2.15	W m^{-1} K^{-1}
$c_{p,r}$	810	J kg^{-1} K^{-1}
ρ_r	2320	kg m^{-3}
k_w	0.58	W m^{-1} K^{-1}
$c_{p,w}$	4200	J kg^{-1} K^{-1}
ρ_w	1000	kg m^{-3}
μ_w	1.3×10^{-3}	kg s^{-1} m^{-1}
D_L	0.01	m^2 s^{-1}
Pr	9.5	-

4.3. Cylindrical full pipe flow simulations

Figure 4.2 shows how τ depends on D_H, L, and v. τ is approximately proportional to $L\ D_H^{-1}\ v^{-1}$. However, τ becomes more dependent on D_H as D_H decreases and less dependent on v as v decreases.

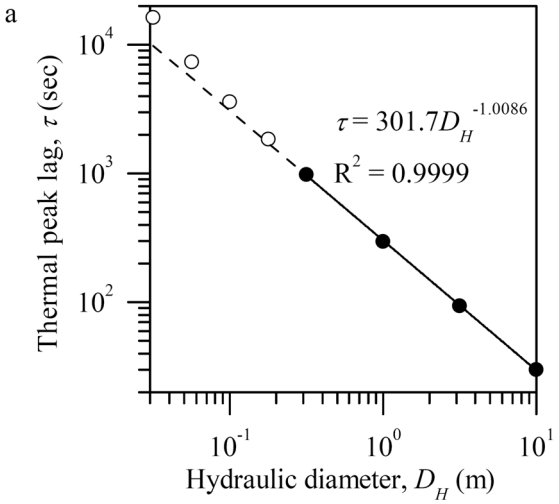

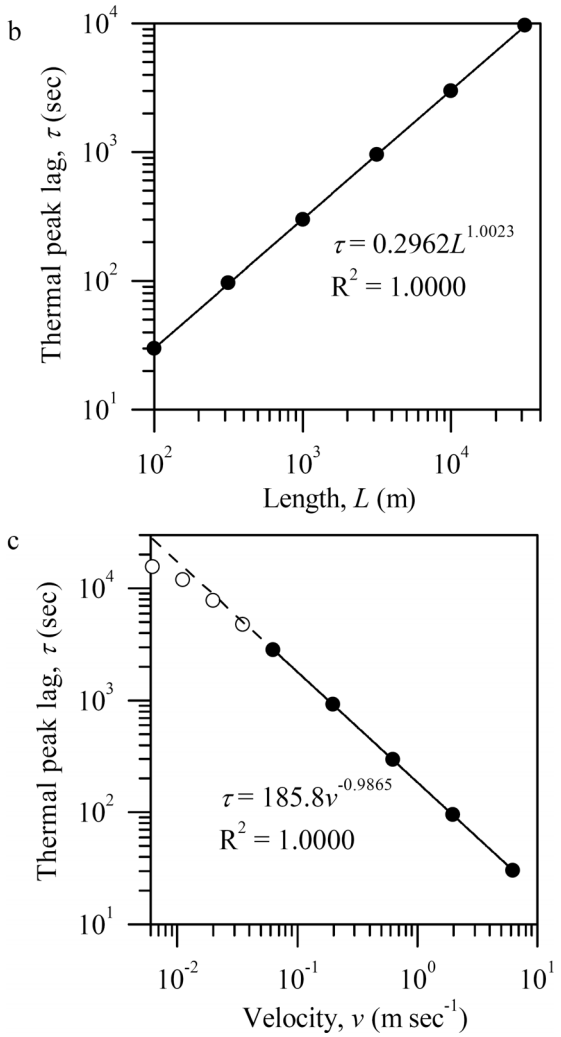

Figure 4.2. Thermal peak lag, τ, as a function of (a) hydraulic diameter, D_H, (b) length, L, and (c) velocity, v. Note the power law relationship in both (a) and (c) include only the filled circles (i.e., larger D_Hs in (a) and faster vs in (b)). The dashed line in both (a) and (c) is simply an extension of each power law relationship, illustrating deviation for smaller D_Hs and slower vs.

The dependence of τ on the recharge parameters R_D and R_A is illustrated in Figure 4.3. τ is approximately proportional to $R_D^{0.5}$, but is independent of R_A.

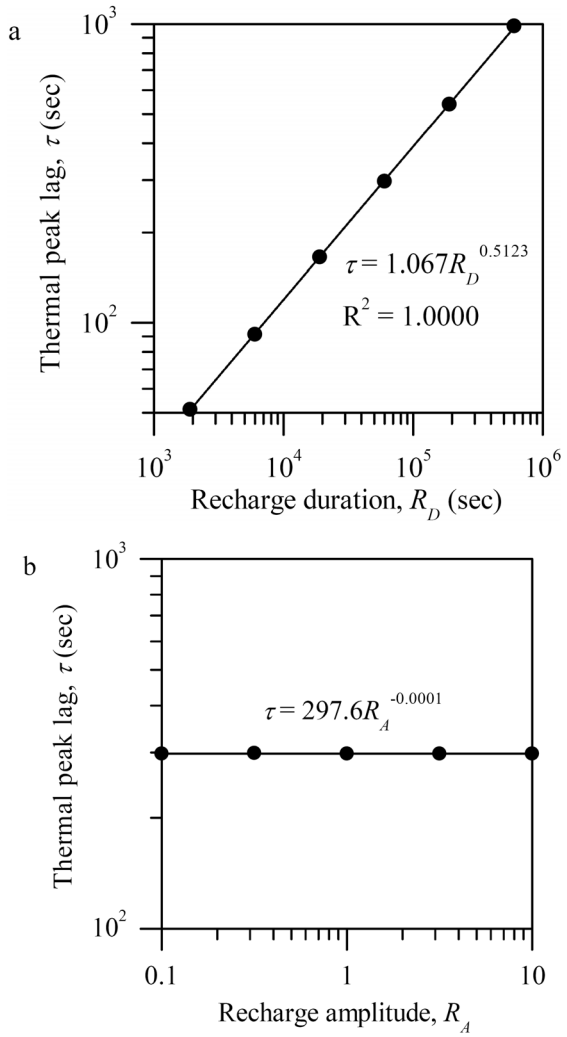

Figure 4.3. Thermal peak lag, τ, as a function of (a) recharge duration, R_D, and (b) recharge amplitude, R_A.

Figure 4.4 portrays how k_r, $c_{p,r}$, and ρ_r affect τ. τ is approximately proportional to $k_r^{0.5}\, c_{p,r}^{0.5}\, \rho_r^{0.5}$.

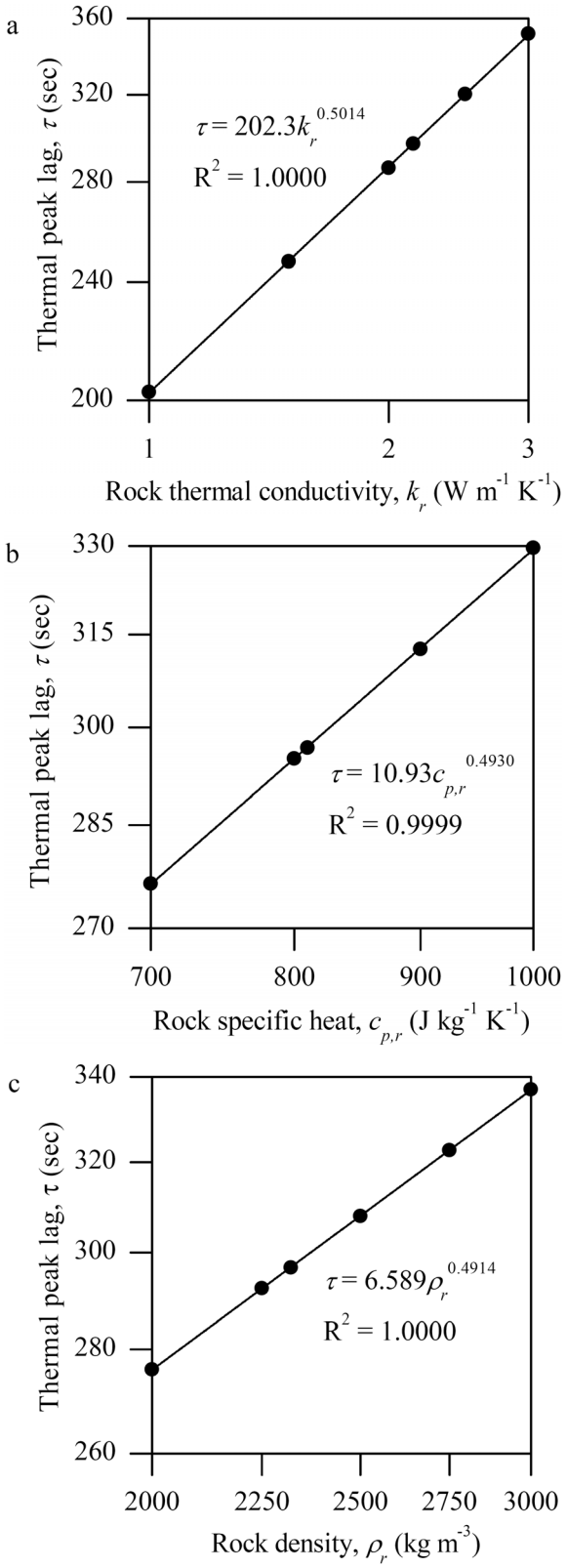

Figure 4.4. Thermal peak lag, τ, as a function of (a) rock thermal conductivity, k_r, (b) rock specific heat, $c_{p,r}$, and (c) rock density, ρ_r.

The influence of k_w, $c_{p,w}$, ρ_w, and μ_w on τ is shown in Figure 4.5. τ is approximately proportional to $c_{p,w}^{-1}\,\rho_w^{-1}$, but is largely independent of k_w and μ_w.

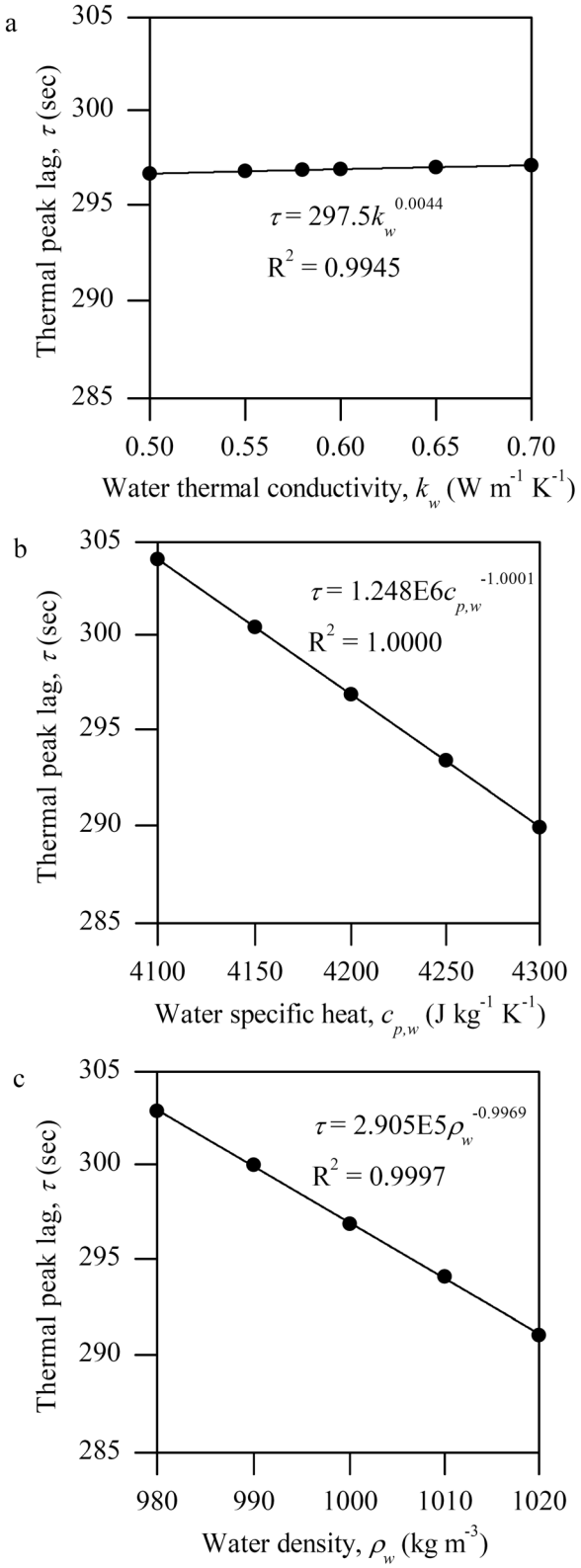

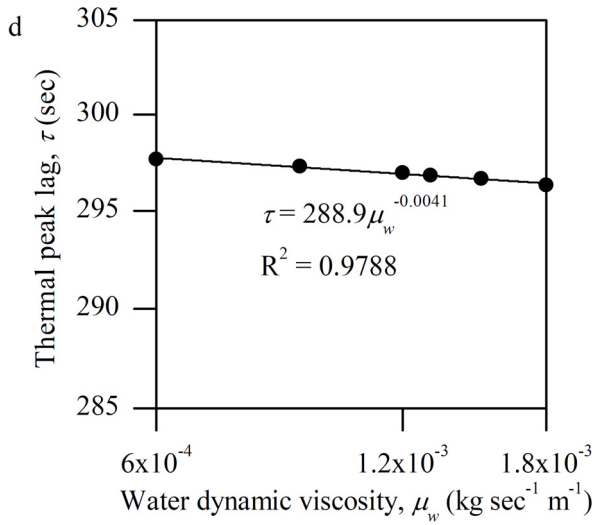

Figure 4.5. Thermal peak lag, τ, as a function of (a) water thermal conductivity, k_w, (b) water specific heat, $c_{p,w}$, (c) water density, ρ_w, and (d) water dynamic viscosity, μ_w.

We propose that all of the above relationships may be combined to form the single function:

$$F = \frac{L(R_D k_r c_{p,r} \rho_r)^{0.5}}{D_H v c_{p,w} \rho_w}, \tag{4.21}$$

which has units of seconds. Figure 4.6 shows the result of plotting F against τ. Simulations that were run with $D_H \geq 1$ m are shown with +s, and those run with $D_H < 1$ m are shown with ×s. Simulations with low vs (i.e., those that deviated from the line in Figure 4.2c) are shown with □s. When F is plotted against τ, simulations with $D_H \geq 1$ m and $v > 0.0352$ m s^{-1} generally fall on a line in log-log space with an exponent of 1. However, the thermal peak lag for most simulations with $D_H < 1$ m generally deviates above the line defined by the simulations with larger D_Hs. Note the two ×s that form a vertical line for the F value of 275,000. These two simulations were run with D_Hs of 0.2 m and 0.0632 m. F remained constant by simultaneously changing L and v. For these two simulations, τ increases as D_H decreases, producing greater deviation for smaller D_Hs. Thus, the thermal lag becomes progressively more dependent on D_H as it decreases for small D_Hs.

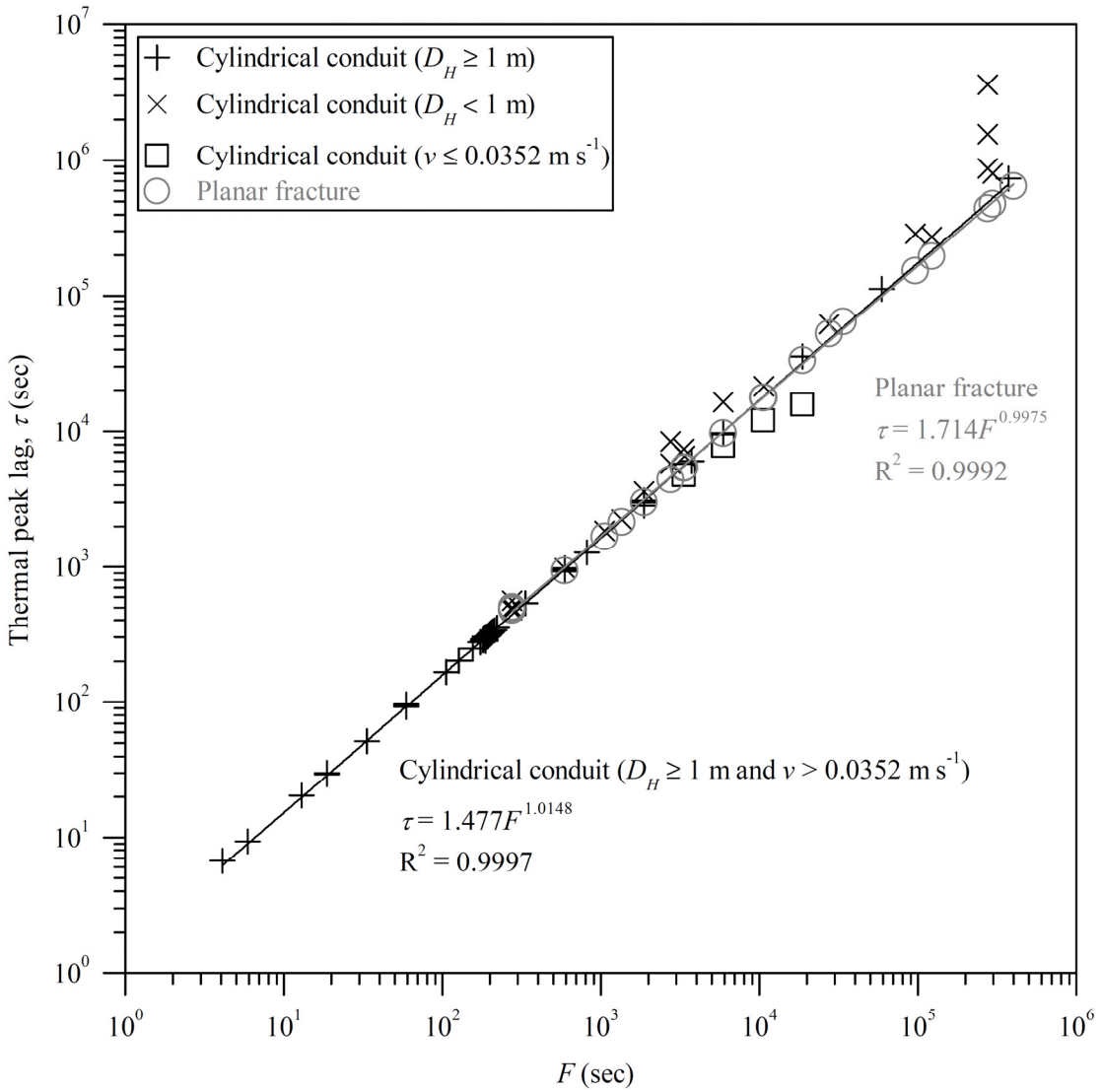

Figure 4.6. Thermal peak lag, τ, as a function of F. Two power law relationships were determined: one for cylindrical conduit simulations with $D_H \geq 1$ m and $v > 0.0352$ m s^{-1} and another for planar fracture simulations.

4.4. Planar full fracture flow simulations

All cylindrical simulations with $D_H < 1$ m (i.e., those that generally deviate above the line) were run in planar coordinates. These planar simulations are also included in Figure 4.6 (shown with ○s) and were run with the same parameters that were used in the cylindrical simulations. The only difference is that these simulations were run with a planar, instead of cylindrical, geometry. When F is plotted against τ for planar

simulations, the resulting line defined by planar simulations is similar to the line defined by cylindrical simulations with $D_H \geq 1$ m and $v > 0.0352$ m s^{-1}.

4.5. Additional considerations

f may also be calculated using the more rigorous, empirical Colebrook-White equation:

$$\frac{1}{\sqrt{f}} = -2\log\left(\frac{\varepsilon}{3.7D_H} + \frac{2.51}{\mathrm{Re}\sqrt{f}}\right). \tag{4.22}$$

Furthermore, 9.5 was used for the Prandtl number, Pr, for all previous simulations. Using the default variables given in Table 4.1 for water's specific heat, dynamic viscosity, and thermal conductivity gives a Pr of 9.41. The four simulations with the smallest D_Hs shown in Figure 4.2a were run again with both of these changes, and Table 4.2 lists identical results between these simulations.

Table 4.2. Comparison of simulations with different Darcy-Weisbach friction factors and Prandtl numbers.

Simulation	Thermal peak lag (sec)	Output peak temp
C3	16,300	1.11
C3 with modified f and Pr	16,300	1.11
C4	7,360	1.43
C4 with modified f and Pr	7,360	1.43
C5	3,590	1.71
C5 with modified f and Pr	3,590	1.71
C6	1,840	1.87
C6 with modified f and Pr	1,840	1.87

4.6. Discussion

k_r, $c_{p,r}$, ρ_r, $c_{p,w}$, and ρ_w vary relatively little in shallow aquifers. Thus, τ is primarily controlled by D_H, L, v, and R_D, with the first three variables having a stronger influence on τ. For these four variables, anything that increases the interaction between water and rock leads to more lag. Thus, there is more lag for small-diameter, long conduits with low average flow-through velocities that receive long duration recharge.

The thermal peak lag becomes more dependent on D_H with smaller, circular conduits. This produces a deviation in Figure 4.6 that arises because of conduction in cylindrical coordinates. Conduits with smaller diameters have larger conduit wall surface

areas to water volume ratios and a greater ratio of thermal penetration depth to conduit radius. Thus, the cylindrical geometry plays an important role during heat exchange in small, circular conduits. The ratio of penetration depth to conduit radius for a large diameter conduit is relatively small, which reduces the importance of its cylindrical geometry. This permits large, circular conduits to be modeled with planar symmetry (Covington et al. in review, 2011). Thus, the power law relationships in Figure 4.6 for cylindrical simulations with large D_Hs and fast vs and for planar simulations are similar. It is likely that a fit which incorporates these two relationships includes many natural full pipe flow scenarios. For example, flow paths with smaller D_H likely occur as fractures (with planar symmetry) instead of circular conduits. Furthermore, peak temperature was lower for cylindrical simulations than it was for planar simulations with the same parameters, making it less likely to see thermal perturbations from small, circular conduits when they exist.

In contrast, τ becomes less dependent on v for lower flow velocities. Advection becomes less significant with lower flow velocities, and this increases the relative importance of conduction. In an attempt to understand this deviation, I modified the simulation with the lowest v in Figure 4.2c in two ways. First, I increased the Pe in Equation 4.6 from 626 to 100,000 to reduce dispersion. However, τ remained constant at a value of 15,700 for these two different simulations. Second, I changed $R^2 L^{-2}$ from 2.5×10^{-7} to 2.5×10^{-17}. If conduction in the rock parallel to the conduit is responsible for the deviation, then decreasing the coefficient $R^2 L^{-2}$ in Equation 4.7 should produce less deviation. However, τ was not changed. Thus, I still do not understand the deviation for lower flow velocities. However, lower flow velocities typically occur in flow paths with smaller D_Hs where thermal perturbations are more likely to be completely damped.

Our model simulates heat transport in a single conduit. Karst aquifers contain numerous conduits of different sizes that form a larger, connected flow network. However, the largest conduits are likely responsible for producing temperature peaks or troughs following a recharge event, as the largest diameter flow paths generally have faster velocities and flow-through times and less thermal damping. Smaller conduits may potentially produce bumps on the thermal recession at a spring that follow the thermal

peak. For the smallest flow paths, water temperature is significantly or totally damped by the time the water reaches a spring. If a spring receives inputs from several large conduits, recharge event perturbations at a spring may incorporate several peaks (e.g., Hess and White 1988). The first thermal peak would provide the most promise for constraining parameters controlling the thermal peak lag. Constraining these parameters from subsequent peaks may be more complicated, particularly if a later peak from another conduit tributary spends a significant amount of time in the master conduit where the temperature in the rock surrounding the flow path has already been changed due to interaction with the water producing the first peak. However, if water flowing through tributary conduits enters the main conduit just before discharging at the spring, the thermal lag of later peaks is little affected by earlier peaks.

Second, our model simulates heat transport in a single conduit of constant D_H. However, the largest conduit in any aquifer displays some variation in D_H along its L. Portions of the conduit with smaller D_H would produce relatively more lag, and portions with larger D_H would produce relatively less lag. Thus, the thermal peak lag at a spring is likely a function of the average D_H for a given conduit.

Finally, our model simulates heat transport in a single conduit with full pipe flow conditions. It is likely that a similar relationship exists for a partially filled conduit with a free surface, where deviation from the full pipe flow relationship would be a function of the portion of the conduit filled with water and the duration of the recharge event. This is because radiation exchange from the free surface to the dry conduit wall can be an important heat transport mechanism in karst conduits (Covington et al. in review, 2011).

Determination of a thermal peak lag requires high resolution data for a conservative tracer. It is not uncommon for a monitoring location to have equipment installed that is capable of recording water level/discharge, electrical conductivity, and temperature. In general, water level/discharge data has limited use in determining thermal peak lag. Initial hydrograph perturbations often record arrival of pre-recharge water, a detail which is commonly exploited during full pipe flow to estimate conduit volume and diameter (Ashton 1966; Atkinson 1977b; Sauter 1992; Ryan and Meiman 1996; Birk et al. 2004; Luhmann et al. in review, 2011, Chapter 3 in this thesis). In

contrast, electrical conductivity shows more promise as a conservative tracer. Spring electrical conductivity perturbations record event water contributions (e.g., Raeisi et al. 2007), and electrical conductivity interacts less with the rock surrounding a conduit than temperature (Birk et al. 2006; Covington et al. in prep).

Luhmann et al. (in review, 2011, Chapter 3 in this thesis) conducted a field tracer experiment that involved temperature, conductivity/chloride, and other parameters. They were able to estimate a flow path's D_H using known input data, high-resolution output data, and heat transport simulations which reproduced the damped, lagged thermal signal that resulted from the trace. The dependence of τ on D_H demonstrates the validity of a new technique. Specifically, one may estimate a conduit's D_H by using natural recharge events or tracer experiments without information about inputs or complex simulations. There is likely more error with D_H estimates using this new technique. However, its ease of employment should be of interest to the karst hydrologist.

4.7. Conclusions

As water flows through an aquifer, heat exchange occurs between water and rock if they are in thermal disequilibrium. When thermal equilibrium is not attained, the water-rock interaction produces a thermal signal in the water that lags behind the actual groundwater velocity. Our numerical simulations demonstrate that the thermal peak lag, τ, in a conduit or fracture is dependent on hydraulic diameter, D_H, length, L, and velocity, v, and to a lesser extent, on recharge duration, R_D. The thermal lag in a conduit or fracture is also dependent on rock thermal conductivity, k_r, rock specific heat, $c_{p,r}$, rock density, ρ_r, water specific heat, $c_{p,w}$, and water density, ρ_w. However, these parameters vary little in shallow aquifers. We find that these parameters can be combined in a single, simple function, $F = L\ (R_D\ k_r\ c_{p,r}\ \rho_r)^{1/2}\ (D_H\ v\ c_{p,w}\ \rho_w)^{-1}$, with F given in units of seconds. F shows a power-law relationship with the thermal peak lag, τ, with an exponent of approximately 1. Only small cylindrical conduits and slow flow velocities deviate from this relationship. Additional work is needed to determine if the relationships demonstrated here hold for partially filled conduits or fractures with free water surfaces.

Springs may undergo significant chemical and physical variations following aquifer recharge events. The results presented here underscore the importance of collecting high-resolution data during these events. In some cases, an ideal data recording rate might be on the order of seconds. With high temporal resolution spring data and estimates of conduit length, flow velocity, and recharge duration, for example, the thermal peak lag might be used to estimate the flow path's hydraulic diameter using the relationship demonstrated between the thermal peak lag, τ, and the combined function, F. Even when more than one of these variables is unknown, the relationship might be used to determine possible values for each of the variables to bracket the range of potential scenarios.

Chapter 5

Conclusions and future work

5.1. Conclusions

Water temperature at springs generally provides useful information concerning aquifer geometry and recharge. Temperature monitoring at 25 springs and cave streams in southeastern Minnesota has shown four distinct thermal patterns that can be interpreted in terms of heat exchange effectiveness along a flow path and the nature of recharge. The patterns provide information about the size of the flow path, recharge type and duration, and aquifer depth.

Water temperature is generally an interactive tracer, where heat transport rapidly occurs when water and aquifer rock are at different temperatures. In the pool dump trace at Freiheit Spring, the uranine, chloride, and δD breakthrough curves were essentially identical and conservative. In contrast, the water temperature interacted with the aquifer as it moved along the flow path, producing a damped, lagged thermal signal at the spring. However, both the conservative and nonconservative tracers provided complementary information. The conservative tracers used in conjunction with the discharge pressure pulse permitted an upper bound estimate of conduit volume. Heat transport simulations were run to reproduce the nonconservative temperature signal to determine the hydraulic diameter of the flow path. Together, the tracers were used to estimate a low, wide flow path, in agreement with the observed spring geometry.

The dependence of the thermal peak lag on several variables was illustrated using heat transport simulations. The thermal peak lag is controlled by the length and hydraulic diameter of the flow path, water velocity, recharge duration, and water and rock physical properties. The controlling variables were combined to form a power law relationship with the thermal peak lag. Water and rock physical properties show little variation in shallow aquifer settings. Therefore, the thermal peak lag may be used to provide an estimate of the length and hydraulic diameter of the flow path, water velocity, or recharge duration, especially if some of these variables are known. This is particularly promising to the field of karst hydrology because it potentially permits estimates of flow path geometry using only high resolution data collected from a spring.

Finally, I have also been involved in some other relevant work that is not included in this thesis. One project explores the mechanisms of heat exchange between water and rock in karst conduits (Covington et al. in review, 2011). Rock conduction primarily controls heat exchange in karst conduits, especially over long time scales. Furthermore, radiative heat exchange can be important in conduits with open channel flow. Another project explores process length scales in karst aquifers (Covington et al. in prep, 2011). Water, solutes, sediment, organic debris, and other materials are modified as they move through an aquifer. These modification processes occur over a characteristic length scale, and ultimately control whether an input signal change produces variability in the signal at a spring. Thermal length scales are a function of the time scale associated with input variations. For input variations over short time scales, thermal length scales are much shorter than calcite dissolution length scales. Thus, short time scale thermal perturbations provide maximum information about m-scale conduits, whereas dissolved calcite perturbations provide maximum information about mm- to cm-scale flow paths. As the input time scale increases to seasonal changes, temperature signals probe smaller flow paths that are more comparable to those probed by conductivity signals.

5.2. Future work

Much of this thesis has focused on how water temperature may be used to learn important information about a flow system. There are still numerous questions to address

regarding water temperature. For example, how does advection enhance the skin depth? And to what degree does advection contribute to thermal heterogeneity in an aquifer? Whenever thermal perturbations flow through an aquifer, some of the thermal energy is exchanged with the surrounding rock which modifies the previous thermal regime of the aquifer. Do these disturbed thermal regimes ever completely recover to background conditions before the next advective thermal perturbation?

Furthermore, what information may be gathered from thermal recessions? Hydrograph recessions have been analyzed for more than a century to characterize the recessions, to determine aquifer characteristics, or to estimate discharge. Early quantitative work began with the pioneering work of Boussinesq (1903, 1904) and Maillet (1905). Numerous studies have followed this early work, and they have subsequently been summarized in several publications (e.g., Hall 1968; Tallaksen 1995; Jeannin and Sauter 1998; Dewandel et al. 2003; Ford and Williams 2007). However, Jeannin and Sauter (1998) suggested that it is difficult to determine karst aquifer structure using hydrograph recession analysis. Furthermore, Covington et al. (2009) demonstrated that hydrograph recessions rarely provide information about conduit geometry. However, thermal recessions seem particularly promising to infer aquifer structure since water temperature is so readily modified by a system. These features have never been extensively analyzed

Finally, water temperature is only one of many tracers. As demonstrated with the few tracers used in Chapter 3, each potentially provides unique and complementary information. Hydrologic monitoring would benefit from additional work that seeks to more fully understand the unique information provided by each tracer, exploiting differences in physical or chemical processes, tracer size, etc. Then each unique piece of information may be combined to provide a more complete picture which more fully explains flow and transport in an aquifer.

References

Alexander, E.C., Jr., G.A. Brick, and A.N. Palmer. 2009. The Glaciated Central Lowlands: Minnesota. In *Caves and Karst of the USA*, ed. A.N. Palmer and M.V. Palmer, 146-150. Huntsville, AL: National Speleological Society.

Alexander, E.C., Jr., and R.S. Lively. 1995. Karst-aquifers, caves, and sinkholes (Plates 8 and 9). In *Text Supplement to the Geologic Atlas of Fillmore County, Minnesota, Part C*, ed. R.S. Lively and N.H. Balaban, 10-18. Minnesota Geological Survey County Atlas Series C-8.

Anderson, M.P. 2005. Heat as a ground water tracer. *Ground Water* 43, no. 6: 951-968.

APHA. 1992. *Standard Methods for the Examination of Water and Wastewater*, 18th ed. Washington, D.C.: American Public Health Association Water Works Association, American Water Environment Federation.

Ashton, K. 1966. The analysis of flow data from karst drainage system. *The Transactions of the Cave Research Group* 7, no. 2: 161-203.

Atkinson, T.C. 1977a. Carbon dioxide in the atmosphere of the unsaturated zone: An important control of groundwater hardness in limestones. *Journal of Hydrology* 35, no. 1-2: 111-123.

Atkinson, T.C. 1977b. Diffuse flow and conduit flow in limestone terrain in the Mendip Hills, Somerset (Great Britain). *Journal of Hydrology* 35, no. 1-2: 93-110.

Atkinson, T.C., D.I. Smith, J.J. Lavis, and R.J. Whitaker. 1973. Experiments in tracing underground waters in limestones. *Journal of Hydrology* 19, no. 4: 323-349.

Austin, G.S. 1969. Paleozoic lithostratigraphic nomenclature for southeastern Minnesota. Minnesota Geological Survey Information Circular 6.

Austin, G.S. 1972. Paleozoic lithostratigraphy of southeastern Minnesota. In *Geology of Minnesota: A Centennial Volume*, ed. P.K. Sims and G.B. Morey, 459-473. Minneapolis: Minnesota Geological Survey, University of Minnesota.

Benderitter, Y., B. Roy, and A. Tabbagh. 1993. Flow characterization through heat transfer evidence in a carbonate fractured medium: First approach. *Water Resources Research* 29, no. 11: 3741-3747.

Benischke, R., N. Goldscheider, and C. Smart. 2007. Tracer techniques. In *Methods in Karst Hydrogeology*, ed. N. Goldscheider and D. Drew, 147-170. Leiden: Taylor & Francis/Balkema.

Birk, S. 2002. Characterization of karst systems by simulating aquifer genesis and spring responses: Model development and application to gypsum karst. Ph.D. diss., Tübinger Geowissenschaftliche Arbeiten C60, Institut für Geowissenschaften, Universität Tübingen.

Birk, S., R. Liedl, and M. Sauter. 2004. Identification of localised recharge and conduit flow by combined analysis of hydraulic and physico-chemical spring responses (Urenbrunnen, SW-Germany). *Journal of Hydrology* 286, no. 1-4: 179-193.

Birk, S., R. Liedl, and M. Sauter. 2006. Karst spring responses examined by process-based modeling. *Ground Water* 44, no. 6: 832-836.

Borchardt, M.A., K.R. Bradbury, E.C. Alexander, Jr., R.J. Kolberg, S.C. Alexander, J.R. Archer, L.A. Braatz, B.M. Forest, J.A. Green, and S.K. Spencer. 2011. Norovirus outbreak caused by a new septic system in a dolomite aquifer. *Ground Water* 49, no. 1: 85-97.

Boussinesq, J. 1903. Sur un mode simple d'écoulement des nappes d'eau d'infiltration à lit horizontal, avec rebord vertical tout autour lorsqu'une partie de ce rebord est enlevée depuis la surface jusqu'au fond. *Comptes Rendus, Académie des Sciences (Paris)* 137: 5-11.

Boussinesq, J. 1904. Recherches théoriques sur l'écoulement des nappes d'eau infiltrées dans le sol et sur le débit des sources. *Journal de Mathématiques Pures et Appliquées* 10: 5-78.

Bravo, H.R., J. Feng, and R.J. Hunt. 2002. Using groundwater temperature data to constrain parameter estimation in a groundwater flow model of a wetland system. *Water Resources Research* 38, no. 8. DOI: 10.1029/2000WR000172.

Bredehoeft, J.D., and I.S. Papadopulos. 1965. Rates of vertical groundwater movement estimated from the Earth's thermal profile. *Water Resources Research* 1, no. 2: 325-328.

Budd, D.A., and H.L. Vacher. 2004. Matrix permeability of the confined Floridan Aquifer. *Hydrogeology Journal* 12, no. 5: 531-549.

Bundschuh, J. 1993. Modeling annual variations of spring and groundwater temperatures associated with shallow aquifer systems. *Journal of Hydrology* 142, no. 1-4: 427-444.

Bundschuh, J. 1997. Temporal variations of spring water temperatures in relation to the extents of the heat transport modes occurring in the karstified lower gypsum-Keuper Aquifer (Karnian, southern Germany). In *Proceedings of the 12th International Congress of Speleology; 6th Conference on Limestone Hydrology*

and Fissured Media, ed. P.-Y. Jeannin, 129-132. International Union of Speleology.

Butler, R.W.H., R.E. Holdsworth, and G.E. Lloyd. 1997. The role of basement reactivation in continental deformation. *Journal of the Geological Society* 154, no. 1: 69-71.

Carslaw, H.S., and J.C. Jaeger. 1959. *Conduction of Heat in Solids*, 2nd ed. Oxford: Clarendon.

Chanson, H. 2004. *The Hydraulics of Open Channel Flow: An Introduction*, 2nd ed. Boston: Elsevier Butterwork-Heinemann.

COMSOL. 2008. *COMSOL Multiphysics User's Guide*, Version 3.5.

Covington, M.D., A.J. Luhmann, F. Gabrovšek, M.O. Saar, and C.M. Wicks. 2011. Mechanisms of heat exchange between water and rock in karst conduits. In review, submitted to *Water Resources Research*.

Covington, M.D., A.J. Luhmann, C.M. Wicks, and M.O. Saar. 2011. Process length scales and longitudinal damping in karst conduits. In preparation, to be submitted to *Journal of Geophysical Research-Earth Surface*.

Covington, M.D., C.M. Wicks, and M.O. Saar. 2009. A dimensionless number describing the effects of recharge and geometry on discharge from simple karstic aquifers. *Water Resources Research* 45, no. 11. W11410. DOI: 10.1029/2009WR008004.

Craddock, C. 1972. Keweenawan geology of east-central and southeastern Minnesota. In *Geology of Minnesota: A Centennial Volume*, ed. P.K. Sims and G.B. Morey, 416-424. Minneapolis: Minnesota Geological Survey, University of Minnesota.

Craddock, C., E.C. Thiel, and B. Gross. 1963. A gravity investigation of the Precambrian of southeastern Minnesota and western Wisconsin. *Journal of Geophysical Research* 68, no. 21: 6015-6032.

Craddock, J.P., M. Jackson, B.A. van der Pluijm, and R.T. Versical. 1993. Regional shortening fabrics in eastern North America: Far-field stress transmission from the Appalachian-Ouachita Orogenic Belt. *Tectonics* 12, no. 1: 257-264.

Craddock, J.P., and B.A. van der Pluijm. 1989. Late Paleozoic deformation of the cratonic carbonate cover of eastern North America. *Geology* 17, no. 5: 416-419.

Craddock, J.P., and B.A. van der Pluijm. 1999. Sevier-Laramide deformation of the continental interior from calcite twinning analysis, west-central North America. *Tectonophysics* 305, no. 1-3: 275-286.

Desmarais, K., and S. Rojstaczer. 2002. Inferring source waters from measurements of carbonate spring response to storms. *Journal of Hydrology* 260, no. 1-4: 118-134.

Dewandel, B., P. Lachassagne, M. Bakalowicz, Ph. Weng, and A. Al-Malki. 2003. Evaluation of aquifer thickness by analysing recession hydrographs. Application to the Oman ophiolite hard-rock aquifer. *Journal of Hydrology* 274, no. 1-4: 248-269.

Domenico, P.A., and V.V. Palciauskas. 1973. Theoretical analysis of forced convective heat transfer in a regional ground-water flow. *Geological Society of America Bulletin* 84, no. 12: 3803-3814.

Domenico, P.A., and F.W. Schwartz. 1998. *Physical and Chemical Hydrogeology*, 2nd ed. New York: John Wiley and Sons.

Dreiss, S.J. 1989. Regional scale transport in a karst aquifer: 1. Component separation of spring flow hydrographs. *Water Resources Research* 25, no. 1: 117-125.

Fetter, C.W. 2001. *Applied Hydrogeology*, 4th ed. Upper Saddle River, NJ: Prentice-Hall.

Field, M.S., and S.G. Nash. 1997. Risk assessment methodology for karst aquifers: (1) Estimating karst conduit-flow parameters. *Environmental Monitoring and Assessment* 47, no. 1: 1-21.

Florea, L.J., and H.L. Vacher. 2006. Springflow hydrographs: Eogenetic vs. telogenetic karst. *Ground Water* 44, no. 3: 352-361.

Ford, D., and P. Williams. 2007. *Karst Hydrogeology and Geomorphology*. Chichester, England: John Wiley & Sons.

Freeze, R.A., and J.A. Cherry. 1979. *Groundwater*. Englewood Cliffs, NJ: Prentice-Hall.

Gao, Y., and E.C. Alexander, Jr. 2008. Sinkhole hazard assessment in Minnesota using a decision tree model. *Environmental Geology* 54, no. 5: 945-956.

Gao, Y., E.C. Alexander, Jr., and R.G. Tipping. 2005. Karst database development in Minnesota: Design and data assembly. *Environmental Geology* 47, no. 8: 1072-1082.

Geyer, T., S. Birk, T. Licha, R. Liedl, and M. Sauter. 2007. Multitracer test approach to characterize reactive transport in karst aquifers. *Ground Water* 45, no. 1, 36-45.

Goldscheider, N., D. Drew, and S. Worthington. 2007. Introduction. In *Methods in Karst Hydrogeology*, ed. N. Goldscheider and D. Drew, 1-8. London: Taylor & Francis.

Goldscheider, N., H. Hötzl, W. Käss, and W. Ufrecht. 2003. Combined tracer tests in the karst aquifer of the artesian mineral springs of Stuttgart, Germany. *Environmental Geology* 43, no. 8: 922-929.

Goldscheider, N., J. Meiman, M. Pronk, and C. Smart. 2008. Tracer tests in karst hydrogeology and speleology. *International Journal of Speleology* 37, no. 1: 27-40.

Golterman, H.L., R.S. Clymo, and M.A.M. Ohnstad. 1978. *Methods for Physical and Chemical Analysis of Fresh Waters: IBP Handbook No 8*, 2nd ed. Oxford: Blackwell Scientific.

Grasso, D.A., and P.Y. Jeannin. 2002. A global experimental system approach of karst springs' hydrographs and chemographs. *Ground Water* 40, no. 6: 608-617.

Grasso, D.A., P.Y. Jeannin, and F. Zwahlen. 2003. A deterministic approach to the coupled analysis of karst springs' hydrographs and chemographs. *Journal of Hydrology* 271, no. 1-4: 65-76.

Green, J.A., A.J. Luhmann, A.J. Peters, A.C. Runkel, E.C. Alexander, Jr., and S.C. Alexander. 2008. Dye tracing within the St. Lawrence confining unit in southeastern Minnesota. In *Sinkholes and the Engineering and Environmental Impacts of Karst: Proceedings of the Eleventh Multidisciplinary Conference*, ed. L.B. Yuhr, E.C. Alexander, Jr., and B.F. Beck, 477-484. Reston, VA: American Society of Civil Engineers.

Groves, C. 2007. Hydrological methods. In *Methods in Karst Hydrogeology*, ed. N. Goldscheider and D. Drew, 45-64. Leiden: Taylor & Francis/Balkema.

Hall, F.R. 1968. Base-flow recessions–a review. *Water Resources Research* 4, no. 5: 973-983.

Hallberg, G.R., R.D. Libra, E.A. Bettis, III, and B.E. Hoyer. 1984. Hydrogeologic and water quality investigations in the Big Spring Basin, Clayton County, Iowa, 1983 water year. Iowa Geological Survey Open File Report 84-4.

Hess, J.W., and W.B. White. 1988. Storm response of the karstic carbonate aquifer of southcentral Kentucky. *Journal of Hydrology* 99, no. 3-4: 235-252.

Hobbs, H.C. 1995. Plate 3 – Surficial geology. In Geological Atlas of Fillmore County, Minnesota. Minnesota Geological Survey County Atlas Series C-8.

Hobbs, H.C. 2002. Quaternary geology of Wabasha County, Minnesota. In *Contributions to the geology of Wabasha County, Minnesota*, project manager A.C. Runkel, 28-37. Minnesota Geological Survey Report of Investigations 59.

Hobbs, H.C., and J.E. Goebel. 1982. Geologic Map of Minnesota, Quaternary Geology. Minnesota Geological Survey State Map Series S-1.

Hückinghaus, D., R. Liedl, and M. Sauter. 1997. Characterization of karst aquifers by heat transfer. In *Proceedings of the 12th International Congress of Speleology; 6th Conference on Limestone Hydrology and Fissured Media*, ed. P.-Y. Jeannin, 145-148. International Union of Speleology.

Hudleston, P.J. 2007a. Personal communication, June 5, Minneapolis, Minnesota.

Hudleston, P.J. 2007b. Email, June 27.

Incropera, F.P., D.P. Dewitt, T.L. Bergman, and A.S. Lavine. 2007. *Fundamentals of Heat and Mass Transfer*. Hoboken, NJ: John Wiley & Sons.

Jakucs, L. 1959. Neue methoden der höhlenforschung in Ungarn und ihre ergebnisse. *Die Höhle* 10, no. 4: 88-98.

Jeannin, P.-Y., and M. Sauter. 1998. Analysis of karst hydrodynamic behaviour using global approaches: A review. *Bulletin d'Hydrogéologie* 16: 31-48.

Jiang, Y., and A.D. Woodbury. 2006. A full-Bayesian approach to the inverse problem for steady-state groundwater flow and heat transport. *Geophysical Journal International* 167, no. 3: 1501-1512.

Käss, W. 1998. *Tracing Technique in Geohydrology*. Rotterdam: A.A. Balkema.

Kiraly, L. 1975. Rapport sur l'état actuel des connaissances dans le domaine des caractères physiques des roches karstiques. In *Hydrogeology of Karstic Terrains*, International Union of Geological Sciences, Series B, Number 3, ed. A. Burger and L. Dubertret, 53-67. Paris: International Association of Hydrogeologists.

Klimchouk, A.B., and D.C. Ford. 2000. Types of karst and evolution of hydrogeologic setting. In *Speleogenesis: Evolution of Karst Aquifers*, ed. A.B. Klimchouk, D.C. Ford, A.N. Palmer, and W. Dreybrodt, 45-53. Huntsville, Ala.: National Speleological Society.

Krause, P., D.P. Boyle, and F. Bäse. 2005. Comparison of different efficiency criteria for hydrological model assessment. *Advances in Geosciences* 5: 89-97.

Lakey, B., and N.C. Krothe. 1996. Stable isotopic variation of storm discharge from a perennial karst spring, Indiana. *Water Resources Research* 32, no. 3: 721-731.

Lascu, I., and J.M. Feinberg. 2011. Speleothem magnetism. *Quarternary Science Reviews*. In press.

Lee, E.S., and N.C. Krothe. 2001. A four-component mixing model for water in a karst terrain in south-central Indiana, USA. Using solute concentration and stable isotopes as tracers. *Chemical Geology* 179, no. 1-4: 129-143.

Legates, D.R., and G.J. McCabe, Jr. 1999. Evaluating the use of "goodness-of-fit" measures in hydrologic and hydroclimatic model validation. *Water Resources Research* 35, no. 1: 233-241.

Liedl, R., S. Renner, and M. Sauter. 1998. Obtaining information about fracture geometry from heat flow data in karst systems. *Bulletin d'Hydrogéologie*, no. 16: 143-153.

Liedl, R., and M. Sauter. 1998. Modelling of aquifer genesis and heat transport in karst systems. *Bulletin d'Hydrogéologie*, no. 16: 185-200.

Liu, Z., C. Groves, D. Yuan, and J. Meiman. 2004. South China karst aquifer storm-scale hydrochemistry. *Ground Water* 42, no. 4: 491-499.

Luhmann, A.J., M.D. Covington, S.C. Alexander, S.Y. Chai, B.F. Schwartz, J.T. Groten, and E.C. Alexander, Jr. 2011. Comparison of discharge, chloride, temperature, uranine, δD, and suspended sediment responses from a multiple tracer test in karst. In *Proceedings of the 12th Multidisciplinary Conference on Sinkholes and the Engineering and Environmental Impacts of Karst*, ed. J. Caldwell and L. Yuhr. In press.

Luhmann, A.J., M.D. Covington, S.C. Alexander, S.Y. Chai, B.F. Schwartz, J.T. Groten, and E.C. Alexander, Jr. 2011. Comparing natural and artificial tracers in karst and using them to estimate flow path geometry. In review, submitted to *Journal of Hydrology*.

Luhmann, A.J., M.D. Covington, A.J. Peters, S.C. Alexander, C.T. Anger, J.A. Green, A.C. Runkel, and E.C. Alexander, Jr. 2011. Classification of thermal patterns at karst springs and cave streams. *Ground Water* 49, no. 3: 324-335.

Maillet, E. 1905. *Essais d'Hydraulique souterraine et fluviale*. Paris: Hermann.

Manga, M. 2001. Using springs to study groundwater flow and active geologic processes. *Annual Review of Earth and Planetary Sciences* 29, 201-228.

Markle, J.M., and R.A. Schincariol. 2007. Thermal plume transport from sand and gravel pits – Potential thermal impacts on cool water streams. *Journal of Hydrology* 338, no. 3-4: 174-195.

Martin, J.B., and R.W. Dean. 1999. Temperature as a natural tracer of short residence times for groundwater in karst aquifers. In *Karst Modeling, Karst Waters Institute Special Publication 5*, ed. A.N. Palmer, M.V. Palmer, and I.D. Sasowsky, 236-242. Charles Town, WV: Karst Waters Institute.

Martin, J.B., and R.W. Dean. 2001. Exchange of water between conduits and matrix in the Floridan Aquifer. *Chemical Geology* 179, no. 1-4: 145-165.

Midwestern Regional Climate Center. 2010. http://mcc.sws.uiuc.edu/.

Molson, J.W., E.O. Frind, and C.D. Palmer. 1992. Thermal energy storage in an unconfined aquifer 2. Model development, validation, and application. *Water Resources Research* 28, no. 10: 2857-2867.

Molson, J., P. Pehme, J.A. Cherry, and B.L. Parker. 2007. Numerical analysis of HEAT transport within fractured sedimentary rock: Implications for temperature probes. In *Proceedings of the NGWA/U.S. EPA Fractured Rock Conference: State of the Science and Measuring Success in Remediation*.

Mongelli, F., and P. Pagliarulo. 1997. Influence of water recharge on heat transfer in a semi-infinite aquifer. *Geothermics* 26, no. 3: 365-378.

Moore, P.J., J.B. Martin, and E.J. Screaton. 2009. Geochemical and statistical evidence of recharge, mixing, and controls on spring discharge in an eogenetic karst aquifer. *Journal of Hydrology* 376, no. 3-4: 443-455.

Morey, G.B. 1972. Petrology of Keweenawan sandstones in the subsurface of southeastern Minnesota. In *Geology of Minnesota: A Centennial Volume*, ed. P.K. Sims and G.B. Morey, 436-449. Minneapolis: Minnesota Geological Survey, University of Minnesota.

Morey, G.B. 1982. Bedrock geology of Minnesota. *Rocks and Minerals* 57, no. 3: 109-113.

Mossler, J.H. 1995. Bedrock geology (Plate 2). In *Text Supplement to the Geologic Atlas of Fillmore County, Minnesota, Part C*, ed. R.S. Lively and N.H. Balaban, 1-5. Minnesota Geological Survey County Atlas Series C-8.

Mossler, J.H. 2002. Bedrock geology of Wabasha County, Minnesota. In *Contributions to the geology of Wabasha County, Minnesota*, project manager A.C. Runkel, 6-27. Minnesota Geological Survey Report of Investigations 59.

Mossler, J.H. 2008. Paleozoic stratigraphic nomenclature for Minnesota. Minnesota Geological Survey Report of Investigations 65.

Nash, J.E., and J.V. Sutcliffe. 1970. River flow forecasting through conceptual models part 1 – A discussion of principles. *Journal of Hydrology* 10, no. 3: 282-290.

Newson, M.D. 1971. A model of subterranean limestone erosion in the British Isles based on hydrology. *Transactions of the Institute of British Geographers*, no. 54: 55-70.

Palmer, A.N. 1991. Origin and morphology of limestone caves. *Geological Society of America Bulletin* 103, no. 1: 1-21.

Palmer, A.N. 2007. *Cave Geology*. Dayton, OH: Cave Books.

Palmer, C.D., D.W. Blowes, E.O. Frind, and J.W. Molson. 1992. Thermal energy storage in an unconfined aquifer 1. Field injection experiment. *Water Resources Research* 28, no. 10: 2845-2856.

Perrin, J., P.-Y. Jeannin, and F. Cornaton. 2007. The role of tributary mixing in chemical variations at a karst spring, Milandre, Switzerland. *Journal of Hydrology* 332, no. 1-2: 158-173.

Quinlan, J.F., G.J. Davies, and S.R.H. Worthington. 1992. Rationale for the design of cost- effective groundwater monitoring systems in limestone and dolomite terranes: Cost-effective as conceived is not cost-effective as built if the system design and sampling frequency inadequately consider site hydrogeology. In *8th Waste Testing and Quality Assurance Symposium Proceedings*, 552-570. Washington, D.C.: U.S. Environmental Protection Agency.

Quinlan, J.F., and J.A. Ray. 1995. Normalized base-flow discharge of groundwater basins: A useful parameter for estimating recharge area of springs and for recognizing drainage anomalies in karst terranes. In *Proceedings, Karst Geohazards: Engineering and Environmental Problems in Karst Terrane*, ed. B.F. Beck, 149-164. Rotterdam: A.A. Balkema.

Raeisi, E., C. Groves, and J. Meiman. 2007. Effects of partial and full pipe flow on hydrochemographs of Logsdon river, Mammoth Cave Kentucky USA. *Journal of Hydrology* 337, no. 1-2: 1-10.

Ritorto, M., E.J. Screaton, J.B. Martin, and P.J. Moore. 2009. Relative importance and chemical effects of diffuse and focused recharge in an eogenetic karst aquifer: an example from the unconfined upper Floridan Aquifer, USA. *Hydrogeology Journal* 17, no. 7: 1687-1698.

Roy, B., and Y. Benderitter. 1986. Transferts thermiques naturels dans un système aquifer carbonate fissure peu profound. *Bulletin de la Société Géologique de France* 2, no. 4: 661-666.

Runkel, A.C., R.G. Tipping, E.C. Alexander, Jr., and S.C. Alexander. 2006. Hydrostratigraphic characterization of intergranular and secondary porosity in part of the Cambrian sandstone aquifer system of the cratonic interior of North America: Improving predictability of hydrogeologic properties. *Sedimentary Geology* 184, no. 3-4: 281-304.

Runkel, A.C., R.G. Tipping, E.C. Alexander, Jr., J.A. Green, J.H. Mossler, and S.C. Alexander. 2003. Hydrogeology of the Paleozoic bedrock in southeastern Minnesota. Minnesota Geological Survey Report of Investigations 61.

Ryan, M., and J. Meiman. 1996. An examination of short-term variations in water quality at a karst spring in Kentucky. *Ground Water* 34, no. 1: 23-30.

Saar, M.O. 2011. Review: Geothermal heat as a tracer of large-scale groundwater flow and as a means to determine permeability fields. *Hydrogeology Journal* 19, no. 1: 31-52.

Sauter, M. 1992. Quantification and forecasting of regional groundwater flow and transport in a karst aquifer (Gallusquelle, Malm, SW. Germany). Ph.D. diss., Tübinger Geowissenschaftliche Arbeiten C13, Institut und Museum für Geologie und Paläontologie, Universität Tübingen.

Screaton, E., J.B. Martin, B. Ginn, and L. Smith. 2004. Conduit properties and karstification in the unconfined Floridan Aquifer. *Ground Water* 42, no. 3: 338-346.

Shuster, E.T., and W.B. White. 1971. Seasonal fluctuations in the chemistry of limestone springs: A possible means for characterizing carbonate aquifers. *Journal of Hydrology* 14, no. 2: 93-128.

Singhal, B.B.S., and R.P. Gupta. 2010. *Applied Hydrogeology of Fractured Rocks*, 2nd ed. Dordrecht: Springer.

Smart, C.C. 1988. Quantitative tracing of the Maligne karst system, Alberta, Canada. *Journal of Hydrology* 98, no. 3-4: 185-204.

Smart, C., and S.R.H. Worthington. 2004. Springs. In *Encyclopedia of Caves and Karst Science*, ed. J. Gunn, 699-703. New York: Fitzroy Dearborn.

Smart, P.L., and S.L. Hobbs. 1986. Characterisation of carbonate aquifers: A conceptual base. In *Proceedings: Environmental Problems in Karst Terranes and Their Solutions*, 1-14. Dublin, OH: National Water Well Association.

Smart, P.L., and P. Hodge. 1980. Determination of the character of the Longwood sinks to Cheddar resurgence conduit using an artificial pulse wave. *Transactions of the British Cave Research Association* 7, no. 4: 208-211.

Springer, A.E., and L.E. Stevens. 2009. Spheres of discharge of springs. *Hydrogeology Journal* 17, no 1: 83-93.

Stallman, R.W. 1963. Computation of ground-water velocity from temperature data. In *Methods of Collecting and Interpreting Ground-Water Data*, ed. R. Bentall, 36-46. Water Supply Paper 1544-H. Washington, DC: USGS.

Stallman, R.W. 1965. Steady one-dimensional fluid flow in a semi-infinite porous medium with sinusoidal surface temperature. *Journal of Geophysical Research* 70, no. 12: 2821-2827.

Suzuki, S. 1960. Percolation measurements based on heat flow through soil with special reference to paddy fields. *Journal of Geophysical Research* 65, no. 9: 2883-2885.

Swanson, S.K., J.M. Bahr, K.R. Bradbury, and K.M. Anderson. 2006. Evidence for preferential flow through sandstone aquifers in southern Wisconsin. *Sedimentary Geology* 184, no. 3-4: 331-342.

Tallaksen, L.M. 1995. A review of baseflow recession analysis. *Journal of Hydrology* 165, no. 1-4: 349-370.

Ternan, J.L. 1972. Comments on the use of a calcium hardness variability index in the study of carbonate aquifers: With reference to the Central Pennines, England. *Journal of Hydrology* 16, no. 4: 317-321.

Tipping, R.G., A.C. Runkel, E.C. Alexander, Jr., S.C. Alexander, and J.A. Green. 2006. Evidence for hydraulic heterogeneity and anisotropy in the mostly carbonate Prairie du Chien Group, southeastern Minnesota, USA. *Sedimentary Geology* 184, no. 3-4: 305-330.

Vacher, H.L., and J.E. Mylroie. 2002. Eogenetic karst from the perspective of an equivalent porous medium. *Carbonates and Evaporites* 17, no. 2: 182-196.

van der Kamp, G., and S. Bachu. 1989. Use of dimensional analysis in the study of thermal effects of various hydrogeological regimes. In *Hydrogeological Regimes and Their Subsurface Thermal Effects*, ed. A.E. Beck, G. Garven, and L. Stegena, 23-28, Geophysical Monograph 47. Washington, DC: American Geophysical Union.

Vojtechovska, A., J. Bruthans, and F. Krejca. 2010. Comparison of conduit volumes obtained from direct measurements and artificial tracer tests. *Journal of Cave and Karst Studies* 72, no. 3: 156-160.

Wang, K., P.-Y. Shen, and A.E. Beck. 1989. A solution to the inverse problem of coupled hydrological and thermal regimes. In *Hydrogeological Regimes and Their Subsurface Thermal Effects*, ed. A.E. Beck, G. Garven, and L. Stegena, 7-22, Geophysical Monograph 47. Washington, DC: American Geophysical Union.

White, W.B. 1988. *Geomorphology and Hydrology of Karst Terrains*. New York: Oxford University Press.

White, W.B. 1989. Introduction to the karst hydrology of the Mammoth Cave Area. In *Karst Hydrology: Concepts from the Mammoth Cave Area*, ed. W.B. White and E.L. White, 1-13. New York: Van Nostrand Reinhold.

White, W.B. 1999. Conceptual models for karstic aquifers. In *Karst Modeling, Karst Waters Institute Special Publication 5*, ed. A.N. Palmer, M.V. Palmer, and I.D. Sasowsky, 11-16. Charles Town, WV: Karst Waters Institute.

White, W.B. 2002. Karst hydrology: Recent developments and open questions. *Engineering Geology* 65, no. 2-3: 85-105.

White, W.B., and E.L. White. 1989. *Karst Hydrology: Concepts from the Mammoth Cave Area*. New York: Van Nostrand Reinhold.

Williams, P., and Y.T. Fong. 2010. "World Map of Carbonate Rock Outcrops v3.0," The University of Auckland, School of Environment, http://web.env.auckland.ac.nz/our_research/karst/.

Woodbury, A.D., and L. Smith. 1988. Simultaneous inversion of hydrogeologic and thermal data, 2. Incorporation of thermal data. *Water Resources Research* 23, no. 8: 356-372.

Worthington, S.R.H. 1999. A comprehensive strategy for understanding flow in carbonate aquifers. In *Karst Modeling, Karst Waters Institute Special Publication 5*, ed. A.N. Palmer, M.V. Palmer, and I.D. Sasowsky, 30-37. Charles Town, WV: Karst Waters Institute.

Worthington, S.R.H., G.J. Davies, and J.F. Quinlan. 1992. Geochemistry of springs in temperate carbonate aquifers: Recharge type explains most of the variation. In *Cinquième Colloque d'Hydrologie en Pays Calcaire et en Milieu Fissuré. Fifth Colloquium on Hydrology in limestone and fractured environment*, ed. P. Chauve and F. Zwahlen, 341-347. Besançon, France: Université de Besançon.

Worthington, S.R.H., D.C. Ford, and P.A. Beddows. 2000. Porosity and permeability enhancement in unconfined carbonate aquifers as a result of solution. In *Speleogenesis: Evolution of Karst Aquifers*, ed. A.V. Klimchouk, D.C. Ford, A.N. Palmer, and W. Dreybrodt, 220-223. Huntsville, AL: National Speleological Society of America.

Zoback, M.L., and M.D. Zoback. 1989. Tectonic stress field of the continental United States. In *Geophysical Framework of the Continental United States*, ed. L.C. Pakiser and W.D. Mooney, 523-539. Boulder, CO: Geological Society of America.

Appendix A

Temperature, electrical conductivity, water level, discharge, and precipitation data and field notes from monitoring sites

I deployed and maintained data loggers at twelve springs, five surface streams, and two cave streams. Data were collected at each site for at least some portion of the entire monitoring period from August 2008 to May 2011. All loggers measured and recorded temperature. Campbell Scientific data loggers also measured and recorded electrical conductivity, and most of the Campbell loggers measured and recorded water level as well. Weirs were installed at Freiheit Spring and the ephemeral stream in the Cherry Grove Blind Valley Scientific and Natural Area (SNA) to convert water level to discharge. The weir at Freiheit was in place for only a portion of the entire monitoring period at the spring. The weir at the Cherry Grove Blind Valley SNA was in place during the entire monitoring period there. Finally, precipitation data were collected above Goliath Cave and Bat River Cave.

This appendix primarily includes manual measurements and field notes from every field site to aid the future user of this data. Text files that contain the data recorded by data loggers are included online as supplementary files to this thesis. File names are included in this appendix near the beginning of each monitoring site section. The name of each text file generally includes the Karst Features Database (KFDB) number for the site, the dates that bracket the monitoring period, and letter codes that indicate the kind of data available in each file. Letter codes include T (temperature in ºC), C (electrical conductivity in µS/cm), L (water level in ft), D (discharge in L/sec), V (voltage), P (precipitation in in), and I (light intensity in lux). The order of the letter codes indicate the column order of the data in each file. Thus, a file with "TCL" in its filename indicates that the final three columns in the file correspond to temperature, electrical conductivity, and water level, respectively, which follow the initial columns specifying date and time of the data. Light intensity is included in files collected by HOBO data loggers because these loggers had a tendency to heat up when exposed to direct sunlight and record high values. Thus, when light intensity is > 0 lux, water temperature data is not as accurate.

The first three columns of the text files that include the Campbell data logger data correspond to the year, day of year, and time (in HHMM), respectively, when each data point was recorded. There were 366 days in 2008 because it was a leap year; thus, Dec. 31, 2008 is day 366. There were 365 days in 2009-2011; thus, Dec. 31 for each of these years corresponds to day 365. The first four columns of the text files that include the data collected by HOBO loggers correspond to the year, month, day of month, and time, respectively, when each data point was recorded.

Most of the data logger data are the raw data that were collected, unless otherwise noted. I have not spent the time to clean it up for three reasons. First, it would take a

long time to do so. Second, cleaning up the data is somewhat subjective. And third, it will be easier for a future user of this data to identify problems with the raw data if I have not already modified it with my own subjective method. I have included all of my relevant field notes in this appendix. This includes the dates and times that I downloaded my data loggers to indicate times when I may have moved a pressure transducer, etc.

Times of manual measurements provided in this appendix observe Daylight Savings Time shifts. However, time on data loggers was always set to equivalent summer time. Thus, times in data logger files agree with Daylight Savings Time when it is in place (i.e., ~March to November), and are one hour ahead during non-Daylight Savings Time months (i.e., ~November to March).

Electrical conductivity is a temperature dependent variable. Therefore, the *in situ* temperature is generally recorded when a conductivity measurement is made. An empirical equation is then commonly used to convert the conductivity value to a temperature corrected conductivity value at some reference temperature to facilitate comparison of measurements made at different temperatures. Sorensen and Glass (1987) and Talbot et al. (1990) compare some of the most commonly used empirical equations that describe conductivity's temperature dependence. This thesis uses the following equation:

$$C_e(25°C) = \frac{C_e(T)}{1 - K(25 - T)}, \tag{A.1}$$

where C_e is electrical conductivity at a temperature T in ºC, K is a constant that characterizes the temperature dependence of electrical conductivity, and 25 is the reference temperature in ºC. However, the electrical conductivity data in this thesis may be temperature corrected using a different empirical equation with the reported temperatures and electrical conductivities if a future user so desires.

Talbot et al. (1990) obtained K using several river water samples in England, including some taken from carbonate areas. Talbot et al.'s (1990) mean K is 0.0192. Ground water chemistry in Minnesota has more magnesium than the water's reported in Talbot et al. (1990). However, the primary components in both regions are HCO_3^- and Ca^{2+}. Therefore, this thesis uses Talbot et al.'s (1990) value to two significant digits or 0.019. Text files that contain Campbell data logger data include temperature corrected conductivity. Manual measurements in the tables of this appendix include both non-temperature-corrected conductivity and temperature-corrected conductivity (TC Cond.).

The Thermo Orion 105 conductivity probe used for manual electrical conductivity measurements was calibrated periodically. Calibrations involved four standards: deionized water and three KCl standards that ranged from approximately 0.002 to 0.007 M KCl. KCl standards were prepared by mixing KCl and deionized water in a 1L Nalgene bottle. The mass of KCl and deionized water was recorded, and deionized water was boiled with heat or a vacuum pump to remove CO_2 (aq). The mass of deionized water was then divided by water density at 25ºC to determine deionized water volume and enable molarity concentrations to be determined. The standards were put in a water bath overnight, and conductivity, temperature-corrected conductivity, and temperature were recorded the following day for each of the standards. Golterman et al. (1978, Section 3.1) and APHA (1992, Section 2510 Conductivity) were used to determine what the conductivity should have been for each standard at a given temperature. Then the cell

constant in the conductivity probe was adjusted so that measurements were generally <1% of the expected value at the measured temperature. Additional measurements were conducted to confirm the new cell constant. New standards were prepared on Jan. 13, 2009; Mar. 13, 2009; and Mar. 22, 2010. The cell constant was confirmed or changed on the following days: Jan. 15, 2009; Feb. 13, 2009; Mar. 16, 2009; Apr. 17, 2009; May 26, 2009; June 22, 2009; Aug. 24, 2009; Oct. 15, 2009; Dec. 11, 2009; Mar. 23, 2010; May 4, 2010. The Engineered Systems & Designs (ESD) conductivity probe was purchased and used for manual measurements beginning in June 2010 because the Thermo Orion 105 conductivity probe no longer worked consistently. However, the ESD conductivity probe was never calibrated.

Finally, most of the table footnotes in this appendix indicate the glass thermometer or the conductivity probe used to make manual measurements. The same superscript letter is used for each thermometer/probe throughout this appendix for consistency. These general footnotes are only listed here to avoid redundancy and include the following:

[a] glass thermometer #3314.
[b] glass thermometer #3336.
[c] glass thermometer #3314, liquid separated in thermometer.
[d] Thermo Orion 105 conductivity probe.
[e] Engineered Systems & Designs (ESD) conductivity probe.
[f] glass thermometer #2499.

MN23:A0001 (Seven Springs)
Hobo and Campbell: 557889 m E, 4830462 m N (± 4.4 m) - This UTM location was taken ~ 7 m from the emanation point.

Data Logger Files
MN23A0001_100501-110203_TI.txt
MN23A0001_110203-110502_TCL.txt

Data Logger Notes
HOBO data logger installed: May 1, 2010.
HOBO data logger downloaded: Aug. 19, 2010 17:12; Oct. 20, 2010 12:03; Feb. 3, 2011 10:41.
HOBO data logger removed: Feb. 3, 2011.
Campbell data logger installed: Feb. 3, 2011.
Campbell data logger downloaded: Mar. 16, 2011 12:07; May 2, 2011 14:55.
Campbell data logger removed: May 2, 2011.

Table A.1. Manual measurements at MN23:A0001 (Seven Springs).

Year	Month	Day	Time	Temp. (ºC)	Cond. (µS/cm)	TC Cond. (µS/cm)	Time	Depth to Water [g] (ft)
2010	5	1	11:35	11.85 [b]	321 [d]	428		
2010	8	19	~17:25	18.0 [a]	462 [e]	533		
2010	10	20	~12:10	11.2 [a]	409 [e]	554		
2011	2	3	10:40	2.85 [a]	343 [e]	592		
2011	3	16	12:22	4.85 [a]	326 [e]	528	12:39	2.92
2011	5	2	15:10	7.5 [f]	339 [e]	508	15:15	2.75

See page 103 for general footnotes [a-f].
[g] Measured from a point on a rock above the water surface.

Field Notes
Mar. 16, 2011: Temperature/conductivity probe and pressure transducer had been moved by spring flow. The pressure transducer was at the surface of the flow when we first got here. I moved them at 12:10 and covered them with rocks.
May 2, 2011: I moved some rocks where I measure depth to water before I did this measurement.

MN23:A0033 (Trout Spring)
562517 m E, 4828219 m N (± 8.4 m)

Data Logger Files
MN23A0033_090904-100819_TCL.txt

Data Logger Notes
Campbell data logger installed: Sept. 4, 2009.
Campbell data logger downloaded: Sept. 30, 2009 18:06; Nov. 20, 2009 11:12; Jan. 6, 2010 12:38; Feb. 12, 2010 11:42; Mar. 24, 2010 11:25; May 5, 2010 11:30-12:00; June 16, 2010 12:46; July 15, 2010 12:35; Sept. 1, 2010 14:44.
Campbell data logger removed: Aug. 19, 2010.

Table A.2. Manual measurements at MN23:A0033 (Trout Spring).

Year	Month	Day	Time	Temp. (ºC)	Cond. (µS/cm)	TC Cond. (µS/cm)	Time	Depth to Water [g] (ft)
2009	9	4	15:55	9.3 [a]	431 [d]	614		
2009	9	30	18:38	9.1 [a]	432 [d]	619		
2009	11	20	~11:40	8.6 [a]	419 [d]	609	~11:45	3.81
2010	1	6	12:52	8.0 [a]	413 [d]	610	12:55	4.01
2010	2	12	11:59	8.15 [a]	418 [d]	615	12:02	4.11
2010	3	24	11:45	8.1 [a]	386 [d]	569	11:54	3.51
2010	5	5	12:17	9.3 [b]	392 [d]	559	12:23	3.73
2010	6	16	13:10	10.5 [a]	382 [e]	527	13:14	3.38
2010	7	15	13:25	10.0 [c]	432 [e]	604	13:31	3.46
2010	8	19	15:20	9.8 [a]	442 [e]	621	15:26	3.69
2011	3	16	10:55	7.7 [a]	368 [e]	548		

See page 103 for general footnotes [a-f].
[g] Measured from a corner of a rock above the water surface.

Field Notes
Sept. 30, 2009: I moved the temperature/conductivity probe and pressure transducer. I also measured discharge (see Appendix D for details).
Nov. 20, 2009: Temperature/conductivity probe and pressure transducer were moved (possibly by a storm pulse) since last time I was here (Sept. 30, 2009). I checked the internal opening of the temperature/conductivity probe, and it contained no sediment.
Mar. 24, 2010: Depth to water hand measurement is ± 3/8 in because of rapid flow.
June 16, 2010: Depth to water hand measurement is ± 1/4 in.
July 15, 2010: The data logger was moved since last time I was here (June 16, 2010). The temperature shown by the logger is significantly different from my hand measurement. Looking at the data, someone or something messed with the logger between 7:30 and 8:00 on July 5, 2010. I accidently stopped

the logger, but I got it running again at 13:09. I moved the temperature/conductivity probe and pressure transducer at ~13:35. I cleaned algae from the temperature/conductivity probe.

Aug. 19, 2010: The tip of the rock that I use for my depth to water hand measurement had been broken off. Therefore, there is more error in this measurement. I couldn't download the data logger because it was wet. However, I was able to download the data from the data logger back in the lab on Sept. 1, 2010. Still, absolute values of temperature data recorded by data logger were incorrect since 8:00 on July 5, 2010; this error affects conductivity measurements.

MN23:A0034 (Black Rock Spring)
562574 m E, 4828227 m N (± 7.7 m)

Data Logger Files
MN23A0034_100928-110502_TCL.txt

Data Logger Notes
Campbell data logger installed: Sept. 28, 2010.
Campbell data logger downloaded: Nov. 10, 2010 13:27; Dec. 20, 2010 11:08; Feb. 3, 2011 12:00; Mar. 16, 2011 10:04; May 2, 2011 10:53.
Campbell data logger removed: May 2, 2011.

Table A.3. Manual measurements at MN23:A0034 (Black Rock Spring).

Year	Month	Day	Time	Temp. (ºC)	Cond. (µS/cm)	TC Cond. (µS/cm)	Time	Depth to Water [g] (ft)
2009	11	20	11:48	8.6 [d]	420 [d]	610		
2010	8	19	~15:40	9.8 [a]	443 [e]	623		
2010	9	28	~14:17	10.05 [a]	436 [e]	609	14:27	0.688
2010	11	10	13:44	8.8 [a]	431 [e]	623	13:49	1.667
2010	12	20	11:23	8.1 [a]	416 [e]	613		
2011	2	3	12:17	8.1 [a]	424 [e]	625		
2011	3	16	10:14	7.8 [a]	368 [e]	547		
2011	5	2	10:59	8.35 [f]	406 [e]	594	11:03	1.042

See page 103 for general footnotes [a-f].
[g] Measured from a corner of a rock above the water surface.

Field Notes
Sept. 30, 2009: I measured discharge (see Appendix D for details).
Nov. 10, 2010: At 13:52, there was no sediment in the internal opening of the temperature/conductivity probe. I moved both the temperature/conductivity probe and the pressure transducer deeper in the water at 13:53. Water level was much lower than last time when logger was installed (Sept. 28, 2010).
Dec. 20, 2010: I didn't take a depth to water hand measurement because there was a large snow pile at the emanation point.
Feb. 3, 2011: I didn't take a depth to water hand measurement because there was a large snow pile at the emanation point.
Mar. 16, 2011: I didn't take a depth to water hand measurement because there was a large snow pile at the emanation point.
May 2, 2011: I found the pressure transducer out of water.

MN23:A0041 (Freiheit Spring – Downstream Emanation)
554978 m E, 4839445 m N (± 3.5 m)

Data Logger Files
MN23A0041_081031-110502_TCLD.txt
Like all other text files including data collected with a Campbell data logger, the first three columns of this text file correspond to the year, day of year, and time, respectively, when each data point was recorded. The fourth column includes time in seconds in addition to time provided in the third column (in HHMM) when high-resolution data were recorded during two pool traces.

Data Logger Notes
Campbell data logger installed: Oct. 31, 2008.
Campbell data logger downloaded: Nov. 24, 2008 10:39; Dec. 19, 2008 11:22; Jan. 19, 2009 10:28; Feb. 16, 2009 10:20; Mar. 18, 2009 11:10; Mar. 29, 2009 10:10; Mar. 29, 2009 18:30-19:00; Apr. 24, 2009 10:34; May 28, 2009 19:09; June 3, 2009 10:42; June 3, 2009 12:57; June 9, 2009 18:54; June 17, 2009 12:49; June 17, 2009 18:39; June 24, 2009 15:13; June 26, 2009 11:00-11:30; July 2, 2009 12:01, 13:41, 18:37; July 14, 2009 13:57; Aug. 26, 2009 14:26; Sept. 25, 2009 14:00-14:30; Oct. 24, 2009 13:33; Nov. 20, 2009 14:11; Jan. 6, 2010 9:49; Feb. 12, 2010 10:16; Mar. 24, 2010 9:37; May 5, 2010 9:35; May 27, 2010 13:51; June 10, 2010 12:00; June 16, 2010 16:21; July 15, 2010 16:26; Aug. 19, 2010 19:07; Aug. 26, 2010 11:35; Aug. 30, 2010 11:47, 15:35, 16:49, 17:32; Aug. 31, 2010 11:50; Sept. 2, 2010 15:37, 19:20; Sept. 28, 2010 10:47; Nov. 10, 2010 10:35; Dec. 20, 2010 13:56; Feb. 3, 2011 15:27; Mar. 16, 2011 18:56; May 2, 2011 20:37.
Campbell data logger removed: May 2, 2011.
The data logger was temporarily removed on Aug. 26, 2009 and reinstalled on Sept. 4, 2009.

Table A.4. Manual measurements at MN23:A0041 (Freiheit Spring – Downstream Emanation).

Year	Month	Day	Time	Temp. (ºC)	Cond. (µS/cm)	TC Cond. (µS/cm)	Time	Depth to Water [g] (ft)	Time	Depth to Water [h] (ft)
2008	10	31		8.7 [a]	422 [d]	611				
2008	11	24		8.7 [a]	419 [d]	607				
2008	12	19		8.7 [a]	420 [d]	609				
2009	1	19	~10:45	8.7 [a]	417 [d]	604				
2009	2	16	10:44	7.45 [a]	350 [d]	525				
2009	3	18	11:27	7.6 [a]	324 [d]	484				
2009	3	29	~19:10	8.1 [a]	369 [d]	544				
2009	4	24	16:06	8.4 [a]	391 [d]	571	~15:55	1.148		
2009	5	27	16:00	8.7 [a]	391 [d]	566	15:55	0.990		
2009	5	27	19:42	8.7 [a]	393 [d]	569	19:46	0.995		
2009	5	28	19:17	8.6 [a]	379 [d]	551	~19:20	0.995		

2009	6	3	12:37	9.1 [a]	379 [d]	543	~13:55	0.969		
2009	6	8	15:55	8.8 [a]	324 [d]	468	~15:55	0.708		
2009	6	8	18:44	8.9 [a]	298 [d]	429				
2009	6	9	9:47	9.2 [a]	344 [d]	492	9:57	0.750		
2009	6	9	14:34	9.05 [a]	348 [d]	499				
2009	6	9	17:38	9.0 [a]	347 [d]	499	17:44	0.750		
2009	6	17	17:31	9.0 [a]	376 [d]	540	17:36	0.865		
2009	6	24	15:23	9.45 [a]	384 [d]	545	14:33	0.896		
2009	7	2	14:55		399 [d]	567	11:52	0.979		
2009	7	2	15:05	9.4 [a]						
2009	7	14	13:25	9.2 [a]	395 [d]	564				
2009	8	26	11:41	8.7 [a]			11:38	1.099		
2009	8	26	15:51	8.8 [a]	403 [d]	582	15:55	1.099		
2009	9	4	11:52	8.7 [a]	403 [d]	584	11:55	1.036		
2009	9	22					19:09	1.047		
2009	9	25	14:37	8.7 [a]	405 [d]	587	14:39	1.026		
2009	10	24	14:03	8.7 [a]	392 [d]	568	14:05	1.047		
2009	11	20	14:35	8.65 [a]	398 [d]	577	14:31	1.156		
2010	1	6	10:11	8.5 [a]	404 [d]	588	10:16	1.247		
2010	2	12	10:30	8.5 [a]	403 [d]	587	10:34	1.245		
2010	3	24	9:51	7.85 [a]	360 [d]	534	9:58	1.02 [i]		
2010	5	5	10:33	8.8 [b]	388 [d]	561	9:57	1.151		
2010	5	5					10:10	1.073		
2010	5	5					10:39	1.073		
2010	5	27					14:00	0.172		
2010	6	10					12:10	0.281		
2010	6	16	16:33	9.3 [a]			16:36	-0.010	16:38	0.406
2010	7	15	16:38	10.0 [c]	379 [e]	530	16:45	0.208	16:49	0.620
2010	8	19	19:19	9.05 [a]	412 [e]	591	19:26	0.302	19:31	0.745
2010	8	25	18:25	9.05 [a]	415 [e]	595	18:16	0.307	18:18	0.719
2010	8	26	8:49	9.1 [a]	423 [e]	606	10:20	0.307	10:21	0.719
2010	8	30	14:00	8.65 [a]	402 [e]	583	14:07	0.318	14:10	0.734
2010	8	31	13:03	8.8 [a]	415 [e]	600	13:12	0.318	13:14	0.740
2010	9	2	14:30	9.1 [a]	407 [e]	583	14:41	0.318	14:39	0.734
2010	9	28							9:07	0.276

2010	9	28							9:37	0.276
2010	9	28	10:10	10.55 [a]	432 [e]	595	11:06	-0.135	11:10	0.281
2010	9	28					11:26	-0.128	11:24	0.281
2010	11	10	10:49	8.95 [a]	423 [e]	609	10:58	0.333	11:00	0.740
2010	12	20	14:09	8.5 [a]	420 [e]	612	14:18	0.297	14:21	0.698
2011	2	3	15:42	8.4 [a]	403 [e]	589	15:45	0.354	15:49	0.755
2011	3	16	19:05	8.1 [j]	379 [e]	558	19:12	0.063	19:13	0.458
2011	5	2	20:27	8.0 [f]	382 [e]	563			18:22	0.313

See page 103 for general footnotes [a-f].

[g] Measured from the top of the pole where the pressure transducer was attached.

[h] Measured from the top of the weir.

[i] Water depth measurement is ± 0.01 ft because of high water with fluctuating levels.

[j] Temperature measurement from data logger.

Notes

The pressure transducer was initially covered by a rock in a pool just downstream of the emanation. On Apr. 24, 2009, the pressure transducer was attached to a pole, and the pole was pounded into the pool bottom to hopefully prevent the pressure transducer from moving. The pressure transducer was changed on May 5, 2010 (see Field Note below). A 120º v-notch weir was installed at Freiheit Spring on May 26, 2010. Some water leaked around the right edge of the weir structure following its construction. This leak was fixed on Aug. 25, 2010. However, the leak reappeared at least by Oct. 20, 2010 and was still present when the weir was removed on May 2, 2011.

The Freiheit Spring text file which includes the data recorded by the data logger contains water level from Oct. 31, 2008-May 26, 2010 and water level and discharge from May 27, 2010-May 2, 2011. Discharge measurements may be used to develop a rating curve from Oct. 31, 2008-May 26, 2010 (see Appendix D). The survey and manual level measurement on Aug. 31, 2010 were used to determine water level above the bottom of the v-notch. Thus, water level in the text file from May 27, 2010-May 2, 2011 is level above the bottom of the v-notch. Discharge was determined using the equation for a 120º v-notch weir:

$$Q = 4.33H^{2.5}, \tag{A.2}$$

where Q is discharge in ft^3/sec and H is the height of water above the bottom of the v-notch in feet. (The distance from the v-notch to the top of the weir structure was 1.23 ft. Thus, if water level was more than 1.23 ft above the v-notch, then discharge is underestimated.) Discharge was then calibrated using the salt dilution discharge measurements from Aug. 25 – Sept. 28, 2010 (see Appendix D). Discharge is included in the text file with units of liters/sec. However, there was flow around the right edge of the weir from May 26, 2010 to Aug. 25, 2010 and from sometime between Sept. 28 and Oct. 20, 2010 to May 2, 2011. Furthermore, the landowners put a grate in front of the v-notch from sometime between Aug. 26 and 30, 2010 to sometime between Sept. 28 and Oct. 20, 2010. Both of these factors introduce additional error in discharge values. I removed the grate on the days that I was at Freiheit Spring.

Three multiple tracer tests were conducted at Freiheit Spring. Chapter 3 documents the second trace on Aug. 30, 2010. The initial one was conducted on July 2, 2009. For this trace, a smaller, plastic swimming pool was filled next to sinkhole MN23:D2631 with approximately 4,500 L of groundwater from the Kolling well. 2.508 kg of NaCl and 2.518 kg of NaBr were added to the water to increase its conductivity. Just before the pool

water was poured into the sinkhole, the water had a temperature-corrected electrical conductivity of 2050 µS/cm (1.9% per ºC from 25ºC) and a temperature of 15.8 ºC. The draining of the pool began at 14:15. It took approximately 12 minutes for the pool to completely drain. Some ponding occurred in the sinkhole while the pool was drained, but the sinkhole was completely drained within a couple of minutes after we were done pouring water out of the pool.

The third multiple tracer test was conducted at Freiheit Spring on Sept. 2, 2010. The larger, plastic swimming pool was again filled next to sinkhole MN23:D2631 with groundwater from the Kolling well on Aug. 30-31, 2010. The water was heated using one propane burner and a 55 L washtub for several hours on Sept. 2, 2010. 33.02 kg of salt were added to the water to increase its conductivity. Just before the water in the pool was poured into the sinkhole, the water had a temperature-corrected conductivity of 4610 µS/cm (1.9% per ºC from 25ºC) and a temperature of 21.6 ºC. Pool volume for the second trace was 13,633 ± 2% L. Unlike the Aug. 30, 2010 trace, samples were not analyzed for anions from this trace. However, pool volume, V_2, was determined for the Sept. 2, 2010 trace with the following equation:

$$V_2 = \frac{V_1 M_2 C_{e,2}}{M_1 C_{e,1}}, \tag{A.3}$$

where V_1 is pool volume during the trace on Aug. 30, 2010, M_1 and M_2 are the mass of salt that was added to the pool for the Aug. 30, 2010 and Sept. 2, 2010 traces, respectively, and $C_{e,1}$ and $C_{e,2}$ are temperature-corrected electrical conductivities in the pool during the Aug. 30, 2010 and Sept. 2, 2010 traces, respectively. Some of the pool was released into the sinkhole from 16:27 to 16:28. The average pool depth at this point was 40.2 cm, down from a depth of 89.1 cm before the pour. The rest of the pool was released into the sinkhole in three min and fifty-five s, beginning at 16:52. Water did not pond during the second release. A little more than half of the pool depth was poured during the first release because the pool was wider at its base. We tried to pour two slugs of water that were approximately equal in volume.

Field Notes

Jan. 19, 2009: I scraped the internal opening of the temperature/conductivity probe with a stick, but it appeared clean.
Feb. 16, 2009: I cleaned the internal opening of the temperature/conductivity probe, but it appeared clean. The probe was out from the emanation point, but it was still under water. I moved the pressure transducer.
Mar. 29, 2009: I removed some sediment from the internal opening of the temperature/conductivity probe.
Apr. 24, 2009: I cleaned the internal opening of the temperature/conductivity probe, but it appeared clean. I also measured discharge (see Appendix D for details).
May 5, 2009: I cleaned the internal opening of the temperature/conductivity probe, but it appeared clean.
May 27, 2009: I measured discharge twice (see Appendix D for details).
May 28, 2009: I measured discharge (see Appendix D for details).
June 3, 2009: I scraped the internal opening of the temperature/conductivity probe, but it appeared clean. I also measured discharge (see Appendix D for details).
June 8, 2009: I measured discharge four times (see Appendix D for details).
June 9, 2009: I measured discharge twice (see Appendix D for details).
June 17, 2009: At 17:23, I removed sediment from the internal opening of the temperature/conductivity probe. I also measured discharge (see Appendix D for details).

June 24, 2009: At 13:10, I scraped the internal opening of the temperature/conductivity probe, but it appeared clean. I also measured discharge (see Appendix D for details).
July 2, 2009: I removed the extra ISCO program from the data logger; the data logger with only pressure transducer and temperature/conductivity probe instructions was running at 12:30. At 13:48, I changed the data logger output interval to 1 minute. At18:37, I changed the data logger output interval to 10 minutes.
July 14, 2009: I changed the data logger output interval to 30 minutes. I also measured discharge (see Appendix D for details).
Aug. 26, 2009: I removed the data logger from Freiheit Spring because it wasn't working properly.
Sept. 4, 2009: I reinstalled the data logger at Freiheit Spring. I also measured discharge (see Appendix D for details).
Sept. 22, 2009: I measured discharge (see Appendix D for details).
Sept. 25, 2009: I cleaned the internal opening of the temperature/conductivity probe; there was a little bit of sediment at one end of the opening.
Oct. 24, 2009: I accidently disconnected one of the pressure transducer wires from the data logger when I moved the logger to dry out the inside of the containment box. At ~14:15, I disconnected the red wire for the temperature/conductivity probe from the data logger, then retrimmed and reconnected it. Water temperature on the data logger doesn't agree with my manual temperature measurement.
At 14:24, I checked the internal opening of the temperature/conductivity probe, but it appeared clean.
Nov. 20, 2009: I changed the data logger and the temperature/conductivity probe.
Mar. 24, 2010: There was no sediment in the internal opening of the temperature/conductivity probe at 10:02.
May 5, 2010: I changed the pressure transducer, and it was connected to the data logger at 10:20. I measured the water level from a temporary stick both before I removed the old pressure transducer and after I installed the new pressure transducer, and water level remained constant during the change. At 10:45, I removed a few grains of sediment from the internal opening of the temperature/conductivity probe.
May 26, 2010: Calvin Alexander, Scott Alexander, and Cale Anger installed a 120º v-notch weir at Freiheit Spring. There was a little water flowing around the right edge of the weir. See survey notes on Aug. 26, 2010 and Aug. 31, 2010 for distances between the bottom of the weir's v-notch and locations where depth to water measurements were taken.
May 27, 2010: The data logger was recording error values for water level. I reprogrammed the data logger with a larger range for the pressure transducer.
June 16, 2010: I forgot to check the internal opening of the temperature/conductivity probe for sediment.
July 15, 2010: At 16:42, I removed a little sediment from the internal opening of the temperature/conductivity probe. There was some water flowing in from the right side of the weir structure, so all of the flow is not flowing through the v-notch. I'm not sure if the water flowing around the weir structure is more now than other times since the weir was built. There does appear to be air below the downstream side of the v-notch.
Aug. 19, 2010: At 19:24, I removed a little bit of sediment from the internal opening of the temperature/conductivity probe. At 19:29, I cleared a few small sticks and other debris at the v-notch. There is air below the downstream side of the v-notch. There appears to be more water coming in from the right side of the weir structure than there was last time (July 15, 2010).
Aug. 25, 2010: We started working to repair the leak on the right side of the weir structure at ~13:00. The leak was stopped sometime between 13:30-14:30. I measured discharge twice (see Appendix D for details).
Aug. 26, 2010: I conducted a survey at Freiheit Spring. The top of the fencepost in the pond where depth to water measurements are taken is 0.81 ft higher than the bottom of the weir's v-notch. At 11:39, I checked the internal opening of the temperature/conductivity probe, but it appeared clean. I also measured discharge twice (see Appendix D for details).
Aug. 30, 2010: At 10:30, Scott Alexander removed a grate from in front of the v-notch which was obstructing flow. One of the landowners put the grate there sometime since I was here last (Aug. 26, 2010) to keep trout in pond. At 11:50, I changed the data logger output interval to 1 minute. At 12:05, I

checked the internal opening of the temperature/conductivity probe, but it appeared clean. Before the pool was dumped, I reset the time on both data loggers so that they were reading the same time. At 15:54, I changed the data logger output interval to 1 second. At 17:35, I changed the data logger output interval to 1 minute. At ~20:48, I put the grate back in front of the v-notch. I also measured discharge (see Appendix D for details).

Aug. 31, 2010: I moved the grate from in front of the v-notch at 10:39. I changed the data logger output interval to 10 minutes at 11:53. At 13:10, I checked the internal opening of the temperature/conductivity probe, but it appeared clean. I again conducted a survey at Freiheit Spring. The top of the fencepost in the pond where depth to water measurements are taken is 0.81 ft higher than the bottom of the weir's v-notch, in agreement with the survey on Aug. 26, 2010. The top of the weir where additional depth to water measurements are taken is 1.23 ft higher than the bottom of the weir's v-notch. At 14:54, I put the grate back in front of the v-notch. I also measured discharge twice (see Appendix D for details).

Sept. 2, 2010: At ~10:10, I moved the grate from in front of the v-notch. At 11:40, I changed the data logger output interval to 1 minute. At 16:06, I checked the internal opening of the temperature/conductivity probe, but it appeared clean. At 16:10, I changed the data logger output interval to 1 second. At 18:28, I changed the data logger output interval to 1 minute. At 19:20, I changed the data logger output interval to 10 minutes. Between 19:40 and 20:00, I put the grate back in front of the v-notch.

Sept. 28, 2010: At 8:44, I moved the grate from in front of the v-notch. Water was flowing over the weir structure. At 10:49, I changed the data logger output interval to 30 minutes. At 11:02, I removed sediment from the internal opening of the temperature/conductivity probe; it was full of sediment. At 11:08, I moved a small stick and some leaves on the right side of the v-notch that I missed earlier. I used the level recorded by the data logger at 11:30 in my calibration for the discharge measurement at 10:04 (see Appendix D). The 30 minute average level recorded at 11:30 was in agreement with real-time data from the data logger at 11:28, by which time the water level had likely stabilized after I removed the debris at the v-notch at 11:08. At 11:32, I put the grate back in front of the v-notch.

Oct. 20, 2010: The grate was no longer in front of the weir's v-notch. (I emailed the landowners on Oct. 2, 2010 to ask them to remove the grate, and they removed it sometime since then.) There was also no debris in front of the v-notch. However, there appears to be some flow around the right edge of the weir structure again.

Nov. 10, 2010: There was no debris in front of the weir's v-notch. I removed a few grains of sediment from the internal opening of the temperature/conductivity probe. There appears to be a similar amount of flow around the right edge and the right seam of the weir structure as there was on Oct. 20, 2010.

Dec. 20, 2010: There was a little tree hanging down into the pond a bit just upstream of the weir. I couldn't move the tree, but it probably wasn't really affecting the water level. At 14:27, I removed a little bit of sediment from the internal opening of the temperature/conductivity probe. There was no debris in front of the v-notch when I arrived.

Feb. 3, 2011: There was no debris in front of the weir's v-notch when I arrived. However, I removed some vegetation just upstream of the v-notch at 15:52. There is still a little flow coming in along the right side of the weir structure. This flow is no more than 10% of the total flow, and it is probably comparable to the amount of flow coming in along the right side of the weir structure last time (Dec. 20, 2010). At 15:59, I removed a minor amount of sediment from the internal opening of the temperature/conductivity probe.

Mar. 16, 2011: I forgot to check the internal opening of the temperature/conductivity probe.

May 2, 2011: I forgot to check the internal opening of the temperature/conductivity probe. The landowners had moved rock and soil at and near the spring since last time I was here (Mar. 16, 2011). I measured discharge twice (see Appendix D for details).I then removed the weir (which is shown in the level and discharge record at the end of the text file for this site).

MN23:A0041 (Freiheit Spring – Middle Emanation)
554979 m E, 4839440 m N (± 4.8 m)

Data Logger Files
MN23A0041_100825-100928_TCL.txt

Data Logger Notes
Campbell data logger installed: Aug 25, 2010.
Campbell data logger downloaded: Aug. 26, 2010 8:58; Aug. 30, 2010 12:00, 15:51, 16:32, 17:05, 17:41, 19:28; Aug. 31, 2010 11:56; Sept. 2, 2010 15:40, 17:17, 19:21; Sept. 28, 2010 9:02, 9:42.
Campbell data logger removed: Sept. 28, 2010.

Table A.5. Manual measurements at MN23:A0041 (Freiheit Spring – Middle Emanation).

Year	Month	Day	Time	Temp. (ºC)	Cond. (µS/cm)	TC Cond. (µS/cm)	Time	Depth to Water [g] (ft)
2010	8	26	8:55	9.1 [a]	422 [e]	605	11:44	0.29
2010	8	30	14:03	8.65 [a]	403 [e]	585	14:16	0.32
2010	8	31	13:06	8.8 [a]	415 [e]	600	15:01	0.32
2010	9	2	14:32	9.1 [a]	406 [e]	582	14:44	0.32
2010	9	2	14:36	9.1 [a, h]	408 [e, h]	585 [h]		
2010	9	28	10:14	10.55 [a]	431 [e]	594		

See page 103 for general footnotes [a-f].
[g] Measured from a corner of a rock above the water surface.
[h] Manual temperature and conductivity measurements taken at the far upstream emanation.

Field Notes
Aug. 26, 2010: At ~9:00, I removed the data logger so that I could use it for discharge measurements. However, I reinstalled the logger at the middle emanation at 11:30. At 11:39, I removed a slug on one end of the second temperature/conductivity probe.
Aug. 30, 2010: I found the pressure transducer out of water. I checked the internal opening of the temperature/conductivity probe, but it appeared clean. At 12:00, I changed the data logger output interval to 1 minute. Before the pool was dumped, I reset the time on both data loggers so that they were reading the same time. At 15:53, I changed the data logger output interval to 1 second. At 17:44, I changed the data logger output interval to 1 minute. At ~19:30, I removed the data logger so that I could use it for a discharge measurement. However, I reinstalled the logger at the middle emanation at 20:40.
Aug. 31, 2010: At ~12:00, I removed the data logger so that I could use it for discharge measurements. However, I reinstalled the logger at the middle emanation at 13:58. At 13:10, I checked the internal opening of the temperature/conductivity probe, but it appeared clean.
Sept. 2, 2010: At 11:41, I changed the data logger output interval to 1 minute. At 12:05, I changed the time of this logger so that it was the same as the logger at the downstream emanation. At 16:06, I checked the internal opening of the temperature/conductivity probe, but it appeared clean. At 16:36, I

changed the data logger output interval to 1 second. At 18:31, I changed the data logger output interval to 1 minute. At 19:20, I changed the data logger output interval to 10 minutes.

MN23:A0098 (Lanesboro Fish Hatchery)
581005 m E, 4838929 m N (± 8.1 m) - This UTM location was taken approximately 15 ft from the front of the building which contains the spring pool that the data logger is monitoring.

Data Logger Files
MN23A0098_080812-081031_TC.txt

Data Logger Notes
Campbell data logger installed: Aug. 12, 2008.
Campbell data logger downloaded: Oct. 31, 2008 14:49; I downloaded this logger one other time before Oct. 31, 2008, likely on Sept. 5, 12, or 19, 2008.
Campbell data logger removed: Oct. 31, 2008.

I did not take any manual measurements at this site.

MN23:A0875 (Vreeman Spring)
Hobo: 561033 m E, 4830347 m N (± 4.7 m)

Data Logger Files
MN23A0875_100501-110502_TI.txt

Data Logger Notes
HOBO data logger installed: May 1, 2010.
HOBO data logger downloaded: June 10, 2010 13:22; Aug. 26, 2010 12:35; Oct. 20, 2010 12:40; May 2, 2011 9:15.
HOBO data logger removed: May 2, 2011.

Table A.6. Manual measurements at MN23:A0875 (Vreeman Spring).

Year	Month	Day	Time	Temp. (ºC)	Cond. (µS/cm)	TC Cond. (µS/cm)
2009	11	20	12:42	9.4 [a]	399 [d]	567
2010	5	1	18:35	8.7 [b]		
2010	8	26	~12:40	10.6 [a]	451 [e]	621
2010	10	20	~12:50	10.0 [a]	454 [e]	635
2011	5	2	9:14	8.55 [f]	414 [e]	602

See page 103 for general footnotes [a-f].

Field Notes
Sept. 30, 2009: I measured discharge four times (see Appendix D for details).
Oct. 20, 2010: The hollow log in the spring run where the data logger was installed had been filled in with sediment, and this possibly shielded the data logger from water somewhat.

MN23:A0887 (Grover Spring)
555535 m E, 4841102 m N (± 2.9 m)

Data Logger Files
MN23A0887_100527-100825_TI.txt

Data Logger Notes
HOBO data logger installed: May 27, 2010
HOBO data logger downloaded: Aug. 25, 2010 15:48

Table A.7. Manual measurements at MN23:A0887 (Grover Spring).

Year	Month	Day	Time	Temp. (ºC)	Cond. (µS/cm)	TC Cond. (µS/cm)
2010	8	25	~15:55	15.3 [a]	479 [e]	587

See page 103 for general footnotes [a-f].

Field Notes
Aug. 25, 2010: Data logger was out of water on vegetation when I found it. The logger was likely moved on July 17, 2010, and the record from July 18 1:15-Aug. 25, 2010 records air surface temperature.
Oct. 20, 2010: Data logger had been covered by gravel since last time I was here (Aug. 25, 2010) during landscaping work.

MN23:X0016 (Stream in Goliath's Cave at David's Entrance)
559447 m E, 4825749 m N (± 3.3 m)

Data Logger Files
MN23X0016_080313-110316_TCLP.txt

Data Logger Notes
Campbell data logger installed: Mar. 2006. However, a new temperature/conductivity probe and a new pressure transducer were installed on Mar. 13, 2008 which produced better data. Therefore, the record in this thesis begins Mar. 13, 2008. I started downloading the data logger and maintaining the equipment at this site on Oct. 17, 2008.
Campbell data logger downloaded: May 22, 2008; June 3, 2008 18:24; June 12, 2008; Oct. 17, 2008; Nov. 24, 2008 10:00; Dec. 19, 2008 10:00-10:30; Jan. 19, 2009 9:44; Feb. 16, 2009 ~9:45; Mar. 18, 2009 10:27; Apr. 24, 2009 13:26; June 3, 2009 10:02; June 24, 2009 10:40; July 14, 2009 10:41; Aug. 26, 2009 13:05; Oct. 6, 2009 10:27; Oct. 24, 2009 14:58; Dec. 3, 2009 16:00-16:30; Jan. 6, 2010 13:30-14:00; Feb. 12, 2010 14:16; Mar. 24, 2010 13:12; May 5, 2010 14:36; June 16, 2010 10:43; July 15, 2010 10:34; Aug. 19, 2010 13:12; Sept. 28, 2010 16:39; Nov. 10, 2010 15:43; Dec. 20, 2010 12:29; Feb. 3, 2011 8:34; Mar. 16, 2011 16:38.
Campbell data logger removed: Mar. 16, 2011.

Table A.8. Manual measurements at MN23:X0016 (Stream in Goliath's Cave at David's Entrance).

Year	Month	Day	Time	Temp. (ºC)	Cond. (µS/cm)	TC Cond. (µS/cm)	Time	Depth to Water [g] (ft)
2009	7	14	~12:25	9.1 [a]	302 [d, h]	433 [h]		
2009	10	6	~11:50	9.3 [a]	108.7 [d]	155		
2009	10	24	~15:40	9.0 [a]	226 [d]	325	~15:45	0.490 [i]
2010	3	24	~13:40	7.2 [a]	271 [d]	409	~13:45	0.583
2010	5	5	~15:05	8.4 [b]	294 [d]	429	~15:10	0.578
2010	6	16	~11:10	11.45 [a]	312 [e]	420	~11:15	0.479
2010	7	15	~11:05	9.175 [c]	328 [e]	469	~11:10	0.599
2010	8	19	~13:35	9.2 [a]	325 [e]	464	~13:40	0.609
2010	9	28	~16:54	11.15 [a]	340 [e]	461	~16:58	0.526
2010	11	10	~16:07	9.1 [a]	348 [e]	499	~16:20	0.635
2011	3	16	~17:40	3.8 [a]	112 [e]	188	~17:50	0.385

See page 103 for general footnotes [a-f].
[g] Measured from the bottom side of the bottom step on the back and upstream side of the ladder at the shaft entrance.
[h] My manual conductivity measurement was taken during the tail of the salt dilution discharge measurement. However, conductivity had almost returned to background when I did the manual measurement.
[i] I'm not sure if this depth to water measurement was taken on the bottom or top side of the bottom step.

Field Notes

June 24, 2009: I found a severed cable for the rain gauge, so it wasn't working. Looking at the data, the cable was fully severed sometime after 23:30 on Mar. 10, 2009.

July 14, 2009: I moved the probe and pressure transducer as I removed sediment from the internal opening of the temperature/conductivity probe. I also measured discharge (see Appendix D for details).

Aug. 26, 2009: I changed the rain gauge sometime between June 24, 2009 and Aug. 26, 2009, but I forgot to write this down in my field notes. I know I changed the rain gauge at least by Aug. 26, 2009.

Oct. 6, 2009: I changed the pressure transducer. The old pressure transducer was partially severed on Nov. 17, 2008. Therefore, level data from Nov. 17, 2008 to Oct. 6, 2009 is of limited use. However, it may show qualitative response to recharge events.

Oct. 24, 2009: Rain gauge is clean. I moved the temperature/conductivity probe and pressure transducer, and I removed sediment from the internal opening of the temperature/conductivity probe and the surrounding PVC well screen.

Jan. 6, 2010: I removed ice from the rain gauge bucket.

Feb. 12, 2010: Rain gauge is clean.

Mar. 24, 2010: Rain gauge is clean. I moved the temperature/conductivity probe and pressure transducer at ~13:50 as I removed sediment which covered the temperature/conductivity probe.

May 5, 2010: Rain gauge is clean. I moved the temperature/conductivity probe and pressure transducer as I removed some sediment from the internal opening of the temperature/conductivity probe and PVC well screen.

June 16, 2010: Rain gauge is clean. I moved the temperature/conductivity probe and pressure transducer as I removed sediment from the internal opening of the temperature/conductivity probe and PVC well screen; internal opening of probe was full of sediment.

July 15, 2010: Rain gauge is clean. I moved three small rocks to make my depth to water hand measurement. I also moved the temperature/conductivity probe and pressure transducer as I removed sediment from the internal opening of the temperature/conductivity probe and PVC well screen; probe and well screen were full of sediment. Finally, I dug out the place where PVC well screen is to ensure probes remain below water at ~11:15.

Aug. 19, 2010: Rain gauge is clean. I moved the temperature/conductivity probe and pressure transducer at ~13:45 as I removed sediment from the internal opening of the temperature/conductivity probe and PVC well screen.

Sept. 28, 2010: Rain gauge is clean. I moved the temperature/conductivity probe and pressure transducer at ~17:00 as I removed sediment from the internal opening of the temperature/conductivity probe and PVC well screen.

Nov. 10, 2010: Rain gauge is clean. I moved the temperature/conductivity probe and pressure transducer at ~16:20. There was no sediment in the internal opening of the temperature/conductivity probe.

MN23:X0117 (Stream in Bat River Cave at shaft entrance)
557628 m E, 4846619 m N

Data Logger Files
MN23X0117_080626-090826_TCLP.txt
I'm not sure if the level data at this site from 080626-080812 is in feet like the rest of the level data in this file.

Data Logger Notes
Campbell data logger installed: June 12, 2008. However, the earliest data in the text file for this site goes from June 26 – Aug. 12, 2008. I'm not sure if these dates are correct; they don't correspond to the June 12, 2008 installation date or the download date of July 12, 2008. I started downloading the data logger at this site on Nov. 24, 2008.
Campbell data logger downloaded: July 12, 2008; Nov. 24, 2008; Dec. 19, 2008 12:39; Jan. 19, 2009 11:24; Feb. 16, 2009 11:13; Mar. 18 2009 11:57; Apr. 24, 2009 16:29; June 3, 2009 14:41; July 14, 2009 14:30; Aug. 26, 2009 9:36.
Campbell data logger removed: Aug. 26, 2009.

Table A.9. Manual measurements at MN23:X0117 (Stream in Bat River Cave at shaft entrance).

Year	Month	Day	Time	Temp. (ºC)	Cond. (µS/cm)	TC Cond. (µS/cm)
2008	10	31		9.1 [d]	452 [d]	648
2009	8	26	~10:00	8.8 [a]	426 [d]	615

See page 103 for general footnotes [a-f].

Field Notes
Aug. 26, 2009: The internal opening of the temperature/conductivity probe was full of sediment.

MN23:X0131 (Stream flowing through culvert under 161st Ave.)
554035 m E, 4838488 m N (± 3.1 m)

Data Logger Files
MN23X0131_100616-110502_TCL.txt

Data Logger Notes
Campbell data logger installed: June 16, 2010.
Campbell data logger downloaded: July 15, 2010 15:37; Aug. 19, 2010 18:04; Sept. 28, 2010 11:51; Nov. 10, 2010 11:24; Feb. 3, 2011 16:20; Mar. 16, 2011 18:22; May 2, 2011 16:14.
Campbell data logger removed: May 2, 2011.

Table A.10. Manual measurements at MN23:X0131 (Stream flowing through culvert under 161st Ave.).

Year	Month	Day	Time	Temp. (ºC)	Cond. (µS/cm)	TC Cond. (µS/cm)	Time	Water Depth [g] (ft)
2010	6	16	~15:50	19.2 [a]			~15:55	1.07
2010	7	15	15:50	22.1 [c]	524 [e]	555	16:00	0.36
2010	8	19	18:36	23.3 [a]	534 [e]	552	18:41	0.19
2010	9	28	12:00	13.95 [a]	476 [e]	602	12:05	0.88
2010	11	10	11:40	10.1 [a]	418 [e]	583	11:53	0.22
2010	11	10	12:07	10.9 [a]				
2011	3	16	18:18	4.5 [a]	190 [e]	311	18:33	0.66
2011	5	2	16:04	7.45 [f]	356 [e]	534	16:11	0.56 [h]

See page 103 for general footnotes [a-f].
[g] Measured from the lowest spot on the 10th corrugation from the upstream side of the culvert.
[h] Water depth measurement is ± 0.02 ft because of rapid flow.

Notes
The conductivity/temperature probe and the pressure transducer monitored temperature, conductivity, and water level at the upstream end of a culvert during the entire monitoring period. The culvert was 45.5 ft long and 6 ft in diameter. Distance from one corrugation peak to the next peak is 3 in, and corrugations are 1 in deep. The pressure transducer was placed on top of corrugations on the culvert floor and was covered by a rock. I conducted a survey at this site on Aug. 31, 2010. The culvert bottom at 41.42 ft from the downstream edge of the culvert was 0.29 ft higher than the culvert bottom at 4.03 ft from the downstream edge of the culvert. The culvert bottom at 22.48 ft from the downstream edge of the culvert was 0.11 ft higher than the culvert bottom at 4.03 from the downstream edge of the culvert.

Field Notes
July 15, 2010: At 16:05, I removed sediment and scraped a tiny slug from the internal opening of the temperature/conductivity probe.

Aug. 19, 2010: I accidently disconnected the data logger from the battery, but I got the logger running again at 18:27. The temperature/conductivity probe had been moved upstream of the culvert since the last time I was here (July 15, 2010). I moved the probe back close to its original location. At 18:47, I scraped the internal opening of the temperature/conductivity probe. I bumped the pressure transducer at 18:48.
Aug. 31, 2010: I removed mud from the internal opening of the temperature/conductivity probe; it was full of mud.
Sept. 28, 2010: I removed sediment from the internal opening of the temperature/conductivity probe; it was full of sediment. I moved the pressure transducer to the deepest flow in the culvert.
Nov. 10, 2010: At 12:00, I removed sediment from the internal opening of the temperature/conductivity probe; it was full of sediment. I moved the pressure transducer while removing debris at 12:04.
Dec. 20, 2010: The battery had power and was connected to the data logger, but the logger was not running correctly. I got the logger running again at 13:21.
Mar. 16, 2011: At 18:35, I removed some sediment from the internal opening of the temperature/conductivity probe. I may have bumped the pressure transducer.
May 2, 2011: There was a log in front of the culvert which has dammed up debris. There was some grass around both the temperature/conductivity probe and the pressure transducer, and they had been moved likely by high flow. The pressure transducer was not in the deepest flow. There was some sediment in the internal opening of the temperature/conductivity probe.

MN23:X0141 (Stream in Cherry Grove Blind Valley Scientific and Natural Area)
Weir: 559055 m E, 4825688 m N (± 5.1 m)

Data Logger Files
MN23X0141_091203-101110_TCL.txt

Data Logger Notes
Campbell data logger installed: Dec. 3, 2009.
Campbell data logger downloaded: Jan. 6, 2010 14:09; Feb. 12, 2010 13:15; Mar. 24, 2010 14:16; May 5, 2010 13:33; June 16, 2010 9:55; July 15, 2010 9:34; Aug. 19, 2010 12:17; Sept. 28, 2010 16:06; Nov. 10, 2010 15:10.
Campbell data logger removed: Nov. 10, 2010.

Table A.11. Manual measurements at MN23:X0141 (Stream in Cherry Grove Blind Valley Scientific and Natural Area).

Year	Month	Day	Time	Temp. (ºC)	Cond. (µS/cm)	TC Cond. (µS/cm)	Time	Depth to Water [g] (ft)	Time	Depth to Water [h] (ft)
2009	12	3	~15:40	0.25 [a]	327 [d]	617				
2010	3	24	14:30	7.45 [a]	336 [d]	504	14:33	1.570	14:36	1.146
2010	3	24					14:54	1.594	14:57	1.161
2010	5	5	13:50	12.5 [b]			13:57	1.573	13:59	1.135
2010	6	16	10:12	14.8 [a]	369 [e]	458	10:17	1.068	10:23	0.620
2010	7	15	9:52	17.95 [a]	598 [e]	690	10:01	1.844	10:06	1.427
2010	8	19	12:30	21.1 [a]	561 [e]	606	12:39	1.906	12:48	1.505
2010	9	28	16:14	16.0 [a]	454 [e]	548	16:18	1.417	16:21	0.969

See page 103 for general footnotes [a-f].
[g] Measured from the top of the post where the pressure transducer was attached.
[h] Measured from the top of the weir.

Notes

A 90º v-notch weir was installed at the Cherry Grove Blind Valley Scientific and Natural Area on Dec. 3, 2009. The data logger file at this site includes water level data, which needs to be converted to level above the v-notch. This can be done using the survey information provided in the Aug. 26, 2010 field notes below and the depth to water manual measurements provided in Table A.11. The fence post that the pressure transducer was connected to likely moved during the monitoring period, so these offsets need to be corrected when converting to level above the v-notch. Then the weir equation for a 90º v-notch weir may be used to calculate discharge, which is

$$Q = 2.5H^{2.5}, \tag{A.4}$$

where Q is discharge in ft^3/sec and H is the height of water above the bottom of the v-notch in feet. The distance from the v-notch to the top of the weir structure was 1.63 ft. Thus, if water level was more than 1.63 ft above the v-notch, then discharge is underestimated.

Field Notes

Jan. 6, 2010: I accidently stopped the data logger, but I got it running again at ~14:30. The sinking stream was frozen.

Feb. 12, 2010: The sinking stream was frozen.

Mar. 24, 2010: I cleared debris from the weir's v-notch at 14:37. I removed sediment from the internal opening of the temperature/conductivity probe at 14:42. Mark White from Forestville State Park told me that there was flow occurring around the edges of the weir last week, so I wasn't capturing all of the higher flow through the v-notch.

May 5, 2010: There was no sediment in the internal opening of the temperature/conductivity probe. I added some soil, gravel, and 3 large rocks to east edge of weir at ~14:15. There was air behind the flow on the downstream edge of the v-notch, and the v-notch was clear of debris.

June 16, 2010: At 9:52, I removed two large sticks from the weir's v-notch. I didn't check to see if there was sediment in the internal opening of the temperature/conductivity probe because the water was higher than my knee high boots. There is no backflooding of the weir, but it is close. However, I don't believe there was air space below the downstream edge of the v-notch.

July 15, 2010: At 9:29, I removed two branches from the weir's v-notch (~ 4 in by ~ 2 ft and ~ 4 in by ~ 5 ft). At 9:56, I removed some leaves and little sticks at the temperature/conductivity probe. There was air behind the flow on the downstream edge of the v-notch.

Aug. 19, 2010: At 12:41, I removed some mud from the internal opening of the temperature/conductivity probe; it was filled with mud. There was no debris at the weir's v-notch, and there was air behind the flow on the downstream edge of the v-notch.

Aug. 26, 2010: There is no water flowing at the Cherry Grove Blind Valley Scientific and Natural Area. I conducted a survey at this site. The top of the fencepost where depth to water measurements are taken is 2.11 ft higher than the bottom of the weir's v-notch. The top of the weir where additional depth to water measurements are taken is 1.63 ft higher than the bottom of the weir's v-notch. *Sept. 28, 2010*: There may have been sediment in the internal opening of the temperature/conductivity probe. I may have moved the pressure transducer and the pole that the pressure transducer was attached to while I removed sediment above the pressure transducer which had accumulated on top of it since it was installed. There was no debris at the weir's v-notch.

Nov. 10, 2010: The cables for both the temperature/conductivity probe and the pressure transducer had been burned on Nov. 8, 2010. There was no flow at the SNA.

MN23:X0142 (South Branch of the Root River at County 5)
Hobo: 559231 m E, 4830584 m N (± 4.4 m)

Data Logger Files
MN23X0142_100501-110502_TI.txt

Data Logger Notes
HOBO data logger installed: May 1, 2010.
HOBO data logger downloaded: July 15, 2010 14:44; Aug. 26, 2010 14:57; Oct. 20, 2010 11:18; May 2, 2011 9:40.
HOBO data logger removed: May 2, 2011.

Table A.12. Manual measurements at MN23:X0142 (South Branch of the Root River at County 5).

Year	Month	Day	Time	Temp. (ºC)	Cond. (µS/cm)	TC Cond. (µS/cm)
2010	5	1	10:52	12.8 [b]	341 [d]	444
2010	6	16	~14:30	18.6 [a]	324 [e]	369
2010	7	15	~14:55	21.825 [c]	467 [e]	497
2010	8	26	~15:10	20.6 [a]	473 [e]	516
2010	10	20	~11:30	11.0 [a]	407 [e]	554
2011	5	2	9:45	6.7 [f]	334 [e]	512

See page 103 for general footnotes [a-f].

Field Notes
Oct. 20, 2010: The data logger was out of the water when I found it. The data shows that some light intensity data > 0 lux occurred from Sept. 25 – Oct. 20, 2010. Light intensity during the preceding four months was 0 lux. Therefore, the data logger was moved sometime around Sept. 25, 2010, and some or all of the period from Sept. 25 – Oct. 20, 2010 records surface temperature.

MN23:X0143, MN23:X0144, and MN23:X0145 (South Branch of the Root River at Mystery Cave)
MN 23:X0143 (1st Hobo data logger): 555665 m E, 4829514 m N (± 4.2 m)
MN 23:X0144 (2nd Hobo data logger): 555677 m E, 4829530 m N (± 3.4 m)
MN 23:X0145 (Campbell data logger): 555682 m E, 4829598 m N (± 4.0 m)

Data Logger Files
MN23X0143_MN23X0144_100501-110316_TI.txt
MN23X0145_110203-110502_TCL.txt

Data Logger Notes
1st HOBO data logger installed: May 1, 2010.
1st HOBO data logger downloaded: June 10, 2010 12:47; Aug. 26, 2010 13:17.
2nd HOBO data logger installed: Oct. 20, 2010.
2nd HOBO data logger downloaded: Mar. 16, 2011 14:05.
2nd HOBO data logger removed: Mar. 16, 2011.
Campbell data logger installed: Feb. 3, 2011.
Campbell data logger downloaded: Mar. 16, 2011 13:31; May 2, 2011 13:02.
Campbell data logger removed: May 2, 2011.

Table A.13. Manual measurements at MN23:X0143, MN23:X0144, and MN23:X0145 (South Branch of the Root River at Mystery Cave).

Year	Month	Day	Time	Temp. (ºC)	Cond. (µS/cm)	TC Cond. (µS/cm)	Time	Depth to Water [g] (ft)
2010	8	26	13:40	18.4 [a, h]	461 [e, h]	527 [h]		
2010	10	20	10:36	8.2 [a, i]	373 [e, i]	548 [i]		
2011	3	16	13:53	4.9 [a, j]	306 [e, j]	495 [j]	14:12	14.1
2011	5	2	12:52	6.1 [f, i]	325 [e, i]	507 [i]		
2011	5	2	13:14	6.1 [f, j]	326 [e, j]	509 [j]		

See page 103 for general footnotes [a-f].
[g] Measured from the top of the hand railing on the bridge that crosses the South Branch of the Root River near the Mystery Cave I Entrance, on the cave entrance side of the bridge sign closest to the cave entrance.
[h] Manual temperature and conductivity measurements taken near the 1st HOBO data logger monitoring location.
[i] Manual temperature and conductivity measurements taken near the 2nd HOBO data logger monitoring location.
[j] Manual temperature and conductivity measurements taken near the Campbell data logger monitoring location.

Field Notes
Aug. 26, 2010: Data logger was along the edge of the river just below water; the string that was tied to it had been cut. I reconnected the HOBO and the holey rock to the fencepost with new string.

Oct. 20, 2010: I couldn't find the HOBO data logger. I deployed a new HOBO data logger ~ 25 m downstream of 1st HOBO monitoring location.
Feb. 3, 2011: The surface of the South Branch of the Root River at Mystery Cave was frozen. Therefore, I set the temperature/conductivity probe and the pressure transducer on top of the ice to capture snowmelt when it occurs.
Mar. 16, 2011: I moved the temperature/conductivity probe and the pressure transducer and taped them to a large rock so that they hopefully wouldn't move.
May 2, 2011: There was some sediment in the internal opening of the temperature/conductivity probe.

MN23:X0146 (Spring Valley Creek below Old Timber Bridge on Grover's property)
Hobo: 555491 m E, 4841170 m N (± 4.4 m)

Data Logger Files
MN23X0146_100527-101020_TI.txt

Data Logger Notes
HOBO data logger installed: May 27, 2010.
HOBO data logger downloaded: Aug. 25, 2010 16:07; Oct. 20, 2010 13:46.

Table A.14. Manual measurements at MN23:X0146 (Spring Valley Creek below Old Timber Bridge on Grover's property).

Year	Month	Day	Time	Temp. (ºC)	Cond. (µS/cm)	TC Cond. (µS/cm)
2010	8	25	~16:23	19.55 [a]	510 [e]	569
2010	10	20	14:00	9.9 [a]	420 [e]	589
2011	5	2	17:20	7.05 [f]	358 [e]	543

See page 103 for general footnotes [a-f].

Field Notes
May 2, 2011: I couldn't find the HOBO data logger.

MN85:A0005 (Little Green Spring East)
581179 m E, 4881772 m N (± 11.3 m)

Data Logger Files
MN85A0005_081031-091024_TCV.txt
The "V" in the text file name stands for voltage. The pressure transducer no longer worked after the data logger was removed, so the pressure transducer was never calibrated.

Data Logger Notes
Campbell data logger installed: Oct. 31, 2008.
Campbell data logger downloaded: Nov. 24, 2008 15:48; Dec. 19, 2008 16:53; Jan. 19, 2009 16:53; Feb. 16, 2009 16:26; Mar. 18 2009 17:45; Apr. 24, 2009 20:00; June 3, 2009 19:18; July 14, 2009 18:45; Aug. 26, 2009 19:25; Oct. 24, 2009 9:18.
Campbell data logger removed: Dec. 14, 2009.

Table A.15. Manual measurements at MN85:A0005 (Little Green Spring East).

Year	Month	Day	Time	Temp. (ºC)	Cond. (µS/cm)	TC Cond. (µS/cm)	Time	Depth to Water [g] (ft)
2008	10	31		9.0 [a]	403 [d]	579		
2008	11	24		9.0 [a]	398 [d]	571		
2008	12	19		8.9 [a]	407 [d]	586		
2009	1	19	~17:05	9.0 [a]	400 [d]	575		
2009	2	16	16:40	8.95 [a]	396 [d]	570		
2009	3	18	17:58	8.9 [a]	394 [d]	568		
2009	4	24	20:15	8.8 [a]	397 [d]	574		
2009	6	3	19:33	8.85 [a]	397 [d]	573		
2009	7	14	18:57	8.9 [a]				
2009	8	26	19:40	8.9 [a]	397 [d]	572		
2009	10	24	9:38	8.9 [a]	395 [d]	569	9:46	2.62
2009	12	14	15:40	8.8 [a]	404 [d]	584	15:45	2.69

See page 103 for general footnotes [a-f].
[g] Measured from a point on top edge of the cement structure above the water surface.

Field Notes
Jan. 19, 2009: I scraped the internal opening of the temperature/conductivity probe with a stick; the internal opening was not clean. I found a dead possum in the water just upstream of the probe and the pressure transducer. There were also leaves around the probe and transducer in the metal pipe that obstructed some flow.

Feb. 16, 2009: I checked the internal opening of the temperature/conductivity probe, but it appeared clean.
June 3, 2009: I accidently stopped the logger, but I got it running again at 20:00.
Aug. 26, 2009: I moved some rocks around the pressure transducer to force most of the flow through the metal pipe. At 19:46, I cleaned the temperature/conductivity probe with 1 N HCl and a brush, but the probe appeared clean.
Oct. 24, 2009: I moved the temperature/conductivity probe and the pressure transducer at 9:42 to clear leaf litter from the metal pipe. The internal opening of the temperature/conductivity probe appeared clean.
Dec. 14, 2009: The data logger was not working. I was not able to download the data since the last time I was here (Oct. 24, 2009).

MN85:A0053 (Wunderlich Spring)
594088 m E, 4860696 m N

Data Logger Files
MN85A0053_080812-081031_TC.txt

Data Logger Notes
Campbell data logger installed: Aug. 12, 2008.
Campbell data logger downloaded: Aug. 29, 2008; Sept. 5, 2008; Sept. 12, 2008; Sept. 19, 2008; Oct. 3, 2008; Oct. 17, 2008; Oct. 31, 2008 10:00.
Campbell data logger removed: Oct. 31, 2008.

Table A.16. Manual measurements at MN85:A0053 (Wunderlich Spring).

Year	Month	Day	Temp. (ºC)	Cond. (µS/cm)	TC Cond. (µS/cm)
2008	8	12	8.8 [a]	328 [d]	474
2008	8	29	9.0 [a]	358 [d]	514
2008	9	5	9.1 [a]	367 [d]	526
2008	9	12	9.2 [a]	368 [d]	525
2008	9	19	9.1 [a]	367 [d]	526
2008	10	3	9.2 [a]	366 [d]	523
2008	10	17	9.3 [a]	367 [d]	523
2008	10	31	9.3 [a]	367 [d]	523

See page 103 for general footnotes [a-f].

Field Notes
Sept. 12, 2008: I moved the temperature/conductivity probe.
Sept. 19, 2008: I moved the temperature/conductivity probe.
Oct. 3, 2008: I moved the temperature/conductivity probe.
Oct. 17, 2008: I moved the temperature/conductivity probe.

MN85:A0255 (Borson Spring – Boils)
596230 m E, 4857541 m N (± 4.4 m)

Data Logger Files
MN85A0255_Boils_100106-101110_TCL.txt

Data Logger Notes
Campbell data logger installed: Jan. 6, 2010.
Campbell data logger downloaded: Feb. 12, 2010 16:28; Mar. 24, 2010 16:38; May 5, 2010 16:48; June 16, 2010 ~18:05; July 15, 2010 18:05; Aug. 19, 2010 9:41; Sept. 28, 2010 18:33; Nov. 10, 2010 9:15.
Campbell data logger removed: Nov. 10, 2010.

Table A.17. Manual measurements at MN85:A0255 (Borson Spring – Boils).

Year	Month	Day	Time	Temp. (ºC)	Cond. (µS/cm)	TC Cond. (µS/cm)	Time	Depth to Water [g] (ft)
2010	1	6	17:35	8.95 [a]	359 [d]	517		
2010	2	12	15:59	8.9 [a]	358 [d]	516	16:50	0.104
2010	3	24	16:57	9.1 [a]	360 [d]	516	17:46	0.052
2010	5	5	17:18	9.1 [b]			17:46	0.094
2010	6	16	18:31	8.9 [a]			18:53	0.073
2010	7	15	18:31	8.8 [c]	361 [e]	522	18:57	-0.161
2010	8	19	10:05	9.0 [a]	363 [e]	522	10:42	-0.083
2010	9	28	19:09	9.0 [a]	374 [e]	537	19:11	-0.292
2010	11	10	8:44	9.1 [a]	375 [e]	537	8:46	-0.099
2010	12	20					9:12	0.000

See page 103 for general footnotes [a-f].
[g] Measured from a corner of a rock. The rock corner was below water for the negative measurements.

Field Notes
Feb. 12, 2010: The 7 wire ground was disconnected from the A547 Interface for the temperature/conductivity probe. Looking at the data, I either never connected this wire or it became disconnected when I was working with the logger when I installed the logger on *Jan. 6, 2010*. I connected the wire at 16:41.
Mar. 24, 2010: The pressure transducer had been moved since last time I was here (Feb. 12, 2010). I moved it back close to its original position at 16:59.
May 5, 2010: I disconnected and trimmed the white wire for the temperature/conductivity probe. I also disconnected the red wire for the temperature/conductivity probe momentarily. I reconnected the wires at 17:00; both were connected when I got here.
June 16, 2010: The data logger was covered with ants, but it was still running. I changed the data logger and the temperature/conductivity probe. I also tried to seal the box that holds the data logger better. The new data logger is running correctly at 19:41.

July 15, 2010: There were some ants in and around the logger, but it appears to be running correctly.

MN85:A0255 (Borson Spring – Emanation)
596221 m E, 4857540 m N (± 4.6 m)

Data Logger Files
MN85A0255_Emanation_080812-101220_TCL.txt

Data Logger Notes
Campbell data logger installed: Aug. 12, 2008.
Campbell data logger downloaded: Aug. 29, 2008; Sept. 5, 2008; Sept. 12, 2008; Sept. 19, 2008; Oct. 3, 2008; Oct. 17, 2008; Oct. 31, 2008 ~10:51; Nov. 24, 2008 13:39; Dec. 19, 2008 14:41; Jan. 19, 2009 14:10; Feb. 16, 2009 13:45; Mar. 18, 2009 14:50; Apr. 24, 2009 18:01; June 3, 2009 17:11; Aug. 26, 2009 17:00; Oct. 24, 2009 10:50; Dec. 14, 2009 11:52; Jan. 6, 2010 17:13; Feb. 12, 2010 16:04; Mar. 24, 2010 17:04; May 5, 2010 17:24; June 16, 2010 18:37; July 15, 2010 18:36; Aug. 19, 2010 10:13; Sept. 28, 2010 18:45; Nov. 10, 2010 8:50; Dec. 20, 2010 8:59.
Campbell data logger removed: Dec. 20, 2010.

Table A.18. Manual measurements at MN85:A0255 (Borson Spring – Emanation).

Year	Month	Day	Time	Temp. (ºC)	Cond. (µS/cm)	TC Cond. (µS/cm)	Time	Depth to Water [g] (ft)
2008	8	12		8.9 [a]	324 [d]	467		
2008	8	29		9.1 [a]	342 [d]	491		
2008	9	5		9.0 [a]	343 [d]	492		
2008	9	12		9.1 [a]	342 [d]	491		
2008	9	19		9.0 [a]	341 [d]	490		
2008	10	3		9.1 [a]	344 [d]	492		
2008	10	17		9.1 [a]	342 [d]	491		
2008	10	31		9.1 [a]	346 [d]	495		
2008	11	24		9.1 [a]	340 [d]	487		
2008	12	19		9.2 [a]	347 [d]	496		
2009	1	19	~14:15	9.2 [a]	342 [d]	489		
2009	2	16	14:01	9.2 [a]	339 [d]	484		
2009	3	18	15:00	9.3 [d]	339 [d]	483		
2009	4	24	18:13	9.1 [a]	337 [d]	483		
2009	6	3	17:20	9.2 [a]	337 [d]	482		
2009	7	14	16:57	9.0 [a]	336 [d]	483		
2009	8	26	17:20	8.9 [a]	336 [d]	484		
2009	10	24	11:01	8.9 [a]	336 [d]	484		
2009	12	14	12:07	8.8 [a]	340 [d]	491		

2010	1	6	17:25	8.8 [a]	341 [d]	493		
2010	2	12	16:15	8.9 [a]	342 [d]	493		
2010	3	24	17:40	9.05 [a]	339 [d]	486		
2010	5	5	17:36	9.1 [b]	340 [d]	487		
2010	6	16	18:45	8.9 [a]				
2010	7	15	18:51	8.7 [c]	338 [e]	490		
2010	8	19	10:24	8.8 [a]	340 [e]	491	10:35	0.40
2010	9	28	18:55	8.8 [a]	354 [e]	511	19:00	0.18 [h]
2010	11	10	9:02	8.9 [a]	351 [e]	506	9:10	0.40
2010	12	20	9:06	8.9 [a]	339 [e]	488		

See page 103 for general footnotes [a-f].

[g] Measured from a corner of a rock above the water surface. Also see the depth to water measurements at Borson Spring – Boils. The level measurements at the Boils were taken just downstream of the Emanation.

[h] It was getting dark when I took the depth to water measurement so it was tough to see. Also, the rock I used to take depth to water measurements wobbled, but I believe it was still in the same place.

Field Notes

Oct. 31, 2008: I added a pressure transducer at this site to monitor water level.

Jan. 19, 2009: I scraped the internal opening of the temperature/conductivity probe with a stick, but it appeared clean.

Feb. 16, 2009: I scraped the internal opening of the temperature/conductivity probe; there were some loose sediment grains inside.

June 3, 2009: I cleaned the internal opening of the temperature/conductivity probe; there was a little sediment buildup inside.

July 14, 2009: There were ants all over the data logger, and the logger wasn't running. I got the logger running again at 16:48. I checked the internal opening of the temperature/conductivity probe, and it contained no sediment.

Aug. 26, 2009: I cleaned the temperature/conductivity probe with 1 N HCl and a brush at 17:24, but it appeared clean.

Oct. 24, 2009: I checked the internal opening of the temperature/conductivity probe, but it appeared clean. I moved the probe further back into the emanation point; it was sticking out a bit when I arrived.

Feb. 12, 2010: I checked the internal opening of the temperature/conductivity probe, but it appeared clean. I moved the probe further back into the emanation point at 16:17.

Mar. 24, 2010: I changed the temperature/conductivity probe. I accidently disconnected the battery which stopped the data logger, but I got the logger running again at 17:32.

May 5, 2010: There was no sediment in the internal opening of the temperature/conductivity probe.

June 16, 2010: There was no sediment in the internal opening of the temperature/conductivity probe.

July 15, 2010: At 18:53, there was no sediment in the internal opening of the temperature/conductivity probe.

Aug. 19, 2010: At 10:28, I removed a few grains of sand from the internal opening of the temperature/conductivity probe.

Nov. 10, 2010: At 9:06, there was no sediment in the internal opening of the temperature/conductivity probe.

MN85:A0266 (Krage Spring)
613147 m E, 4861156 m N

Data Logger Files
MN85A0266_080812-100505_TCL.txt

Data Logger Notes
Campbell data logger installed: Aug. 12, 2008.
Campbell data logger downloaded: Oct. 3, 2008; Oct. 31, 2008; Nov. 24, 2008 14:29; Dec. 19, 2008 15:42; Jan. 19, 2009 15:19; Feb. 16, 2009 14:49; Mar. 18 2009 15:50; Apr. 24, 2009 18:48; June 3, 2009 18:01; June 17, 2009 10:34; June 17, 2009 11:03; July 14, 2009 17:32; Aug. 26, 2009 18:04; Oct. 24, 2009 11:54; Dec. 14, 2009 13:02; Jan. 6, 2010 18:17; Feb. 12, 2010 17:38; Mar. 24, 2010 18:41; May 5, 2010 18:51.
Campbell data logger removed: May 5, 2010.

Table A.19. Manual measurements at MN85:A0266 (Krage Spring).

Year	Month	Day	Time	Temp. (ºC)	Cond. (µS/cm)	TC Cond. (µS/cm)	Time	Water Depth [g] (ft)
2008	8	12		8.9 [a]	331 [d]	476		
2008	10	3		9.4 [a]	347 [d]	493		
2008	10	31		9.7 [a]	345 [d]	486		
2008	11	24		9.7 [a]	352 [d]	496		
2008	12	19		9.7 [a]	344 [d]	485		
2009	1	19	~15:30	9.6 [a]	343 [d]	485		
2009	2	16	~15:00	9.4 [a]	338 [d]	480		
2009	3	18	16:04	9.25 [a]	337 [d]	481		
2009	4	24	18:59	8.8 [a]	333 [d]	481		
2009	6	3	18:14	8.7 [a]	332 [d]	481		
2009	6	17	10:55	8.7 [a]	332 [d]	481		
2009	7	14	17:40	8.7 [a]	332 [d]	481		
2009	8	26	18:16	9.0 [a]	335 [d]	481		
2009	10	24	12:06	9.6 [a]	341 [d]	482	12:13	0.297
2009	12	14	13:17	9.7 [a]	346 [d]	488	14:00	0.255
2010	1	6	18:28	9.7 [a]	347 [d]	489	18:33	0.266
2010	2	12	18:25	9.5 [a]	344 [d]	488	18:29	0.260
2010	3	24	19:09	9.2 [a]	342 [d]	489	19:12	0.281
2010	5	5	18:50	9.0 [b]			18:39	0.266

See page 103 for general footnotes [a-f].

[g] Measured from a corner of a rock below the water surface.

Field Notes
Jan. 19, 2009: I scraped the internal opening of the temperature/conductivity probe with a stick, but it appeared clean.
Feb. 16, 2009: The internal opening of the temperature/conductivity probe appeared clean.
June 17, 2009: I cleaned the internal opening of the temperature/conductivity probe, but it appeared clean.
July 14, 2009: I checked the internal opening of the temperature/conductivity probe, and it contained no sediment.
Aug. 26, 2009: I cleaned the temperature/conductivity probe with 1 N HCl and a brush at 18:22, but it appeared clean.
Dec. 14, 2009: I calibrated the pressure transducer at Krage Spring to convert voltage to water level measurements. I checked the internal opening of the temperature/conductivity probe, and it contained no sediment.
Feb. 12, 2010: I changed the data logger, and the new data logger was running at 18:19. I also changed the box which holds the data logger which will hopefully keep the data logger drier. I checked the internal opening of the temperature/conductivity probe, and it appeared clean.
Mar. 24, 2010: I stopped the data logger when I changed the desiccant, but the logger was running again at 19:00. I checked the internal opening of the temperature/conductivity probe, and it appeared clean.

MN85:A0312 (Ehlenfeldt Spring)
594213 m E, 4860095 m N

Data Logger Files
MN85A0312_080812-090714_TC.txt

Data Logger Notes
Campbell data logger installed: Aug. 12, 2008.
Campbell data logger downloaded: Aug. 29, 2008; Sept. 5, 2008; Sept. 12, 2008; Sept. 19, 2008; Oct. 3, 2008; Oct. 17, 2008; Oct. 31, 2008 ~10:21; Nov. 24, 2008 12:58; Dec. 19, 2008 14:03; Jan. 19, 2009 13:00; Feb. 16, 2009 12:46; Mar. 18 2009 13:05; Apr. 24, 2009 17:27; June 3, 2009 15:53; July 14, 2009 15:38.
Campbell data logger removed: July 14, 2009.

Table A.20. Manual measurements at MN85:A0312 (Ehlenfeldt Spring).

Year	Month	Day	Time	Temp. (ºC)	Cond. (µS/cm)	TC Cond. (µS/cm)
2008	8	12		8.5 [a]	326 [d]	476
2008	8	29		8.8 [a]	351 [d]	507
2008	9	5		9.0 [a]	358 [d]	514
2008	9	12		9.0 [a]	353 [d]	506
2008	9	19		8.9 [a]	354 [d]	509
2008	10	3		9.2 [a]	360 [d]	514
2008	10	17		9.3 [a]	363 [d]	517
2008	10	31		9.4 [a]	365 [d]	518
2008	11	24		9.5 [a]	363 [d]	515
2008	12	19		9.6 [a]	366 [d]	518
2009	1	19	~13:15	9.7 [a]	365 [d]	515
2009	2	16	~13:00	9.6 [a]	360 [d]	509
2009	3	18	13:32	9.5 [a]	361 [d]	512
2009	4	24	~17:35	9.0 [a]	352 [d]	506
2009	6	3	16:34	8.9 [a]	355 [d]	511
2009	7	14	15:46	8.8 [a]	350 [d]	506

See page 103 for general footnotes [a-f].

Field Notes
Jan. 19, 2009: I scraped the internal opening of the temperature/conductivity probe with a stick, but it appeared clean.

Feb. 16, 2009: I scraped the internal opening of the temperature/conductivity probe, but it appeared clean.
Mar. 18, 2009: I changed the data logger.
Apr. 24, 2009: I scraped the internal opening of the temperature/conductivity probe, but it appeared clean.
June 3, 2009: I changed the temperature/conductivity probe.

MN85:A0313 (Wolfram Spring)
595494 m E, 4857992 m N

I never installed a data logger at this site. However, I took several temperature and conductivity manual measurements (Table A.21).

Table A.21. Manual measurements at MN85:A0313 (Wolfram Spring).

Year	Month	Day	Time	Temp. (ºC)	Cond. (µS/cm)	TC Cond. (µS/cm)
2008	8	29		8.9 [a]	336 [d]	484
2008	9	5		8.9 [a]	335 [d]	483
2008	9	12		8.9 [a]	340 [d]	489
2008	9	19		8.9 [a]	338 [d]	486
2008	10	3		9.0 [a]	338 [d]	485
2008	10	17		9.1 [a]	335 [d]	480
2008	10	31		9.1 [a]	338 [d]	484
2008	11	24		9.2 [a]	343 [d]	490
2009	1	19	~13:45	9.3 [a]	339 [d]	483
2009	2	16	~13:25	9.3 [a]	334 [d]	476
2009	3	18	14:35	9.2 [a]	332 [d]	474
2009	6	3	16:58	8.6 [a]	329 [d]	478

See page 103 for general footnotes [a-f].

Appendix B

Dye, sediment, major anions, and stable isotopes from Freiheit Spring Trace

This appendix includes data from the pool trace at Freiheit Spring on Aug. 30, 2010 (see Chapter 3). Uranine and suspended sediment data are included in Table B.1. Major anion analyses are shown in Table B.2 and were analyzed by Rick Knurr in the Analytical Geochemistry Lab of the University of Minnesota's Department of Geology and Geophysics. Anion analyses included 19 samples from Freiheit Spring, one sample of the Kolling well water that was used to fill the pool, and two samples of the pool water after the tracers were added and well mixed. Anions were analyzed using anion chromatography following EPA method 300.1 with a Dionex ICS 2000 system with an AS19 (4 mm) column, an ASRS 300 (4 mm) suppressor, and a NaOH eluent generator. Anion analysis also used a 1.00 ml/min flow rate, a deionized water external regenerant, a 50 µl injection, and a conductivity detector.

δD and $\delta^{18}O$ analyses are given in Table B.3 and were analyzed at the Schwartz Isotope Lab at Texas State University in San Marcos. The instrument used for the analysis is a Model 908-0008, Los Gatos Research, Liquid Water Stable Isotope Analyzer. This instrument uses Off-Axis Integrated Cavity Ouput Spectroscopy (OA-ICOS) laser technology to simultaneously measure Hydrogen and Oxygen stable isotopic ratios from liquid water samples. All data are reported relative to VSMOW. Samples are prepared in 2 mL glass vials that are loaded into an autosampler attached to the instrument. Each sample is analyzed eight times and the first three analyses are ignored to eliminate the effects of 'sample memory'. Measurement accuracies are generally +0.3‰ for δD and +0.1‰ $\delta^{18}O$, but individual samples are reported with an associated sample standard deviation for each value. Compounds that may affect the accuracy of the analysis include, but are not limited to: organic compounds and salts. For highly saline or mineralized waters, the water is distilled prior to analysis. Distillation involves taking a ~2 mL split of the sample and completely distilling it using an apparatus designed for extracting plant-water samples for isotopic analysis. During each batch run, internal standards are run at the beginning and end of each run, and after every third unknown sample, to allow for correction of instrument drift. Raw data are post-processed in a LIMS system, developed and customized for LGR data by Tyler Coplen at the USGS, Reston. For more information about analysis of stable isotopes, contact Dr. Benjamin Schwartz; Department of Biology; Texas State University - San Marcos; 206 FAB, Freeman Aquatic Station; 601 University Drive; San Marcos, TX 78666; bs37@txstate.edu; office: 1-512-245-7608.

Table B.1. Uranine and suspended sediment from Freiheit Spring (Aug. 30-Sept. 2, 2010).

Location	Date	Time	Uranine	Suspended sediment
			ppb	mg sediment / g water
Detection limit			0.003	0.01
Freiheit Spring	Aug. 30, 2010	16:02:00	< 0.003	< 0.01
Freiheit Spring	Aug. 30, 2010	16:03:00	< 0.003	0.01
Freiheit Spring	Aug. 30, 2010	16:04:00	< 0.003	< 0.01
Freiheit Spring	Aug. 30, 2010	16:05:00	< 0.003	< 0.01
Freiheit Spring	Aug. 30, 2010	16:06:00	< 0.003	< 0.01
Freiheit Spring	Aug. 30, 2010	16:07:00	< 0.003	< 0.01
Freiheit Spring	Aug. 30, 2010	16:08:00	< 0.003	< 0.01
Freiheit Spring	Aug. 30, 2010	16:09:00	< 0.003	< 0.01
Freiheit Spring	Aug. 30, 2010	16:10:00	< 0.003	< 0.01
Freiheit Spring	Aug. 30, 2010	16:11:00	< 0.003	0.01
Freiheit Spring	Aug. 30, 2010	16:11:30	< 0.003	< 0.01
Freiheit Spring	Aug. 30, 2010	16:12:00	< 0.003	< 0.01
Freiheit Spring	Aug. 30, 2010	16:12:30	< 0.003	0.01
Freiheit Spring	Aug. 30, 2010	16:13:00	< 0.003	< 0.01
Freiheit Spring	Aug. 30, 2010	16:13:30	< 0.003	< 0.01
Freiheit Spring	Aug. 30, 2010	16:14:00	< 0.003	< 0.01
Freiheit Spring	Aug. 30, 2010	16:14:30	< 0.003	0.01
Freiheit Spring	Aug. 30, 2010	16:15:00	< 0.003	0.02
Freiheit Spring	Aug. 30, 2010	16:15:30	< 0.003	0.02
Freiheit Spring	Aug. 30, 2010	16:16:00	< 0.003	0.02
Freiheit Spring	Aug. 30, 2010	16:16:30	< 0.003	0.03
Freiheit Spring	Aug. 30, 2010	16:17:00	< 0.003	0.03
Freiheit Spring	Aug. 30, 2010	16:17:30	< 0.003	0.03
Freiheit Spring	Aug. 30, 2010	16:18:00	< 0.003	0.03
Freiheit Spring	Aug. 30, 2010	16:18:30	< 0.003	-
Freiheit Spring	Aug. 30, 2010	16:19:00	0.033	-
Freiheit Spring	Aug. 30, 2010	16:19:30	0.249	-
Freiheit Spring	Aug. 30, 2010	16:20:00	1.12	0.12
Freiheit Spring	Aug. 30, 2010	16:20:30	3.31	0.29
Freiheit Spring	Aug. 30, 2010	16:21:00	7.79	0.57
Freiheit Spring	Aug. 30, 2010	16:21:30	14.0	0.89
Freiheit Spring	Aug. 30, 2010	16:22:00	22.1	1.20
Freiheit Spring	Aug. 30, 2010	16:22:30	30.9	1.49
Freiheit Spring	Aug. 30, 2010	16:23:00	41.0	1.63
Freiheit Spring	Aug. 30, 2010	16:23:30	51.4	1.90
Freiheit Spring	Aug. 30, 2010	16:24:00	61.9	2.02
Freiheit Spring	Aug. 30, 2010	16:24:30	71.6	1.95
Freiheit Spring	Aug. 30, 2010	16:25:00	81.0	1.97
Freiheit Spring	Aug. 30, 2010	16:25:30	91.3	2.09
Freiheit Spring	Aug. 30, 2010	16:26:00	99.3	2.09
Freiheit Spring	Aug. 30, 2010	16:26:30	108	2.04
Freiheit Spring	Aug. 30, 2010	16:27:00	115	1.91
Freiheit Spring	Aug. 30, 2010	16:27:30	123	1.99
Freiheit Spring	Aug. 30, 2010	16:28:00	128	1.85
Freiheit Spring	Aug. 30, 2010	16:28:30	128	1.86
Freiheit Spring	Aug. 30, 2010	16:29:00	135	1.85

Freiheit Spring	Aug. 30, 2010	16:29:30	133	1.81
Freiheit Spring	Aug. 30, 2010	16:30:00	132	1.77
Freiheit Spring	Aug. 30, 2010	16:30:30	126	-
Freiheit Spring	Aug. 30, 2010	16:31:00	128	1.77
Freiheit Spring	Aug. 30, 2010	16:31:30	124	1.71
Freiheit Spring	Aug. 30, 2010	16:32:00	118	1.63
Freiheit Spring	Aug. 30, 2010	16:32:30	110	1.53
Freiheit Spring	Aug. 30, 2010	16:33:00	105	1.42
Freiheit Spring	Aug. 30, 2010	16:33:30	100	1.34
Freiheit Spring	Aug. 30, 2010	16:34:00	93.2	1.13
Freiheit Spring	Aug. 30, 2010	16:34:30	86.6	1.13
Freiheit Spring	Aug. 30, 2010	16:35:00	80.0	1.02
Freiheit Spring	Aug. 30, 2010	16:35:30	73.6	0.91
Freiheit Spring	Aug. 30, 2010	16:36:00	68.1	0.83
Freiheit Spring	Aug. 30, 2010	16:36:30	63.4	0.77
Freiheit Spring	Aug. 30, 2010	16:37:00	59.2	0.68
Freiheit Spring	Aug. 30, 2010	16:37:30	54.7	0.59
Freiheit Spring	Aug. 30, 2010	16:38:00	51.3	0.56
Freiheit Spring	Aug. 30, 2010	16:39	44.6	0.45
Freiheit Spring	Aug. 30, 2010	16:40	39.2	0.38
Freiheit Spring	Aug. 30, 2010	16:41	34.9	0.39
Freiheit Spring	Aug. 30, 2010	16:42	31.3	0.26
Freiheit Spring	Aug. 30, 2010	16:43	28.3	0.23
Freiheit Spring	Aug. 30, 2010	16:44	25.8	0.19
Freiheit Spring	Aug. 30, 2010	16:45	22.9	-
Freiheit Spring	Aug. 30, 2010	16:46	21.2	0.16
Freiheit Spring	Aug. 30, 2010	16:47	19.3	0.11
Freiheit Spring	Aug. 30, 2010	16:48	17.2	0.12
Freiheit Spring	Aug. 30, 2010	16:49	-	0.11
Freiheit Spring	Aug. 30, 2010	16:50	14.9	0.08
Freiheit Spring	Aug. 30, 2010	16:51	13.8	0.10
Freiheit Spring	Aug. 30, 2010	16:52	12.7	0.09
Freiheit Spring	Aug. 30, 2010	16:53	11.6	0.07
Freiheit Spring	Aug. 30, 2010	16:54	10.6	0.07
Freiheit Spring	Aug. 30, 2010	16:55	9.73	0.05
Freiheit Spring	Aug. 30, 2010	16:56	8.95	0.06
Freiheit Spring	Aug. 30, 2010	16:57	8.27	-
Freiheit Spring	Aug. 30, 2010	16:58	7.44	0.07
Freiheit Spring	Aug. 30, 2010	16:59	6.16	0.05
Freiheit Spring	Aug. 30, 2010	17:00	5.75	0.04
Freiheit Spring	Aug. 30, 2010	17:01	4.87	-
Freiheit Spring	Aug. 30, 2010	17:02	4.87	0.03
Freiheit Spring	Aug. 30, 2010	17:04	4.21	0.04
Freiheit Spring	Aug. 30, 2010	17:06	3.66	0.03
Freiheit Spring	Aug. 30, 2010	17:08	3.27	0.02
Freiheit Spring	Aug. 30, 2010	17:10	3.03	0.04
Freiheit Spring	Aug. 30, 2010	17:12	2.53	0.02
Freiheit Spring	Aug. 30, 2010	17:14	2.26	0.02
Freiheit Spring	Aug. 30, 2010	17:16	2.05	< 0.01
Freiheit Spring	Aug. 30, 2010	17:18	1.86	0.03
Freiheit Spring	Aug. 30, 2010	17:20	1.68	0.02
Freiheit Spring	Aug. 30, 2010	17:22	1.51	< 0.01

Freiheit Spring	Aug. 30, 2010	17:24	1.39	0.03
Freiheit Spring	Aug. 30, 2010	17:26	1.28	0.01
Freiheit Spring	Aug. 30, 2010	17:28	1.20	< 0.01
Freiheit Spring	Aug. 30, 2010	17:30	1.09	0.03
Freiheit Spring	Aug. 30, 2010	17:32	1.01	0.01
Freiheit Spring	Aug. 30, 2010	17:34	0.914	0.01
Freiheit Spring	Aug. 30, 2010	17:36	0.882	< 0.01
Freiheit Spring	Aug. 30, 2010	17:38	0.766	-
Freiheit Spring	Aug. 30, 2010	17:40	0.740	< 0.01
Freiheit Spring	Aug. 30, 2010	17:42	0.686	< 0.01
Freiheit Spring	Aug. 30, 2010	17:44	0.638	< 0.01
Freiheit Spring	Aug. 30, 2010	17:46	0.600	< 0.01
Freiheit Spring	Aug. 30, 2010	17:48	0.566	< 0.01
Freiheit Spring	Aug. 30, 2010	17:50	0.541	< 0.01
Freiheit Spring	Aug. 30, 2010	17:52	0.498	< 0.01
Freiheit Spring	Aug. 30, 2010	17:54	0.491	< 0.01
Freiheit Spring	Aug. 30, 2010	17:56	0.459	< 0.01
Freiheit Spring	Aug. 30, 2010	17:58	0.437	< 0.01
Freiheit Spring	Aug. 30, 2010	18:00	0.419	< 0.01
Freiheit Spring	Aug. 30, 2010	18:10	0.350	< 0.01
Freiheit Spring	Aug. 30, 2010	18:20	0.284	< 0.01
Freiheit Spring	Aug. 30, 2010	18:30	0.251	< 0.01
Freiheit Spring	Aug. 30, 2010	18:40	0.238	< 0.01
Freiheit Spring	Aug. 30, 2010	18:50	0.201	< 0.01
Freiheit Spring	Aug. 30, 2010	19:00	0.166	
Freiheit Spring	Aug. 30, 2010	19:20	0.153	
Freiheit Spring	Aug. 30, 2010	19:40	0.124	
Freiheit Spring	Aug. 30, 2010	20:00	0.126	
Freiheit Spring	Aug. 30, 2010	20:20	0.102	
Freiheit Spring	Aug. 30, 2010	20:40	0.100	
Freiheit Spring	Aug. 30, 2010	21:00	0.081	
Freiheit Spring	Aug. 30, 2010	21:20	0.082	
Freiheit Spring	Aug. 30, 2010	21:40	0.071	
Freiheit Spring	Aug. 30, 2010	22:00	0.072	
Freiheit Spring	Aug. 30, 2010	22:20	0.065	
Freiheit Spring	Aug. 30, 2010	22:40	0.063	
Freiheit Spring	Aug. 30, 2010	23:00	0.055	
Freiheit Spring	Aug. 30, 2010	23:20	0.055	
Freiheit Spring	Aug. 30, 2010	23:40	0.046	
Freiheit Spring	Aug. 31, 2010	0:00	0.046	
Freiheit Spring	Aug. 31, 2010	0:20	0.036	
Freiheit Spring	Aug. 31, 2010	0:40	0.039	
Freiheit Spring	Aug. 31, 2010	1:00	0.034	
Freiheit Spring	Aug. 31, 2010	1:20	0.035	
Freiheit Spring	Aug. 31, 2010	1:40	0.031	
Freiheit Spring	Aug. 31, 2010	2:00	0.032	
Freiheit Spring	Aug. 31, 2010	2:20	0.028	
Freiheit Spring	Aug. 31, 2010	2:40	0.029	
Freiheit Spring	Aug. 31, 2010	3:00	0.029	
Freiheit Spring	Aug. 31, 2010	3:20	0.027	
Freiheit Spring	Aug. 31, 2010	3:40	0.025	
Freiheit Spring	Aug. 31, 2010	4:00	0.026	

Freiheit Spring	Aug. 31, 2010	4:20	0.026	
Freiheit Spring	Aug. 31, 2010	4:40	0.026	
Freiheit Spring	Aug. 31, 2010	5:00	0.022	
Freiheit Spring	Aug. 31, 2010	5:20	0.021	
Freiheit Spring	Aug. 31, 2010	5:40	0.020	
Freiheit Spring	Aug. 31, 2010	6:00	0.021	
Freiheit Spring	Aug. 31, 2010	6:20	0.018	
Freiheit Spring	Aug. 31, 2010	6:40	0.019	
Freiheit Spring	Aug. 31, 2010	7:00	0.018	
Freiheit Spring	Aug. 31, 2010	7:20	0.020	
Freiheit Spring	Aug. 31, 2010	7:40	0.017	
Freiheit Spring	Aug. 31, 2010	8:00	0.018	
Freiheit Spring	Aug. 31, 2010	8:20	0.018	
Freiheit Spring	Aug. 31, 2010	8:40	0.017	
Freiheit Spring	Aug. 31, 2010	9:00	0.017	
Freiheit Spring	Aug. 31, 2010	9:20	0.016	
Freiheit Spring	Aug. 31, 2010	9:40	0.015	
Freiheit Spring	Aug. 31, 2010	10:00	0.015	
Freiheit Spring	Aug. 31, 2010	10:20	0.014	
Freiheit Spring	Aug. 31, 2010	10:40	0.014	
Freiheit Spring	Aug. 31, 2010	11:00	0.019	
Freiheit Spring	Aug. 31, 2010	12:30	0.015	
Freiheit Spring	Aug. 31, 2010	14:00	0.014	
Freiheit Spring	Aug. 31, 2010	15:30	0.013	
Freiheit Spring	Aug. 31, 2010	17:00	0.013	
Freiheit Spring	Aug. 31, 2010	18:30	0.011	
Freiheit Spring	Aug. 31, 2010	20:00	0.020	
Freiheit Spring	Aug. 31, 2010	21:30	0.015	
Freiheit Spring	Aug. 31, 2010	23:00	0.019	
Freiheit Spring	Sept. 1, 2010	0:30	0.011	
Freiheit Spring	Sept. 1, 2010	2:00	0.009	
Freiheit Spring	Sept. 1, 2010	3:30	0.008	
Freiheit Spring	Sept. 1, 2010	5:00	0.007	
Freiheit Spring	Sept. 1, 2010	6:30	0.007	
Freiheit Spring	Sept. 1, 2010	8:00	0.007	
Freiheit Spring	Sept. 1, 2010	9:30	0.006	
Freiheit Spring	Sept. 1, 2010	11:00	0.010	
Freiheit Spring	Sept. 1, 2010	12:30	0.007	
Freiheit Spring	Sept. 1, 2010	14:00	0.008	
Freiheit Spring	Sept. 1, 2010	15:30	0.009	
Freiheit Spring	Sept. 1, 2010	17:00	0.008	
Freiheit Spring	Sept. 1, 2010	18:30	0.008	
Freiheit Spring	Sept. 1, 2010	20:00	0.008	
Freiheit Spring	Sept. 1, 2010	21:30	0.008	
Freiheit Spring	Sept. 1, 2010	23:00	0.008	
Freiheit Spring	Sept. 2, 2010	0:30	0.007	
Freiheit Spring	Sept. 2, 2010	2:00	0.007	
Freiheit Spring	Sept. 2, 2010	3:30	0.007	
Freiheit Spring	Sept. 2, 2010	5:00	0.006	
Freiheit Spring	Sept. 2, 2010	6:30	0.006	
Freiheit Spring	Sept. 2, 2010	8:00	0.006	
Freiheit Spring	Sept. 2, 2010	9:30	0.005	

Freiheit Spring	Sept. 2, 2010	11:00	0.004	
Freiheit Spring	Sept. 2, 2010	12:30	0.004	
Freiheit Spring	Sept. 2, 2010	14:00	0.004	
Freiheit Spring	Sept. 2, 2010	15:30	< 0.003	

Table B.2. Major anion water chemistry from Freiheit Spring, Kolling well, and pool (Aug. 30, 2010).

Location	Date	Time	F^-	Cl^-	NO_2^--N	Br^-	NO_3^--N	SO_4^{2-}	PO_4^{3-}-P
			ppm	ppm	ppm	ppm	ppm	ppm	ppm
Detection Limit for 1× dilution (DL1)			0.002	0.005	0.001	0.002	0.001	0.01	0.001
Freiheit Spring	Aug. 30, 2010	16:02:00	0.151	9.780	0.012	0.015	4.757	22.22	0.033
Freiheit Spring	Aug. 30, 2010	16:18:30	0.151	9.861	< 0.003	0.019	4.856	22.40	0.040
Freiheit Spring	Aug. 30, 2010	16:19:00	0.153	10.913	< 0.003	0.017	4.872	22.46	0.036
Freiheit Spring	Aug. 30, 2010	16:19:30	0.153	11.069	< 0.003	0.014	4.853	22.38	0.029
Freiheit Spring	Aug. 30, 2010	16:20:00	0.155	15.170	< 0.003	0.018	4.840	22.40	0.042
Freiheit Spring	Aug. 30, 2010	16:23:00	0.145	200.458	< 0.003	0.051	4.304	22.49	0.068
Freiheit Spring	Aug. 30, 2010	16:25:00	0.143	384.144	< 0.003	0.078	3.768	22.39	0.069
Freiheit Spring	Aug. 30, 2010	16:27:00	0.139	536.325	< 0.003	0.108	3.215	22.15	0.068
Freiheit Spring	Aug. 30, 2010	16:28:00	0.137	591.191	< 0.003	0.116	3.037	22.08	0.068
Freiheit Spring	Aug. 30, 2010	16:28:30	0.144	606.910	< 0.003	0.115	2.964	22.26	0.070
Freiheit Spring	Aug. 30, 2010	16:29:00	0.136	624.814	< 0.003	0.120	2.949	22.08	0.073
Freiheit Spring	Aug. 30, 2010	16:29:30	0.142	629.601	< 0.003	0.120	2.906	22.17	0.083
Freiheit Spring	Aug. 30, 2010	16:30:00	0.141	625.296	< 0.003	0.124	2.907	22.13	0.075
Freiheit Spring	Aug. 30, 2010	16:30:30	0.143	614.357	< 0.003	0.119	2.943	22.15	0.081
Freiheit Spring	Aug. 30, 2010	16:34:00	0.151	440.222	< 0.003	0.090	3.457	22.32	0.060
Freiheit Spring	Aug. 30, 2010	16:37:30	0.146	270.835	< 0.003	0.058	4.058	22.25	0.053
Freiheit Spring	Aug. 30, 2010	16:47:00	0.154	102.388	< 0.003	0.033	4.428	22.45	0.010
Freiheit Spring	Aug. 30, 2010	18:30:00	0.155	12.115	< 0.003	0.018	4.871	22.60	0.023
Freiheit Spring	Aug. 30, 2010	18:50:00	0.153	10.794	< 0.003	0.019	4.898	22.38	0.028
Kolling well	Aug. 30, 2010	11:20	0.147	0.690	< 0.003	< 0.006	0.103	18.14	0.010
Pool (North side)	Aug. 30, 2010	15:45	0.153	1524.388	< 0.003	0.241	0.074	21.31	0.017
Pool (South side)	Aug. 30, 2010	15:45	0.152	1533.591	< 0.003	0.240	0.068	21.27	0.009

Note: Samples were also analyzed for lactate (DL1 = 0.005 ppm), acetate (DL1 = 0.005 ppm), formate (DL1 = 0.005 ppm), oxalate (DL1 = 0.002 ppm), and thiosulfate (DL1 = 0.002 ppm). However, lactate was <0.015 ppm, acetate was < 0.015 ppm, formate was < 0.015 ppm, oxalate was < 0.006 ppm, and thiosulfate was < 0.006 ppm for all of the samples.

Table B.3. δD and $\delta^{18}O$ from Freiheit Spring, Kolling well, and pool (Aug. 30, 2010).

Sample	Date	Time	δD (‰) VSMOW	δD standard deviation	$\delta^{18}O$ (‰) VSMOW	$\delta^{18}O$ standard deviation
Freiheit Spring	Aug. 30, 2010	16:02	-58.39	0.31	-9.34	0.12
Freiheit Spring	Aug. 30, 2010	16:18:30	-58.63	0.5	-9.47	0.1
Freiheit Spring	Aug. 30, 2010	16:19	-58.63	0.38	-9.2	0.12
Freiheit Spring	Aug. 30, 2010	16:19:30	-58.85	0.22	-9.12	0.16
Freiheit Spring	Aug. 30, 2010	16:20	-58	0.27	-9.54	0.08
Freiheit Spring	Aug. 30, 2010	16:23	-47.32	0.36	-9.37	0.16
Freiheit Spring	Aug. 30, 2010	16:25	-36.32	0.49	-9.05	0.09
Freiheit Spring	Aug. 30, 2010	16:27	-28.69	0.48	-9.24	0.09
Freiheit Spring	Aug. 30, 2010	16:28	-25.62	0.31	-9.37	0.08
Freiheit Spring	Aug. 30, 2010	16:28:30	-24.38	0.19	-9.37	0.12
Freiheit Spring	Aug. 30, 2010	16:29	-23.42	0.28	-9.35	0.09
Freiheit Spring	Aug. 30, 2010	16:29:30	-22.82	0.29	-9.23	0.12
Freiheit Spring	Aug. 30, 2010	16:30	-23.14	0.16	-9.41	0.11
Freiheit Spring	Aug. 30, 2010	16:30:30	-24.16	0.07	-9.27	0.08
Freiheit Spring	Aug. 30, 2010	16:34	-33.94	0.23	-9.08	0.13
Freiheit Spring	Aug. 30, 2010	16:37:30	-43.87	0.14	-9.24	0.06
Freiheit Spring	Aug. 30, 2010	16:47	-53.49	0.19	-9.42	0.2
Freiheit Spring	Aug. 30, 2010	18:30	-57.92	0.22	-9.62	0.1
Freiheit Spring	Aug. 30, 2010	18:50	-58.9	0.42	-9.45	0.1
Kolling well	Aug. 30, 2010	11:20	-60.23	0.26	-9.41	0.07
Pool (North side)	Aug. 30, 2010	15:45	29.45	0.23	-9.6	0.08
Pool (South side)	Aug. 30, 2010	15:45	30.18	0.29	-9.35	0.12

Appendix C

Thermal peak lag simulations

This appendix includes details about the thermal peak lag, the output peak temperature, and the variables used for each heat transport simulation from Chapter 4. Table C.1 provides details about cylindrical simulations, and planar simulations are summarized in Table C.2.

Table C.1. Thermal peak lag, output peak temperature, and variables used in cylindrical simulations.

Simulation	Thermal peak lag (sec)	Output peak temp	Variables different from those given in Table 4.1 (units are the same as those given in Table 4.1)
C1	-	1.00 (i.e., completely damped)	$D_H = 0.01$
C2	-	1.00 (i.e., completely damped)	$D_H = 0.0178$
C3	16,300	1.11	$D_H = 0.0316$
C4	7,360	1.43	$D_H = 0.0562$
C5	3,590	1.71	$D_H = 0.1$
C6	1,840	1.87	$D_H = 0.178$
C7	978	1.94	$D_H = 0.316$
C8	297	1.99	-
C9	93.3	2.00	$D_H = 3.16$
C10	30.0	2.00	$D_H = 10$
C11	29.9	2.00	$L = 100$
C12	96.5	2.00	$L = 316$
C13	952	1.96	$L = 3{,}160$
C14	2,990	1.87	$L = 10{,}000$
C15	9,700	1.64	$L = 31{,}600$
C16	15,700	1.31	$v = 0.00626$
C17	11,900	1.48	$v = 0.0111$
C18	7,830	1.65	$v = 0.0198$
C19	4,770	1.78	$v = 0.0352$
C20	2,830	1.87	$v = 0.0626$
C21	924	1.96	$v = 0.198$
C22	95.2	2.00	$v = 1.98$
C23	30.1	2.00	$v = 6.26$
C24	51.4	1.94	$R_D = 1{,}900$
C25	92.5	1.96	$R_D = 6{,}000$
C26	166	1.98	$R_D = 19{,}000$
C27	538	1.99	$R_D = 190{,}000$
C28	983	1.99	$R_D = 600{,}000$
C29	297	1.10	$R_A = 0.1$
C30	298	1.31	$R_A = 0.316$
C31	298	4.12	$R_A = 3.16$
C32	297	10.86	$R_A = 10$
C33	203	1.99	$k_r = 1$

C34	248	1.99	$k_r = 1.5$
C35	286	1.99	$k_r = 2$
C36	320	1.98	$k_r = 2.5$
C37	351	1.98	$k_r = 3$
C38	276	1.99	$c_{p,r} = 700$
C39	295	1.99	$c_{p,r} = 800$
C40	313	1.99	$c_{p,r} = 900$
C41	330	1.98	$c_{p,r} = 1{,}000$
C42	276	1.99	$\rho_r = 2{,}000$
C43	292	1.99	$\rho_r = 2{,}250$
C44	308	1.99	$\rho_r = 2{,}500$
C45	323	1.98	$\rho_r = 2{,}750$
C46	337	1.98	$\rho_r = 3{,}000$
C47	297	1.99	$k_w = 0.5$
C48	297	1.99	$k_w = 0.55$
C49	297	1.99	$k_w = 0.6$
C50	297	1.99	$k_w = 0.65$
C51	297	1.99	$k_w = 0.7$
C52	304	1.99	$c_{p,w} = 4{,}100$
C53	300	1.99	$c_{p,w} = 4{,}150$
C54	293	1.99	$c_{p,w} = 4{,}250$
C55	290	1.99	$c_{p,w} = 4{,}300$
C56	303	1.99	$\rho_w = 980$
C57	300	1.99	$\rho_w = 990$
C58	294	1.99	$\rho_w = 1{,}010$
C59	291	1.99	$\rho_w = 1{,}020$
C60	298	1.99	$\mu_w = 0.0006$
C61	297	1.99	$\mu_w = 0.0009$
C62	297	1.99	$\mu_w = 0.0012$
C63	297	1.99	$\mu_w = 0.0015$
C64	296	1.99	$\mu_w = 0.0018$
C65	-	1.00 (i.e., completely damped)	$D_H = 0.1$; $v = 0.0346$
C66	20.5	2.00	$D_H = 10$; $v = 0.907$
C67	21,400	1.15	$D_H = 0.1$; $v = 0.110$
C68	6.66	2.00	$D_H = 10$; $v = 2.87$
C69	6,530	1.54	$D_H = 0.1$; $v = 0.346$
C70	92.9	2.00	$L = 100$; $v = 0.198$
C71	9,530	1.64	$L = 10{,}000$; $v = 0.198$
C72	9.31	2.00	$L = 100$; $v = 1.98$
C73	946	1.96	$L = 10{,}000$; $v = 1.98$
C74	283	1.89	$v = 0.198$; $R_D = 6{,}000$
C75	3,090	1.98	$v = 0.198$; $R_D = 600{,}000$
C76	29.5	1.99	$v = 1.98$; $R_D = 6{,}000$
C77	295	2.00	$v = 1.98$; $R_D = 600{,}000$
C78	930	1.10	$v = 0.198$; $R_A = 0.1$
C79	930	10.56	$v = 0.198$; $R_A = 10$
C80	94.8	1.10	$v = 1.98$; $R_A = 0.1$
C81	94.5	10.96	$v = 1.98$; $R_A = 10$
C82	2,240	1.87	$D_H = 0.316$; $v = 0.273$
C83	6,040	1.75	$L = 20{,}000$
C84	289	1.99	$L = 100$; $v = 0.0626$

C85	300	1.99	L = 10,000; v = 6.26
C86	-	1.00 (i.e., completely damped)	D_H = 0.05; v = 0.0586; R_D = 6,000,000
C87	733,000	1.51	L = 200,000; R_D = 6,000,000
C88	287,000	1.61	D_H = 0.2; v = 0.0609; R_D = 6,000,000
C89	35,600	1.97	L = 10,000; R_D = 6,000,000
C90	113,000	1.90	L = 10000; v = 0.198; R_D = 6,000,000
C91	-	1.00 (i.e., completely damped)	D_H = 0.02; v = 0.213; R_D = 6,000,000
C92	1,560,000	1.04	D_H = 0.0632; L = 3,430; v = 0.231; R_D = 6,000,000
C93	871,000	1.24	D_H = 0.2; L = 28,600; v = 0.609; R_D = 6,000,000
C94	559	1.04	D_H = 0.02; L = 100; v = 0.213; R_D = 600
C95	478	1.08	D_H = 0.0356; L = 110; v = 0.131; R_D = 600
C96	500	1.12	D_H = 0.0632; L = 343; v = 0.231; R_D = 600
C97	8,440	1.25	D_H = 0.02; L = 100; v = 0.213
C98	5,790	1.52	D_H = 0.0632; L = 343; v = 0.231
C99	-	1.00 (i.e., completely damped)	D_H = 0.02; v = 0.213
C100	-	1.00 (i.e., completely damped)	D_H = 0.0632; L = 3,430; v = 0.231
C101	61,200	1.04	D_H = 0.2; L = 28,600; v = 0.609
C102	1,280	1.95	D_H = 10; L = 20,000; v = 0.287
C103	802,000	1.32	D_H = 0.3; L = 20,000; v = 0.263; R_D = 6,000,000
C104	275,000	1.71	D_H = 0.5; L = 20,000; v = 0.383; R_D = 6,000,000

Table C.2. Thermal peak lag, output peak temperature, and variables used in planar simulations.

Simulation	Thermal peak lag (sec)	Output peak temp	Variables different from those given in Table 4.1 (units are the same as those given in Table 4.1)
P1 (equivalent to C1)	33,200	1.35	D_H = 0.01
P2 (equivalent to C2)	17,700	1.55	D_H = 0.0178
P3 (equivalent to C3)	9,670	1.71	D_H = 0.0316
P4 (equivalent to C4)	5,360	1.82	D_H = 0.0562
P5 (equivalent to C5)	2,990	1.90	D_H = 0.1
P6 (equivalent to C6)	1,670	1.94	D_H = 0.178
P7 (equivalent to C7)	935	1.97	D_H = 0.316
P8 (equivalent to C65)	63,900	1.17	D_H = 0.1; v = 0.0346
P9 (equivalent to C67)	17,700	1.54	D_H = 0.1; v = 0.110
P10 (equivalent to C69)	5,430	1.82	D_H = 0.1; v = 0.346
P11 (equivalent to C82)	2,140	1.92	D_H = 0.316; v = 0.273
P12 (equivalent to C86)	645,000	1.79	D_H = 0.05; v = 0.0586; R_D = 6,000,000
P13 (equivalent to C88)	153,000	1.94	D_H = 0.2; v = 0.0609; R_D = 6,000,000
P14 (equivalent to C91)	443,000	1.85	D_H = 0.02; v = 0.213; R_D = 6,000,000
P15 (equivalent to C92)	443,000	1.85	D_H = 0.0632; L = 3,430; v = 0.231; R_D = 6,000,000
P16 (equivalent to C93)	443,000	1.85	D_H = 0.2; L = 28,600; v = 0.609; R_D = 6,000,000
P17 (equivalent to C94)	503	1.22	D_H = 0.02; L = 100; v = 0.213; R_D = 600

P18 (equivalent to C95)	476	1.22	$D_H = 0.0356$; $L = 110$; $v = 0.131$; $R_D = 600$
P19 (equivalent to C96)	495	1.22	$D_H = 0.0632$; $L = 343$; $v = 0.231$; $R_D = 600$
P20 (equivalent to C97)	4,410	1.85	$D_H = 0.02$; $L = 100$; $v = 0.213$
P21 (equivalent to C98)	4,400	1.85	$D_H = 0.0632$; $L = 343$; $v = 0.231$
P22 (equivalent to C99)	52,200	1.22	$D_H = 0.02$; $v = 0.213$
P23 (equivalent to C100)	52,100	1.22	$D_H = 0.0632$; $L = 3{,}430$; $v = 0.231$
P24 (equivalent to C101)	52,300	1.22	$D_H = 0.2$; $L = 28{,}600$; $v = 0.609$
P25 (equivalent to C103)	478,000	1.84	$D_H = 0.3$; $L = 20{,}000$; $v = 0.263$; $R_D = 6{,}000{,}000$
P26 (equivalent to C104)	195,000	1.93	$D_H = 0.5$; $L = 20{,}000$; $v = 0.383$; $R_D = 6{,}000{,}000$

Appendix D

Discharge measurements

Discharge was measured at several springs, a cave stream and an ephemeral surface stream over the past two years using the salt dilution method, a pygmy meter, or the bucket method. The salt dilution method is a common method to measure discharge in shallow or turbulent flows (e.g., see Section 4.6.6 in Groves 2007). The sudden-injection method was used for all salt dilution discharge measurements in this appendix. Salt was dissolved in a 5 gal bucket of water and was then poured across the cross section of the spring run. Electrical conductivity was measured and recorded by a data logger ~30 m downstream of the salt solution injection point, and background electrical conductivity was subtracted from the breakthrough curve to get the portion of the breakthrough curve that resulted from the salt injection. Standards of known salt concentration were prepared and put in the spring run for sufficient time so that they approached thermal equilibrium with the spring water temperature. Electrical conductivity was measured for each of these standards to determine a conductivity-concentration relationship. This relationship was used to convert the electrical conductivity less background breakthrough curve to concentration, and discharge Q was then calculated using the following equation:

$$Q = \frac{M}{\int_0^t C dt}, \tag{D.1}$$

where M is the salt mass and C the concentration. Salt dilution discharge measurements are reported here with units of L/s. However, the actual units for these measurements are the less common kg/s. It is assumed that 1 L/s = 1 kg/s.

A pygmy meter was used to calculate discharge at some springs. The spring run's cross section was divided into several sections, and the average velocity was determined for each section by measuring velocity at a depth of 0.6 times the total flow depth at each section. Then, discharge, Q, was calculated for each section by multiplying the product of the width and depth of flow for each section (i.e., area, A) by the velocity measurement, v, for that section (i.e., $Q = v\,A$). Finally, summing discharges for each section gives total discharge.

The bucket method was used at two springs where there was relatively little flow that could easily be captured by a bucket. This method measures discharge by dividing a bucket's volume by the time it takes to fill the bucket.

A lot of the discharge measurements in this appendix were taken in late September 2009. Springs were at baseflow due to preceding dry conditions. The goal was to measure baseflow discharge at many of the larger springs in Fillmore County to estimate springshed size using the method proposed by Quinlan and Ray (1995). However, this project was terminated early because of higher spring flows due to significant precipitation in October 2009.

MN23:A2 (Moth Spring), 560137 m E, 4832032 m N (± 2 m), UTM Zone 15: 175 L/s (Sept. 22, 2009 11:53; salt dilution); 134 L/s (Sept. 22, 2009 ~11:45; pygmy meter)

MN23:A3 (Grabau Spring), 560244 m E, 4832069 m N (± 3 m), UTM Zone 15: 41 L/s (Sept. 22, 2009 13:20; salt dilution); 45 L/s (Sept. 22, 2009 ~13:15; pygmy meter)

MN23:A4 (Stagecoach Spring), 563795 m E, 4838166 m N (± 5 m), UTM Zone 15: 75 L/s (Sept. 22, 2009 16:43; salt dilution); 77 L/s (Sept. 22, 2009 17:02; salt dilution); 71 L/s (Sept. 22, 2009 ~16:30; pygmy meter); 78 L/s (Sept. 22, 2009 ~16:45; pygmy meter); 75 L/s (Sept. 22, 2009 ~17:00; pygmy meter)

MN23:A13 (Bat River Spring), 558232 m E, 4846119 m N (± 4.1 m), UTM Zone 15: 6.1 L/s (Sept. 29, 2009 16:02; salt dilution); 6.1 L/s (Sept. 29, 2009 16:48; salt dilution)

MN23:A20 (Odessa Spring): 135 L/s (May 5, 2009 14:23; salt dilution)

MN23:A31 (Rainy Spring), 562890 m E, 4829020 m N (± 3.6 m), UTM Zone 15: 10.5 L/s (Sept. 30, 2009 14:03; salt dilution); 10.6 L/s (Sept. 30, 2009 14:36; salt dilution)

MN23:A33 (Trout Spring), 562517 m E, 4828219 m N (± 8.4 m), UTM Zone 15: 35 L/s (Sept. 30, 2009 17:14; salt dilution); 35 L/s (Sept. 30, 2009 17:43; salt dilution)

MN23:A34 (Black Rock Spring), 562574 m E, 4828227 m N (± 7.7 m), UTM Zone 15: 87 L/s (Sept. 30, 2009 15:56; salt dilution); 78 L/s (Sept. 30, 2009 16:19; salt dilution)

MN23:A36 (Barr Spring), 556673 m E, 4839978 m N (± 4.5 m), UTM Zone 15: spring is dry (Sept. 24, 2009)

MN23:A37 (Fountain Big Spring), 568634 m E, 4844756 m N (± 5 m), UTM Zone 15: 14.3 L/s (Sept. 23, 2009 10:15; salt dilution); 12.0 L/s (Sept. 23, 2009 14:40; pygmy meter)

MN23:A41 (Freiheit Spring), 554978 m E, 4839445 m N (± 3.5 m), UTM Zone 15: 22 L/s (Apr. 24, 2009 15:18; salt dilution); 54 L/s (May 27, 2009 15:38; salt dilution); 51 L/s (May 27, 2009 18:18; salt dilution); 50 L/s (May 28, 2009 18:23; salt dilution, recorded by first data logger); 54 L/s (May 28, 2009 18:23; salt dilution, recorded by second data logger); 54 L/s (June 3, 2009 13:13; salt dilution); 139 L/s (June 8, 2009 15:39; salt dilution); 130 L/s (June 8, 2009 18:37; salt dilution); 130 L/s (June 8, 2009 18:53; salt dilution); 122 L/s (June 8, 2009 20:53; salt dilution); 125 L/s (June 9, 2009 9:37; salt dilution); 128 L/s (June 9, 2009 14:27; salt dilution); 82 L/s (June 17, 2009 17:03; salt dilution); 75 L/s (June 24, 2009 14:25; salt dilution); 36 L/s (July 14, 2009 13:17; salt dilution); 20 L/s (Sept. 4, 2009 11:17; salt dilution); 19 L/s (Sept. 22, 2009 18:45; pygmy meter); 28 L/s (Aug. 25, 2010 17:49; salt dilution); 28 L/s (Aug. 25, 2010 18:10; salt dilution); 28 L/s (Aug. 26, 2010 9:39; salt dilution); 28 L/s (Aug. 26, 2010 10:10; salt dilution); 27 L/s (Aug. 30, 2010 19:52; salt dilution); 26 L/s (Aug. 31, 2010 12:27; salt dilution); 27 L/s (Aug. 31, 2010 12:52; salt dilution); 114 L/s (Sept. 28, 2010 10:04; salt dilution); 133 L/s (May 2, 2011 18:05; salt dilution); 132 L/s (May 2, 2011 18:16; salt dilution)

MN23:A44 (Little Falls Spring), 568734 m E, 4844899 m N (± 7 m), UTM Zone 15: 0.75 L/s (Sept. 23, 2009 11:30; bucket); 0.79 L/s (Sept. 23, 2009 11:30; bucket); 0.76 L/s (Sept. 23, 2009 11:30; bucket)

MN23:A45 (Little Quarry Spring), 568667 m E, 4844776 m N (± 5 m), UTM Zone 15: 2.3 L/s (Sept. 23, 2009 13:49; salt dilution); 1.62 L/s (Sept. 23, 2009 10:00; bucket); 1.73 L/s (Sept. 23, 2009 10:00; bucket); 1.66 L/s (Sept. 23, 2009 10:00; bucket); 1.64 L/s (Sept. 23, 2009 10:38; bucket)

MN23:A47 (Mahood Spring), 556589 m E, 4839893 m N (± 5.2 m), UTM Zone 15: 23 L/s (Sept. 24, 2009 10:34; salt dilution); 22 L/s (Sept. 24, 2009 11:09; salt dilution)

MN23:A48 (Narcissis Rise), 556610 m E, 4839789 m N (± 4.5 m), UTM Zone 15: 23 L/s (Sept. 24, 2009 11:52; salt dilution); 23 L/s (Sept. 24, 2009 12:19; salt dilution)

MN23:A51 (Quarry Spring), 568762 m E, 4844849 m N (± 5 m), UTM Zone 15: 4.4 L/s (Sept. 23, 2009 12:02; salt dilution); 2.5 L/s (Sept. 23, 2009 ~12:40; pygmy meter)

MN23:A52 (Root Spring), 560777 m E, 4832690 m N (± 5 m), UTM Zone 15: 5.2 L/s (Sept. 22, 2009 14:20; salt dilution); 4.8 L/s (Sept. 22, 2009 ~14:15; pygmy meter)

MN23:A57 (Granger Spring): 23 L/s (May 5, 2009 16:56; salt dilution)

MN23:A122 (Tyson Spring), 561401 m E, 4845410 m N (± 4.9 m), UTM Zone 15: 50 L/s (May 27, 2009 11:17; salt dilution); 84 L/s (May 27, 2009 12:14; salt dilution); 8.6 L/s (Sept. 29, 2009 10:25; salt dilution); 8.7 L/s (Sept. 29, 2009 11:21; salt dilution); 5.2 L/s (Sept. 29, 2009 11:45; pygmy meter)

MN23:A144 (Mahoney Spring), 573283 m E, 4843573 m N (± 2.9 m), UTM Zone 15: 5.6 L/s (Sept. 23, 2009 16:54; salt dilution); 5.4 L/s (Sept. 23, 2009 17:30; salt dilution); 3.4 L/s (Sept. 23, 2009 ~18:30; pygmy meter)

MN23:A358 (Hart Spring), 577793 m E, 4826370 m N (± 4.5 m), UTM Zone 15: 3.4 L/s (Sept. 24, 2009 16:49; salt dilution); 3.5 L/s (Sept. 24, 2009 18:06; salt dilution)

MN23:A875 (Vreeman Spring), 561017 m E, 4830295 m N (± 4.1 m), UTM Zone 15: 14.0 L/s (Sept. 30, 2009 9:24; salt dilution); 15.4 L/s (Sept. 30, 2009 10:29; salt dilution); 13.5 L/s (Sept. 30, 2009 ~11:15; pygmy meter); 14.7 L/s (Sept. 30, 2009 11:29; pygmy meter)

MN23:A876 (Turnlaithe Spring), 561098 m E, 4846007 m N (± 4.3 m), UTM Zone 15: 5.2 L/s (Sept. 29, 2009 13:01; salt dilution); 5.2 L/s (Sept. 29, 2009 13:49; salt dilution)

MN23:X0016 (stream in Goliath's Cave at David's Entrance), 559447 m E, 4825749 m N (± 3.3 m), UTM Zone 15: 1.8 L/s (July 14, 2009 11:26; salt dilution)

MN23:X0147 (Downstream of Stream Sink which eventually flows to Freiheit Spring), 554277 m E, 4838995 m N (± 4.3 m), UTM Zone 15: 11.2 L/s (June 17, 2009 14:28; salt dilution)

MN23:X0148 (Upstream of Stream Sink which eventually flows to Freiheit Spring), 554207 m E, 4838809 m N (± 2.2 m), UTM Zone 15: 20 L/s (June 17, 2009 15:09; salt dilution)

Appendix E

Recharge event water chemistry and suspended sediment at Freiheit Spring

Two ISCOs were set up at Freiheit Spring to collect spring water following a storm. The ISCOs were connected to the data logger at the spring so that they would be triggered to begin sampling once water level at the spring exceeded a defined threshold. The first 30 samples were collected on June 9, 2009, sampled by the ISCOs from 4:46 on June 8, 2009 to 14:46 on June 9, 2009. The bottles were replaced and an additional 48 samples were collected on June 17, 2009, sampled by the ISCOs from 18:48 on June 9, 2009 to 10:39 on June 17, 2009. Select samples were analyzed for major cations (Table E.1) and anions (Table E.2) by Rick Knurr in the Analytical Geochemistry Lab of the University of Minnesota's Department of Geology and Geophysics. Cations were analyzed using Inductively Coupled Plasma – Optical Emission Spectrometry (ICP-OES) following EPA Method 200.7 with a Thermo Scientific iCAP 6500 dual view ICP-OES. Anions were analyzed using anion chromatography following EPA method 300.1 with a Dionex ICS 2000 system with an AS20 column and an AMMS III suppressor and a NaOH eluent. Anion analysis also used a 1.20 ml/min flow rate, a 25 mM H_2SO_4 regenerant, a 50 µl injection, and a conductivity detector. pH, conductivity, and suspended sediment were measured for all of the samples in the lab (Table E.3). However, pH is only reported for the first 30 samples in Table E.3. Erroneous pH values were attained for the second batch of water samples likely because of malfunction of the pH meter or because pH was not measured until 1-9 days after the water samples were collected by the ISCOs. Sediment was filtered from the water samples onto a 1 µm glass fiber filter and dried overnight in an oven at 104°C as per Standard Method 2540D from the American Public Health Association, American Water Works Association, Water Environment Federation. The mass of sediment and water was used to calculate suspended sediment concentration. Alkalinity titrations were conducted in the lab for the first 30 samples (Table E.3).

Table E.1. Major cation recharge chemistry at Freiheit Spring (June 8-9, 2009).

Location	Date	Time	Al^{3+}	Ba^{2+}	Ca^{2+}	K^{+}	Mg^{2+}	Na^{+}	P total	Si total	Sr^{2+}
			ppm	ppm	ppm	ppm	ppm	ppm	ppm	ppm	ppm
Detection Limit for 3× dilution (DL3)			0.004	0.006	0.7	0.6	0.4	0.2	0.01	0.2	0.005
Freiheit Spring [a]	June 8, 2009	4:46	< 0.004	0.106	78.0	1.1	26.6	4.3	0.04	6.6	0.098
Freiheit Spring [b]	June 8, 2009	4:46	< 0.004	0.109	78.1	1.2	26.6	4.4	0.08	6.6	0.100
Freiheit Spring [a]	June 8, 2009	5:46	0.016	0.087	77.2	1.3	26.0	4.3	0.06	6.6	0.098
Freiheit Spring [b]	June 8, 2009	6:46	< 0.004	0.111	83.6	1.9	26.8	4.4	0.08	7.2	0.112
Freiheit Spring [a]	June 8, 2009	7:46	0.005	0.116	82.2	2.9	24.3	4.1	0.14	6.8	0.112
Freiheit Spring [b]	June 8, 2009	8:46	< 0.004	0.121	82.6	3.2	24.5	4.2	0.13	6.7	0.113
Freiheit Spring [a]	June 8, 2009	15:46	< 0.004	0.104	70.5	3.2	18.9	3.1	0.13	5.2	0.099
Freiheit Spring [a]	June 8, 2009	19:46	0.004	0.108	64.0	3.2	16.4	2.7	0.16	5.0	0.091
Freiheit Spring [b]	June 9, 2009	0:46	0.007	0.106	68.7	3.2	19.0	3.1	0.14	5.6	0.096
Freiheit Spring [b]	June 9, 2009	14:46	0.008	0.108	73.0	2.5	21.6	3.5	0.11	6.2	0.100

[a] Sample was collected by ISCO #2.

[b] Sample was collected by ISCO #1.

Note: Samples were also analyzed for total Fe (DL3 = 0.08 ppm), Li^{+} (DL3 = 0.03 ppm), and total Mn (DL3 = 0.008 ppm). However, Fe was < 0.08 ppm, Li^{+} was < 0.03 ppm, and total Mn was < 0.008 ppm for all of the samples.

Table E.2. Major anion recharge chemistry, pH, and charge balance at Freiheit Spring (June 8-9, 2009).

Location	Date	Time	pH	Alkalinity	F^-	Cl^-	Br^-	NO_3^--N	SO_4^{2-}	PO_4^{3-}-P	Charge balance
				as ppm CaCO3	ppm	ppm	ppm	ppm	ppm	ppm	%
Detection Limit for 1× dilution (DL1)				12	0.005	0.005	0.01	0.005	0.01	0.005	
Freiheit Spring [a]	June 8, 2009	4:46	7.40	258	0.184	9.332	< 0.01	4.545	17.42	0.049	1.46
Freiheit Spring [b]	June 8, 2009	4:46	7.32	262	0.181	9.311	0.01	4.563	17.89	0.044	0.82
Freiheit Spring [a]	June 8, 2009	5:46	7.39	256	0.161	9.067	< 0.01	4.534	17.10	0.023	1.27
Freiheit Spring [b]	June 8, 2009	6:46	7.30	274	0.171	9.307	0.02	4.566	15.91	0.016	1.65
Freiheit Spring [a]	June 8, 2009	7:46	7.34	273	0.173	8.607	0.01	4.553	14.23	0.030	0.22
Freiheit Spring [b]	June 8, 2009	8:46	7.33	264	0.162	8.856	0.01	4.671	15.17	0.055	1.74
Freiheit Spring [a]	June 8, 2009	15:46	7.37	221	0.133	7.128	< 0.01	4.963	10.05	0.066	0.97
Freiheit Spring [a]	June 8, 2009	19:46	7.23	199	0.143	5.937	< 0.01	4.223	7.60	0.071	1.39
Freiheit Spring [b]	June 9, 2009	0:46	7.36	224	0.126	6.081	< 0.01	4.475	8.17	0.065	0.62
Freiheit Spring [b]	June 9, 2009	14:46	7.37	254	0.138	6.268	< 0.01	4.557	8.85	0.053	-1.16

[a] Sample was collected by ISCO #2.

[b] Sample was collected by ISCO #1.

Note: Samples were also analyzed for acetate (DL1 = 0.005 ppm), formate (DL1 = 0.005 ppm), NO_2^--N (DL1 = 0.005 ppm), ClO_3^- (DL1 = 0.01 ppm), and oxalate (DL1 = 0.01 ppm). However, acetate was < 0.005 ppm, formate was < 0.005 ppm, NO_2^--N was < 0.005 ppm, ClO_3^- was < 0.01 ppm, and oxalate was < 0.01 ppm for all of the samples.

Table E.3. Recharge event pH, conductivity, alkalinity, and suspended sediment at Freiheit Spring (June 8-17, 2009).

Location	Date	Time	pH	Electrical conductivity, temperature corrected (1.9% / ºC)	Alkalinity	Suspended sediment
				µS/cm	as ppm CaCO3	mg sediment / g water
Detection Limit					12	0.001
Freiheit Spring [a]	June 8, 2009	4:46	7.4	532	258	0.004
Freiheit Spring [b]	June 8, 2009	4:46	7.3	532	262	0.003
Freiheit Spring [a]	June 8, 2009	5:46	7.4	526	256	0.024
Freiheit Spring [b]	June 8, 2009	6:46	7.3	548	274	0.082
Freiheit Spring [a]	June 8, 2009	7:46	7.3	538	273	0.162
Freiheit Spring [b]	June 8, 2009	8:46	7.3	530	264	0.306
Freiheit Spring [a]	June 8, 2009	9:46	7.3	533	259	0.334
Freiheit Spring [b]	June 8, 2009	10:46	7.5	503	251	0.598
Freiheit Spring [a]	June 8, 2009	11:46	7.4	483	239	0.557
Freiheit Spring [b]	June 8, 2009	12:46	7.3	471	229	0.487
Freiheit Spring [a]	June 8, 2009	13:46	7.4	469	228	0.335
Freiheit Spring [b]	June 8, 2009	14:46	7.4	467	223	0.305
Freiheit Spring [a]	June 8, 2009	15:46	7.4	458	221	0.250
Freiheit Spring [b]	June 8, 2009	16:46	7.3	443	215	0.253
Freiheit Spring [a]	June 8, 2009	17:46	7.3	423	206	0.198
Freiheit Spring [b]	June 8, 2009	18:46	7.2	412	202	0.204
Freiheit Spring [a]	June 8, 2009	19:46	7.2	415	199	0.173
Freiheit Spring [b]	June 8, 2009	20:46	7.4	410	198	0.178
Freiheit Spring [a]	June 8, 2009	21:46	7.4	423	207	0.133
Freiheit Spring [b]	June 8, 2009	22:46	7.4	438	207	0.144
Freiheit Spring [a]	June 8, 2009	23:46	7.4	444	218	0.124
Freiheit Spring [b]	June 9, 2009	0:46	7.4	458	224	0.143
Freiheit Spring [a]	June 9, 2009	1:46	7.3	465	226	0.116
Freiheit Spring [b]	June 9, 2009	2:46	7.4	467	231	0.139
Freiheit Spring [a]	June 9, 2009	4:46	7.3	476	234	0.102
Freiheit Spring [b]	June 9, 2009	6:46	7.4	478	247	0.117
Freiheit Spring [a]	June 9, 2009	8:46	7.4	481	245	0.091
Freiheit Spring [b]	June 9, 2009	10:46	7.4	483	246	0.095

Freiheit Spring [a]	June 9, 2009	12:46	7.4	487	248	0.075
Freiheit Spring [b]	June 9, 2009	14:46	7.4	489	254	0.089
Freiheit Spring [b]	June 9, 2009	18:48		486		0.075
Freiheit Spring [a]	June 9, 2009	18:49		485		0.057
Freiheit Spring [a]	June 9, 2009	19:49		490		0.055
Freiheit Spring [b]	June 9, 2009	20:48		486		0.069
Freiheit Spring [a]	June 9, 2009	21:49		491		0.055
Freiheit Spring [b]	June 9, 2009	22:48		486		-
Freiheit Spring [a]	June 9, 2009	23:49		489		0.055
Freiheit Spring [b]	June 10, 2009	0:48		484		-
Freiheit Spring [a]	June 10, 2009	1:49		488		0.049
Freiheit Spring [b]	June 10, 2009	2:48		488		0.061
Freiheit Spring [a]	June 10, 2009	3:49		490		0.052
Freiheit Spring [b]	June 10, 2009	4:48		491		0.062
Freiheit Spring [a]	June 10, 2009	5:49		491		0.046
Freiheit Spring [b]	June 10, 2009	6:48		489		0.055
Freiheit Spring [a]	June 10, 2009	7:49		493		0.041
Freiheit Spring [b]	June 10, 2009	8:48		492		0.049
Freiheit Spring [a]	June 10, 2009	9:49		491		0.039
Freiheit Spring [b]	June 10, 2009	10:48		489		0.048
Freiheit Spring [a]	June 10, 2009	11:49		496		0.037
Freiheit Spring [b]	June 10, 2009	12:48		492		0.040
Freiheit Spring [a]	June 10, 2009	13:49		505		0.032
Freiheit Spring [b]	June 10, 2009	14:48		500		0.042
Freiheit Spring [a]	June 10, 2009	15:49		498		0.034
Freiheit Spring [b]	June 10, 2009	16:48		494		0.039
Freiheit Spring [a]	June 10, 2009	18:49		502		0.031
Freiheit Spring [b]	June 10, 2009	20:48		496		0.040
Freiheit Spring [a]	June 10, 2009	22:49		496		0.027
Freiheit Spring [b]	June 11, 2009	0:48		499		0.037
Freiheit Spring [a]	June 11, 2009	2:49		503		0.026
Freiheit Spring [b]	June 11, 2009	4:48		501		0.031
Freiheit Spring [a]	June 11, 2009	12:49		503		0.019
Freiheit Spring [b]	June 11, 2009	21:27		508		0.039
Freiheit Spring [a]	June 12, 2009	5:28		509		0.020

Freiheit Spring [b]	June 12, 2009	14:06		514		0.040
Freiheit Spring [a]	June 12, 2009	22:07		514		0.014
Freiheit Spring [b]	June 13, 2009	6:45		514		0.029
Freiheit Spring [a]	June 13, 2009	14:46		520		0.010
Freiheit Spring [b]	June 13, 2009	23:24		522		0.047
Freiheit Spring [a]	June 14, 2009	7:25		520		0.013
Freiheit Spring [b]	June 14, 2009	16:03		528		0.034
Freiheit Spring [a]	June 15, 2009	0:04		526		0.010
Freiheit Spring [b]	June 15, 2009	8:42		531		0.046
Freiheit Spring [a]	June 15, 2009	16:43		526		0.011
Freiheit Spring [b]	June 16, 2009	1:21		534		0.044
Freiheit Spring [a]	June 16, 2009	9:22		534		0.010
Freiheit Spring [b]	June 16, 2009	18:00		531		0.041
Freiheit Spring [a]	June 17, 2009	2:01		527		0.010
Freiheit Spring [b]	June 17, 2009	10:39		531		0.040

[a] Sample was collected by ISCO #2.
[b] Sample was collected by ISCO #1.

Appendix F

Snow chemistry above Tyson Spring Cave and near Freiheit Spring

A snow sample was collected near the Tyson Spring Cave entrance shaft (MN23:X0111: 561748 m E, 4844989 m N, UTM Zone 15) on Mar. 13, 2009 and near Freiheit Spring (MN23:A0041: 554978 m E, 4839445 m N (± 3.5 m), UTM Zone 15) on Mar. 18, 2009, both in Fillmore County, MN. Samples were collected in a five-gallon bucket, and the bucket used to collect the sample near Freiheit Spring was lined with a clean plastic bag. Samples were melted in the lab. Both samples were analyzed for major cations (Table F.1) and anions (Table F.2) by Rick Knurr in the Analytical Geochemistry Lab of the University of Minnesota's Department of Geology and Geophysics. Cations were analyzed using Inductively Coupled Plasma – Optical Emission Spectrometry (ICP-OES) following EPA Method 200.7 with a Thermo Scientific iCAP 6500 dual view ICP-OES. Anions were analyzed using anion chromatography following EPA method 300.1 with a Dionex ICS 2000 system with an AS20 column and an AMMS III suppressor and a NaOH eluent. Anion analysis also used a 1.00 ml/min flow rate, a 25 mM H_2SO_4 regenerant, a 50 µl injection, and a conductivity detector. Conductivity and pH were measured in the lab for both samples (Table F.2). Alkalinity titrations were conducted on Mar. 17, 2009 for the sample collected near the Tyson Spring Cave entrance shaft and on Mar. 19, 2009 for the sample collected near Freiheit Spring (Table F.2).

Table F.1. Major cation snow chemistry near the Tyson Spring Cave entrance shaft (Mar. 13, 2009) and near Freiheit Spring (Mar. 18, 2009).

Location	Date	Al^{3+}	Ba^{2+}	Ca^{2+}	Fe total	Mg^{2+}	Mn total	Na^{+}	P total	Si total	Sr^{2+}
		ppm	ppm	ppm	ppm	ppm	ppm	ppm	ppm	ppm	ppm
Detection Limit for 2× dilution (DL2)		0.001	0.001	0.03	0.01	0.006	0.001	0.05	0.005	0.02	0.001
Above Tyson Spring Cave [a]	Mar. 13, 2009	0.017	0.060	3.28	0.03	0.099	0.002	0.35	0.009	0.07	0.005
Near Freiheit Spring [b]	Mar. 18, 2009	0.015	0.075	0.89	0.03	0.101	0.004	0.30	0.031	0.05	0.008

Note: Samples were also analyzed for total K^{+} (DL2 = 0.2 ppm) and Li^{+} (DL2 = 0.009 ppm). However, K^{+} was < 0.2 ppm and Li^{+} was < 0.009 ppm for both samples.

[a] Sample was collected near the entrance shaft to Tyson Spring Cave.

[b] Sample was collected on the hillslope just west of Freiheit Spring.

Table F.2. Major anion snow chemistry, pH, conductivity, and charge balance for snow samples collected near the Tyson Spring Cave entrance shaft (Mar. 13, 2009) and near Freiheit Spring (Mar. 18, 2009).

Location	Date	Lab pH	Lab conductivity	Alkalinity	Cl^{-}	NO_2^{-}-N	NO_3^{-}-N	SO_4^{2-}	Charge balance
			µS/cm	as ppm CaCO3	ppm	ppm	ppm	ppm	%
Detection Limit for 1× dilution (DL1)				0.5	0.005	0.005	0.005	0.01	
Above Tyson Spring Cave [a]	Mar. 13, 2009	7.15	18.1	9.4	0.290	0.006	0.184	0.20	-5.9
Near Freiheit Spring [b]	Mar. 18, 2009	7.07	5.9	2.3	0.218	<0.005	0.091	0.17	5.0

Note: Samples were also analyzed for F^{-} (DL1 = 0.005 ppm), acetate (DL1 = 0.005 ppm), formate (DL1 = 0.005 ppm), ClO_3^{-} (DL1 = 0.01 ppm), Br^{-} (DL1 = 0.01 ppm), oxalate (DL1 = 0.01 ppm), and PO_4^{3-}-P (DL1 = 0.005 ppm). However, F^{-} was < 0.005 ppm, acetate was < 0.005 ppm, formate was < 0.005 ppm, ClO_3^{-} was < 0.01 ppm, Br^{-} was < 0.01 ppm, oxalate was < 0.01 ppm, and PO_4^{3-}-P was < 0.005 ppm for both samples.

[a] Sample was collected near the entrance shaft to Tyson Spring Cave.

[b] Sample was collected on the hillslope just west of Freiheit Spring.